Effect of Residual Stress on the Life Prediction of Dry Storage Canisters for Used Nuclear Fuel

by

Bradley P. Black

B.S., Nuclear Engineering (2011)
University of Tennessee, Knoxville

SUBMITTED TO THE DEPARTMENT OF NUCLEAR SCIENCE
AND ENGINEERING
IN PARTIAL FULFILLMENT OF THE REQUIREMENTS OF THE DEGREE OF

MASTER OF SCIENCE IN NUCLEAR SCIENCE AND ENGINEERING
AT THE
MASSACUSETTS ISTITUTE OF TECHNOLOGY

JUNE 2013

Signature of Author:_____
Bradley P. Black
Department of Nuclear Science and Engineering
May 17, 2013

Certified by:_____
Dr. Ron Ballinger
Professor of Nuclear Science and Engineering, and Materials Science and Engineering
Thesis Supervisor

Certified by:_____
Dr. Tom Eagar
Professor of Material Science and Engineering and Engineering Systems
Thesis Reader

Accepted by:_____
Dr. Mujid S. Kazimi
TEPCO Professor of Nuclear Engineering
Chair, Department Committee on Graduate Students

Effect of Residual Stress on the Life Prediction of Dry Storage Canisters for Used Nuclear Fuel

by

Bradley P. Black

Submitted to the Department of Nuclear Science and Engineering on May 17, 2013
in Partial Fulfillment of the Requirements for the Degree of
Master of Science in Nuclear Science and Engineering

ABSTRACT

Used nuclear fuel dry storage canisters will likely be tasked with holding used nuclear fuel for a period longer than originally intended. Originally designed for 20 years, the storage time will likely approach 100 years. These canisters are fabricated from rolled and welded austenitic stainless steel plate. Most of the storage facilities are located on coastal or brackish water sites with environments containing moisture and chloride ions that can cause stress corrosion cracking (SCC). Residual stresses from the welding process provide the tensile stress for crack initiation and propagation which could eventually compromise canister integrity, allowing the release of radioactive material to the environment. If it is assumed that a tensile stress, predominantly from welding, is constant through the material thickness, this would suggest that failure will be initiation controlled. However, prior studies and practical experience indicate that residual stress varies as a function of depth into a welded material, and that stresses can decrease to zero or even go into compression. This would indicate that at some point, crack propagation could be slowed or even be stopped. In order to predict the time to failure of canister material by stress corrosion cracking, it is therefore necessary to know the actual residual stress distribution through the thickness of canister welds. This thesis investigates dry storage canister designs, canister welds, and contributing factors to residual stress, as well as prior studies of residual stress in welded stainless steel piping and chloride stress corrosion crack propagation rates. From this investigation, an estimate is made for the likely residual stress distribution in a typical canister weld, and the effect of residual stress on canister life prediction is examined. The analysis suggests that residual stress distribution has a tremendous impact on a canister's projected time to failure, and that residual tensile stresses in the heat-affected zone of canister welds could become low enough to result in crack arrest.

Thesis Supervisor: Dr. Ron Ballinger
Title: Professor of Nuclear Science and Engineering, Professor of Material Science and Engineering

Acknowledgments

I would first like to thank my advisor, Professor Ron Ballinger, for taking me on as a research assistant for such an interesting and meaningful project, as well as for his guidance and leadership, his continual availability, and his unfailing willingness to help. Thank you for this excellent opportunity.

I would like to thank Professor Tom Eagar for serving as my thesis reader, for his many outstanding anecdotal lessons in structural materials, and for his personal assistance in many areas of this thesis. In addition, thank you to Dr. Sebastien Teysseyre of Idaho National Laboratory for his guidance early on in the direction of my thesis, as well as in the pursuit of residual stress measurement techniques. Thank you to Chris Sheratt of MIT Libraries for her persistence in helping me obtain the most difficult to locate documents, and for going above and beyond in using her network to help locate references half a world away and written only in a foreign language. Thank you to Dr. Yusaku Maruno for his assistance in translating these documents, as well as for bringing several other papers to my attention that I otherwise could not have found. Thank you to Dr. George Rawls of Savannah River National Laboratory for his assistance in providing additional figures from his papers to help me learn more from his work. Thank you to Dr. Peter Andresen of GE Global Research for his help in the areas of stress intensity and crack growth rates.

Thank you to my officemates Elliott Fray and Sara Ferry. Sara for helping me to prepare and present our research together, as well as proofreading and improving upon drafts of my work, and Elliott for his insight and assistance in materials science, for allowing me access to his personal library of materials science textbook, and for providing great company for many long days of working at the lab.

Thank you to my parents for providing their unwavering support, stability, and encouragement, and for everything in between they have provided throughout my entire life, that have allowed me to be the best student and person I can be.

Finally, thank you to my wife Michele for always providing excellent support and encouragement whenever it was needed, for her patience and understanding for all of the time I have committed to my education over the past ten years of our relationship, and for providing me with the vision of our future as the goal to strive towards and the light at the end of the tunnel.

Thank you to anyone I have forgotten and to everyone without which this would not have been possible.

Contents

Acronyms

ASME B&PV- American Society of Mechanical Engineers Boiler and Pressure Vessel Code
BCC- Body Centered Cubic
BFS/ES- BNG Fuel Solutions / EnergySolutions
BNG- British Nuclear Group
CASTOR- Cast Iron Cask for Storage and Transport of Radioactive Material
CGR- Crack Growth Rate
CRIEPI- Central Research Institute of Electric Power Industry
CT- Compact Tension
DHD- Deep Hole Drilling
DPC- Dual Purpose Canister
DSC- Dry Shielded Canister
EDM- Electrical Discharge Machining
EPRI- Electric Power Research Institute
ESCP- Extended Storage Collaboration Program
FCC- Face Centered Cubic
FEM- Finite Element Method
FNC- Frazer-Nash Consultancy
FSC- Fuel Storage Canister
GNB- Gesellschaft fuer Nuklear-Behaelter
GTAW- Gas Tungsten Arc Welding
HSM- Horizontal Storage Module
ID- Inner Diameter
INTEC- Idaho Nuclear Technology and Engineering Center
ISFSI- Independent Spent Fuel Storage Installation
MAGNASTOR- Modular Advanced Generation Nuclear All-Purpose Storage System
MMA- Manual Metal Arc
MPC- Multi Purpose Canister
MVDS- Modular Vault Dry Store
NRC- Nuclear Regulatory Commission
NUHOMS- NuTech Horizontal Modular Storage System
NuPac- Nuclear Packaging Inc.
OD- Outer Diameter
PRA- Probabilistic Risk Assessment
PS- Proof Stress
PT- Dye Penetrant
PWHT- Post-Weld Heat Treatment
RDCPD- Reverse Direct Current Potential Drop
RH- Relative Humidity
SAW- Submerged Arc Welding
SCC- Stress Corrosion Cracking
SNF- Spent Nuclear Fuel
TIG- Tungsten Inert Gas Welding
TSC- Transportable Storage Canister
UMS- Universal Multi-Purpose Canister System

UoB- University of Bristol
VCC- Vertical Concrete Cask
XRD- X-Ray Diffraction

1. Introduction

Dry cask storage was originally intended to be the intermediate stage for the back end of the nuclear fuel cycle. After spending approximately 10 years in spent fuel storage pools, used nuclear fuel would be moved to dry cask storage where it would remain until a deep geological repository could be completed. The cancellation of the Yucca Mountain Nuclear Waste Repository Project has altered these plans, and forced dry cask storage systems to serve for longer than originally intended. Used fuel could now be kept in dry storage for over 100 years.

Dry cask storage designs most commonly consist of a welded austenitic stainless steel canister of types 304/304L or 316/316L, encased in a concrete shell known as an overpack. These casks are located throughout the country in Independent Spent Fuel Storage Installations (IFSFIs) often on the site of nuclear power plants, which themselves are often located in coastal or lake-side regions where a salt air environment may exist (see Figures 1.1 and 1.2). The concrete overpacks allow air to enter near the bottom of the cask and cool the inner canister, allowing for the deposition of airborne chlorides and other potentially aggressive species on the canister surface.

Austenitic stainless steels, particularly types 304 and 304L, are susceptible to pitting and transgranular stress corrosion cracking in chloride containing environments if a continuous aqueous film is maintained on the surface [Jones, 1996]. Under certain conditions, chlorides can undergo deliquescence on the canister surface, a process by which the salts essentially pull moisture out of the air, creating a concentrated salt brine on the canister surface [Chu et al., 2013].

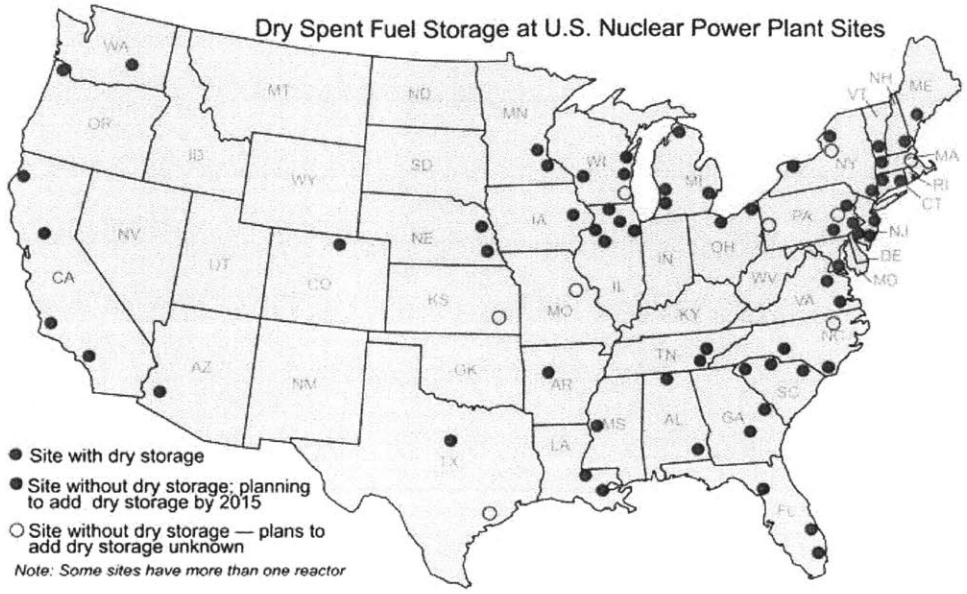

Figure 1.1 - Independent Spent Fuel Storage Installation (IFSFI) locations [Rigby, 2010]

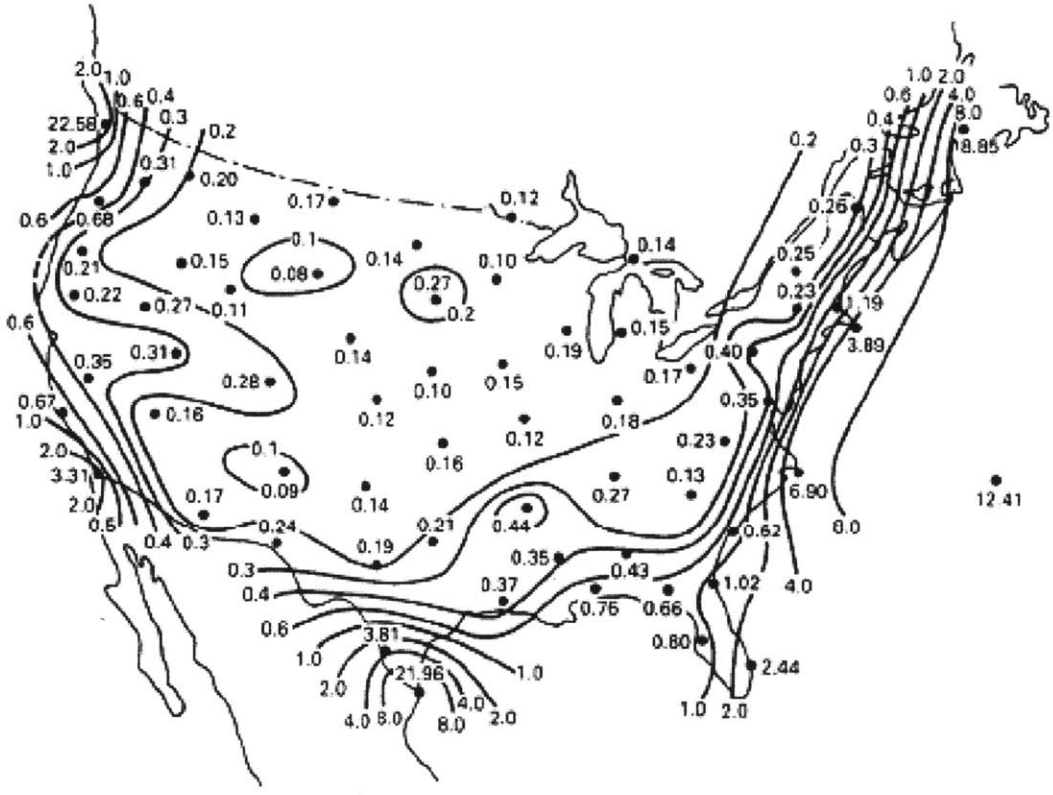

Figure 1.2- Average chloride concentration (ppm) in rainwater [EPRI, 2005]

This deliquesced corrosive solution that can develop, together with elevated temperatures provided by the decay heat from the used fuel, can create the environmental conditions for stress corrosion cracking [Hayashibara et al., 2008]. Stress corrosion cracking (SCC) requires not only a corrosive environment, but also a susceptible material and tensile stress. The magnitude or severity for each of these three requirements is dependent upon that of other two. In other words, given a more corrosive environment, a less susceptible material and lower tensile stress are required for SCC. This relationship is illustrated by the Venn Diagram in Figure 1.3.

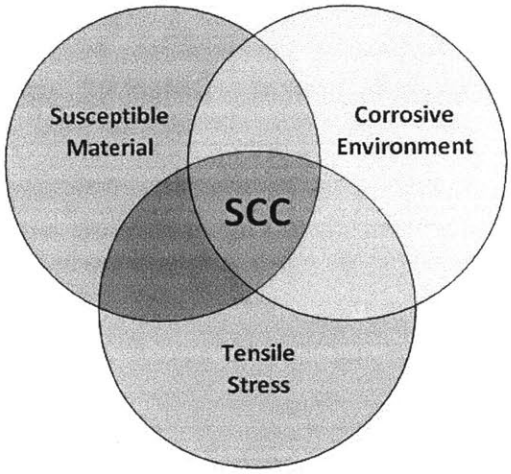

Figure 1.3- Factors necessary for SCC

The susceptible material in this scenario is the sensitized heat-affected zone of the austenitic stainless steel canister welds. Heat input from the welding process results in sensitization of the stainless steel, whereby chromium present throughout the steel is decreased near the grain boundaries due to precipitation of chromium carbides. Carbide precipitation reduces the amount of chromium near the grain boundary, and degrades the passive film locally, leaving the steel vulnerable to intergranular attack.

With a susceptible material in a corrosive environment, all that is required for SCC is the presence of sufficient tensile stress, which is the focus of this thesis. The welding of the canister,

in addition to leaving the steel sensitized, leaves behind highly variable local residual stresses. In the past, studies of SCC in austenitic stainless steels for dry cask storage have utilized test samples that do not account for local residual stress distributions, such as U-bend specimens [Mintz et al., 2010]. Tests such as this purposely induce very high tensile stresses and strains above the threshold to induce SCC, but fail to accurately represent the actual stress distribution near a real canister weld.

In order to accurately characterize the residual stress distribution of actual canister material, a larger project is under way to take high-resolution residual stress measurements of mock-up canister material, provided by the canister vendors and their fabricators, and prepared in exactly the same manner as actual used fuel storage canisters. In anticipation of these measurements, the work in this thesis was completed to guide the design of these mock-up canisters, determine which welds were of greatest interest, choose a residual stress measurement technique, investigate the subtleties and variability of the residual stress profile in canister welds, and to predict their residual stress distributions and the effect of residual stress on time to canister failure by SCC crack growth.

The work completed towards these goals is included below. First, the canister systems themselves are investigated, to gather as much publicly available information as to be able to characterize the mechanical environment in question. Next, an investigation of the canister welds will be discussed in order to understand their impact and variability as well as to determine which areas of the canister are most vulnerable to SCC. Next, in preparation of receiving actual canister material, a literature review of residual stress measurements in welded stainless steels will be discussed in order to understand the factors that influence residual stress as well as to create a prediction of what can be expected of the residual stress state of welded canister

material. Finally, an initial model will be put forth, using these predictions, to estimate the time to failure of used fuel canister material by SCC. It is the goal of this thesis not to provide definitive answers, but rather to lay the groundwork and provide a path forward for developing a model as a function of residual stress, along with other variables such as environment, to predict the time to failure of used fuel storage canisters by stress corrosion cracking.

2. Dry Cask Storage Systems

Six vendors in addition to the Department of Energy have produced over 1000 dry cask storage systems in the United States, the vast majority of which are made by the three leading vendors: Transnuclear, Holtec International, and NAC International. The number of casks and assemblies stored by each vendor is shown in Table 2.1. A typical Independent Spent Fuel Storage Installation with NAC casks is shown in Figure 2.1.

Table 2.1- Vendor Totals as of 2009 [StoreFUEL, 2009]

Vendor	Fuel Assemblies Stored	Total Loaded Casks
Transnuclear	18625	540
Holtec	14398	271
NAC	5106	211
BFS/ES	1833	66
DOE	1464	N/A
GNB	558	26
Westinghouse	533	16
Total:	**42517**	**1130**

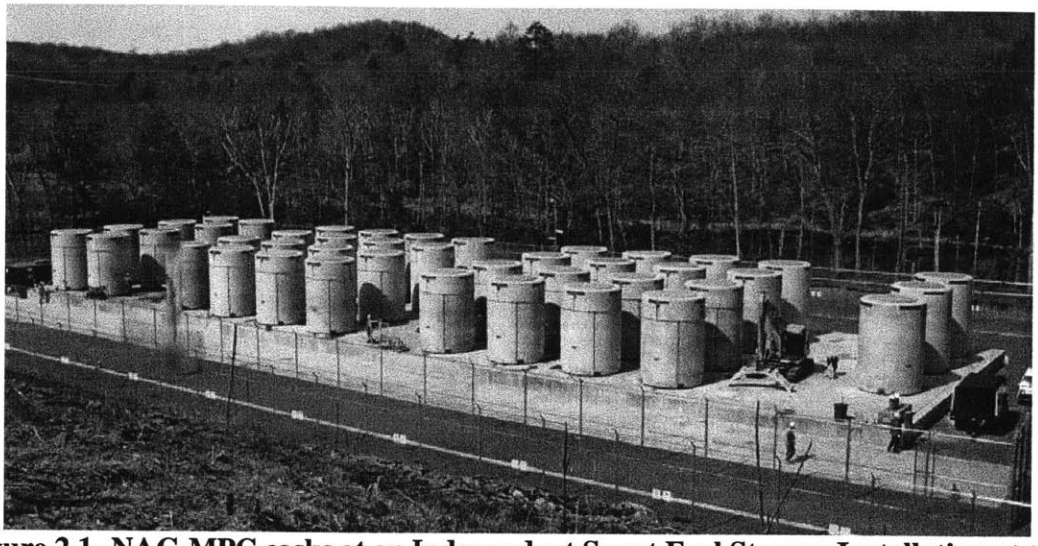

Figure 2.1- NAC-MPC casks at an Independent Spent Fuel Storage Installation at the Connecticut Yankee Nuclear Power Plant site [Rigby, 2010]

Dry storage systems in the US consist of two basic types. There are the non-canisterized, bolted closure, thick-walled metal cask systems, as well as the canisterized systems comprised of thin-walled welded canisters which are inserted into metal and concrete overpacks. While this section will cover both types, the residual stress and crack propagation sections will focus only on the welded, thin-walled canister systems which are vulnerable to SCC.

The thin-walled, welded canisters are all quite similar to one another. Every canister is a right cylinder, with a shell thickness between 1.27cm and 1.59cm (1/2in - 5/8in) thick, fabricated using austenitic stainless steel of Types 304, 316, 304L or 316L. Weld filler metal compositions are typically Type 308 for Type 304 canisters and Type 316 for Type 316 canisters in order to ensure a sufficient fraction of delta ferrite to avoid hot cracking. The empty canisters are lowered into a spent fuel storage pool, filled with used fuel assemblies while submerged, lifted out, drained of water and vacuum dried, backfilled with an inert cover gas (typically helium), and welded shut. Each canister is then encased in more steel, concrete, or other material to provide radiation shielding and/or collision protection for transportation. The diameter and length of the

canisters vary, but are primarily dependent on the type fuel assembly they hold, either the smaller (typically 8 x 8) square arrays of fuel rods for a Boiling Water Reactor (BWR) or the larger (typically 17 x 17) square arrays for a Pressurized Water Reactor (PWR). Several cross sections of a typical used fuel storage cansiter can be seen in Figure 2.2.

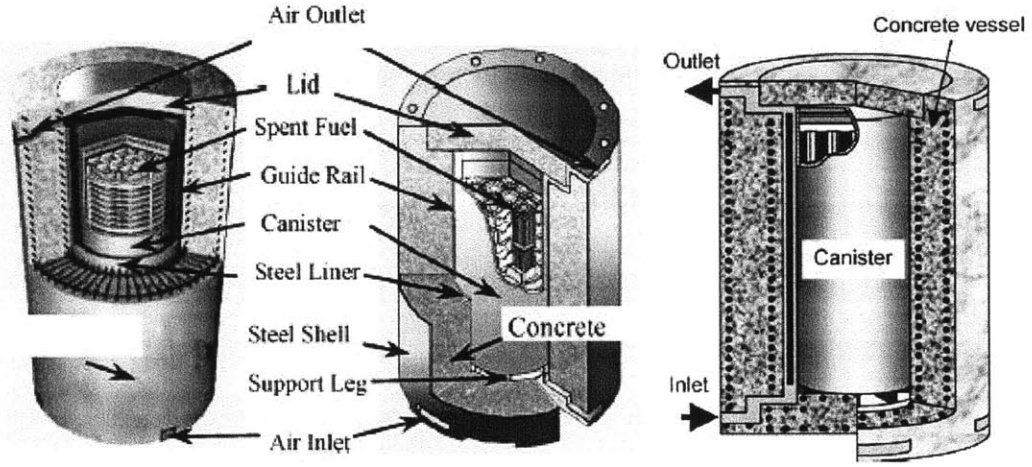

Figure 2.2- Typical used fuel storage canister in concrete cask with air cooling [Saegusa et al., 2008]

In order to characterize the mechanical environment of used fuel storage canister material, it is necessary to first gain a thorough knowledge of the makeup of these used fuel storage systems. For this reason, all publicly available information that could be found on the design and structure of used fuel storage systems currently in use in the US was compiled, with emphasis placed on the three most common canister producers. In addition to providing a basis of understanding for the material and its weld residual stress states, as well as in guiding the design of canister mock-ups for residual stress measurement, this outline will also prove useful in future research on the subject of stress corrosion cracking in used fuel storage systems. Tables further detailing the quantity, location, and dimensions of these canisters can be found in Appendix A.

2.A. Transnuclear

Transnuclear is a subsidiary of AREVA that is headquartered in Columbia, Md. As of 2009, Transnuclear was the largest provider of used fuel storage systems in America, with their casks holding over 44% of all assemblies in dry storage in the US [StoreFUEL, 2009]. Transnuclear produces two lines of dry storage containers for use in the US: the TN family of thick-walled metal casks, and the canisterized NUHOMS system.

2.A.1. TN Metal Casks

The metal TN casks are a line of dual purpose (transportation and storage) casks designed for holding either BWR or PWR assemblies. The first TN metal cask design to be issued a Nuclear Regulatory Commission (NRC) Certificate of Compliance was the TN-24 in 1993 [NRC, 2012]. While there are currently no used fuel assemblies stored in the TN-24 [StoreFUEL, 2009], the TN-32 and TN-68 designs remain in use, holding 32 PWR and 68 BWR assemblies respectively. A newer design, the TN-40 (designed to hold 40 PWR assemblies), is currently under review by the NRC as part of a license amendment for the Prairie Island ISFSI [EPRI, 2010].

As an example of the TN line of casks, a schematic of the TN-68 is shown in Figure 2.3. The cask consists of a confinement vessel with bolted closure, a basket for fuel assemblies, a gamma-ray shield, neutron shield, trunnions for lifting and rotating, pressure monitoring system, and protective weather cover. The confinement vessel is welded carbon steel, bolted with carbon steel lid and inner metallic seal. Vent and drain orifices are covered with closure bolts and inner metallic seals as well. Within the containment vessel is the basket, consisting of slotted plates of stainless steel and neutron absorber, and designed specifically to hold individual fuel assemblies (in this case 68 BWR assemblies, at 13.9cm x 13.9cm) [Todreas and Kazimi, 1990]. The

stainless steel of the basket provides a path for heat conduction while the neutron absorber allows for criticality control.

The inner containment vessel is made up of 19.0cm (7.5in) thick carbon steel that acts as a gamma-ray shield, surrounded by a 15.2cm (6in) thick borated polyester resin neutron shield. [NRC, 2011]. The resin compound is cast in long, narrow aluminum vessels that when grouped around the containment vessel provide the outer neutron shielding. A thin steel envelope surrounds the resin vessels.

The steel lid is bolted on, with a polypropylene disk underneath to provide axial neutron shielding. The outer cask body includes four trunnions for lifting and rotating the cask during loading. The pressure monitoring system (a helium tank with either pressure transducers or switches) continuously monitors the pressure in the spacing between the inner and outer seals on the lid, vent, and port covers [EPRI, 2010].

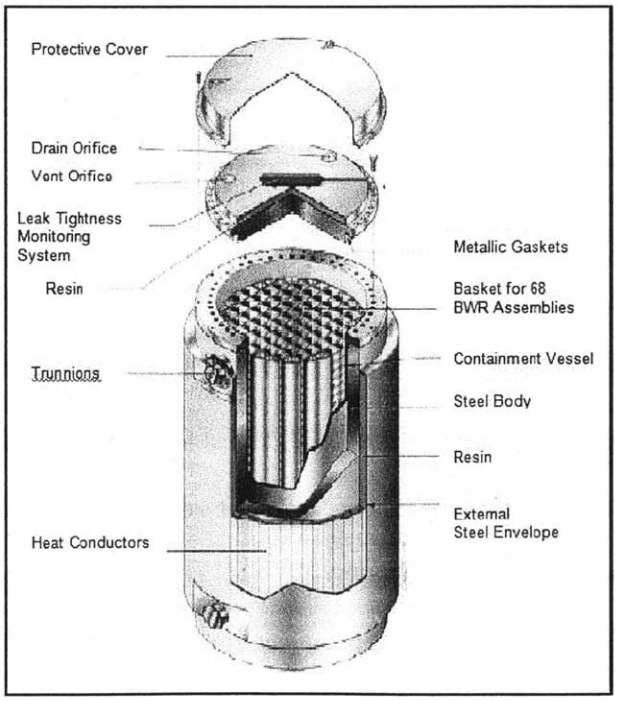

Figure 2.3 - TN-68 Dual Purpose Cask [Bailly, 2005]

2.A.2. NUHOMS

The NUHOMS dry shielded canister (DSC), first approved for use by the NRC in 1995 [NRC, 2012] stores BWR and PWR assemblies horizontally. The NUHOMS (short for NuTech Horizontal Modular Storage System) family of DSCs includes the models 24P, 32P, and 61B. Like many other vendors' canister families, there may be several variations within canisters of equal capacity, such as the NUHOMS 24PT1, 24PT4, 24PHB, and 24PTH. While each holds 24 PWR assemblies, they vary in several regards such as in maximum allowable heat load as well as in external dimensions [EPRI, 2010].

The NUHOMS system consists of a right cylindrical container like every other storage system, but differs from the average storage system in that it is stored horizontally rather than vertically and that it is loaded into its concrete storage module (called a horizontal storage module, or HSM) at the ISFSI. The canister is first loaded into a cask used only to provide shielding during transport, known simply as the Transport Cask (TC), a cylindrical vessel made primarily of stainless steel with bolted cover. It remains in this cask from when it leaves the spent fuel storage pool until it reaches the HSM, whereupon the TC is opened and a hydraulic ram system is used to directly insert the canister into the opening of the HSM (See Figure B.3. in Appendix B). Figure 2.4 shows a schematic of the NUHOMS system.

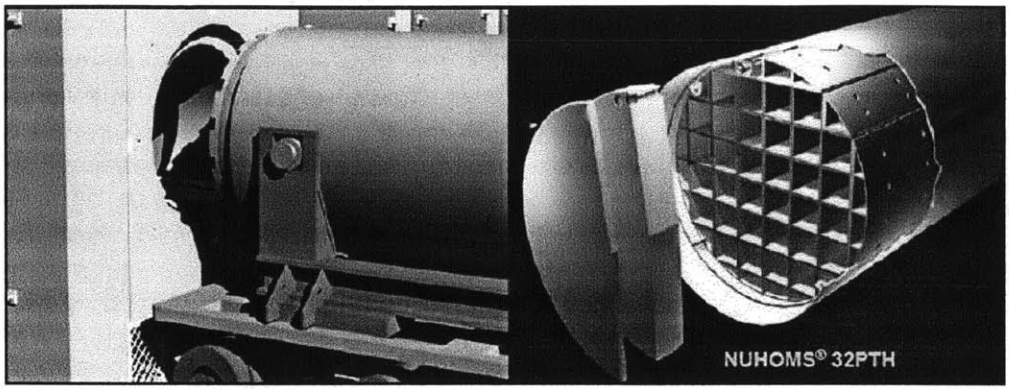

Figure 2.4 - NUHOMS Horizontal Storage Module, Transfer Trailer, and 32PTH DSC [Neider, 2005]

The NUHOMS DSC consists of a thin stainless steel welded cylindrical shell with integral bottom cover plate, bottom shield plug, ram/grapple ring, top shielded plug, top cover plate, and basket assembly. The exterior of the DSC is smooth, as it is designed to slide easily from its transfer cask into the HSM without scratching the surface. The HSM is made of reinforced concrete, typically with internal heat shields (see Figure B.5 in Appendix B) [Kok, 2009]. As shown below in Figure 2.5, there are openings which allow air to flow past and cool the DSC. These openings include wire mesh screens to prevent debris from entering, however salts present in the air can still enter and deposit on the canister surface. The DSC support structure is shown in Figure 2.5, consisting of a structural steel frame with rails. An alternative DSC Support Structure exists for areas with higher levels of seismic activity.

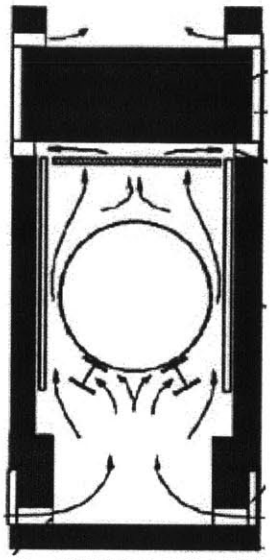

Figure 2.5- Air cooling of a NUHOMS DSC in its HSM [Kok, 2009]

2.B. Holtec International

Headquartered in Marlton, NJ, Holtec is the second largest US vendor of used fuel storage systems. Like Transnuclear, Holtec has two families of dry storage designs: the HI-STAR 100 and HI-STORM 100. Both systems include the use of thin-walled, welded, stainless steel canisters.

2.B.1. HI-STAR 100

The HI-STAR 100, first certified for storage in 1999 and illustrated in Figure 2.6, can hold either 24 PWR fuel assemblies or 68 BWR assemblies. It contains a dual purpose canister (DPC) used for both transportation and storage, surrounded by a metal cask which is also used for both transportation and storage. The DPC consists of a welded cylindrical shell with a honeycombed fuel basket, baseplate, closure ring, and lid. All components that make up the confinement boundary (the canister shell, baseplate, lid, closure ring, and port cover plates) are made of stainless steel [EPRI, 2010]. The canisters are classified as MPC-24, MPC-40, MPC-68, and MPC-68F. MPC stands for multipurpose canister, with the numbers indicating the

maximum number of fuel assemblies that can be held. As of 2009, there were no MPC-24's in use in the US, however, the MPC-68 (used in both the HI-STAR and HI-STORM configuration) was the single most widely used canister in the US (See Table A.2. in Appendix A) [StoreFUEL, 2009].

The HI-STAR 100's metal overpack is a thick walled carbon steel cylinder, with an internal cylindrical cavity for housing the MPC [Holtec, 2010]. It includes inner, intermediate, and enclosure shells that provide the gamma-ray shielding. Neutron shielding is provided around the outer surface of the overpack. The inner shell, which is welded to a cylindrical forging at the bottom and to a heavy flange with bolted closure plate at the top, forms a helium retention boundary. The outer surface of the overpack includes trunnions for lifting and rotating the cask.

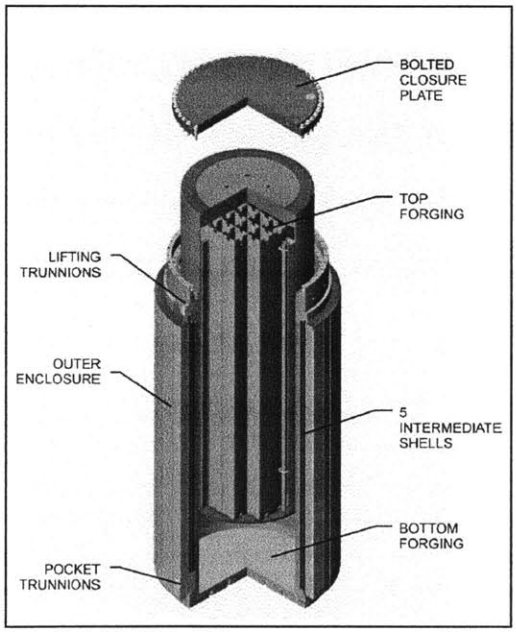

Figure 2.6- HI-STAR 100 storage system [Singh, 2004]

2.B.2. HI-STORM 100

The HI-STORM 100 was first certified for use in 2000, and is illustrated in Figure 2.7. It also utilizes the metal MPCs, but has a concrete storage overpack as opposed to metal cask. The

HI-STORM 100's concrete storage pack is not dual-purpose, but instead is used only for storage. For loading, unloading, and transferring the MPC, a transfer cask (called the HI-TRAC) is used. The HI-STORM 100 holds up to 32 PWR assemblies or 68 BWR assemblies.

The overpack is a cylindrical vessel of steel and concrete. Radial shielding consists of un-reinforced concrete enclosed between two steel shells. There are four air inlets at the bottom of the cask and four at the top. The cask is also penetrated by the drain port plug, pressure port plug, interlid port plug, and pressure sensor. The pressure sensors are electronic, typically with a Ni-plated Cu-Be diaphragm [Rigby, 2010].

There exist several variants of the HI-STORM 100, such as the HI-STORM 100U which is stored underground. In 2009, Holtec applied for certification for the HI-STORM FW (flood and wind) system, which is designed to hold 37 PWR or 89 BWR assemblies. Additionally, the HI-STORM 100A and 100SA variants allow the cask to be anchored to a concrete storage pad in areas of high seismic activity [EPRI, 2010]. Figure 2.7 shows a schematic of a Holtec HI-STORM 100 cask with internal canister.

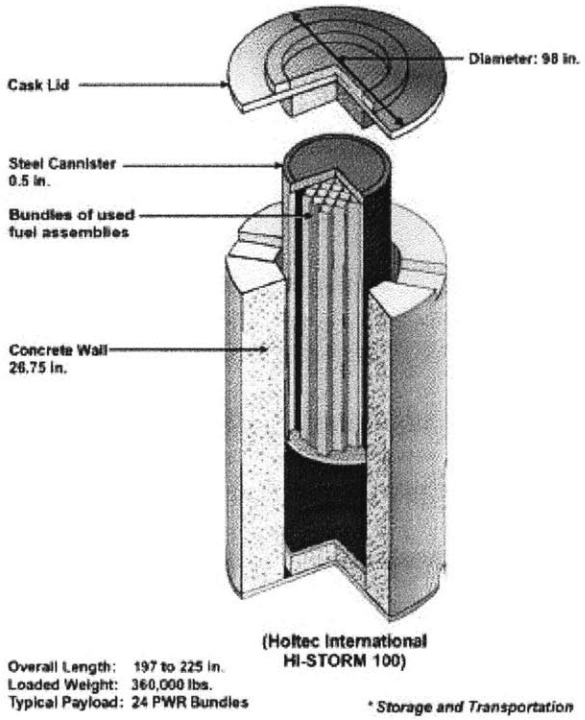

Figure 2.7- Holtec HI-STORM 100 cask [NRC, 2011]

2.C. NAC International

Headquartered in Atlanta, GA, NAC is the third largest provider of dry storage casks in the US. The NAC S/T, a bolted, thick-walled metal cask certified in 1990, was one of the first metal storage casks approved used fuel storage in the US. NAC has since established three new storage system families, each of which is a dual purpose canister storage system. The DPC families include the NAC Universal Multi-Purpose Canister System (NAC UMS), the NAC Multi-Purpose Canister (NAC MPC), and the Modular Advanced Generation Nuclear All-Purpose Storage System (MAGNASTOR).

2.C.1. NAC S/T

There are four variations of the NAC S/T (which are non-DPC cask systems, as opposed to the MPC, UMS and MAGNASTOR). These variations are the NAC S/T, the NAC-C28, the

NAC-I28, and the NAC-STC. They are each vertical metal casks with bolted closure. The Certificates of Compliance for the NAC S/T and NAC-C28 both expired in August of 2010. As of March 2009, only the NAC-I28 held used nuclear fuel.

The NAC S/T casks (illustrated in Figure 2.8) are composed of multiple stainless steel cylinders. Between the inner and outer stainless steel cylinders is a layer of lead for gamma-ray shielding. The inner and outer shells are connected on both the top and bottom of the cask by stainless steel plates and rings. Outside of this shell is a layer of borated synthetic polymer for neutron shielding, which is surrounded by a stainless steel shell whose endplates are welded to the other shells. Within this radial neutron shield are 24 copper and stainless steel fins to aid in the conduction of heat away from the cask internals. Up to six removable trunnions can be attached for moving the cask. The NAC-I28's fuel basket consists of an aluminum and stainless steel grid with borated neutron material for criticality control, and holds up to 28 PWR fuel assemblies [EPRI, 2010].

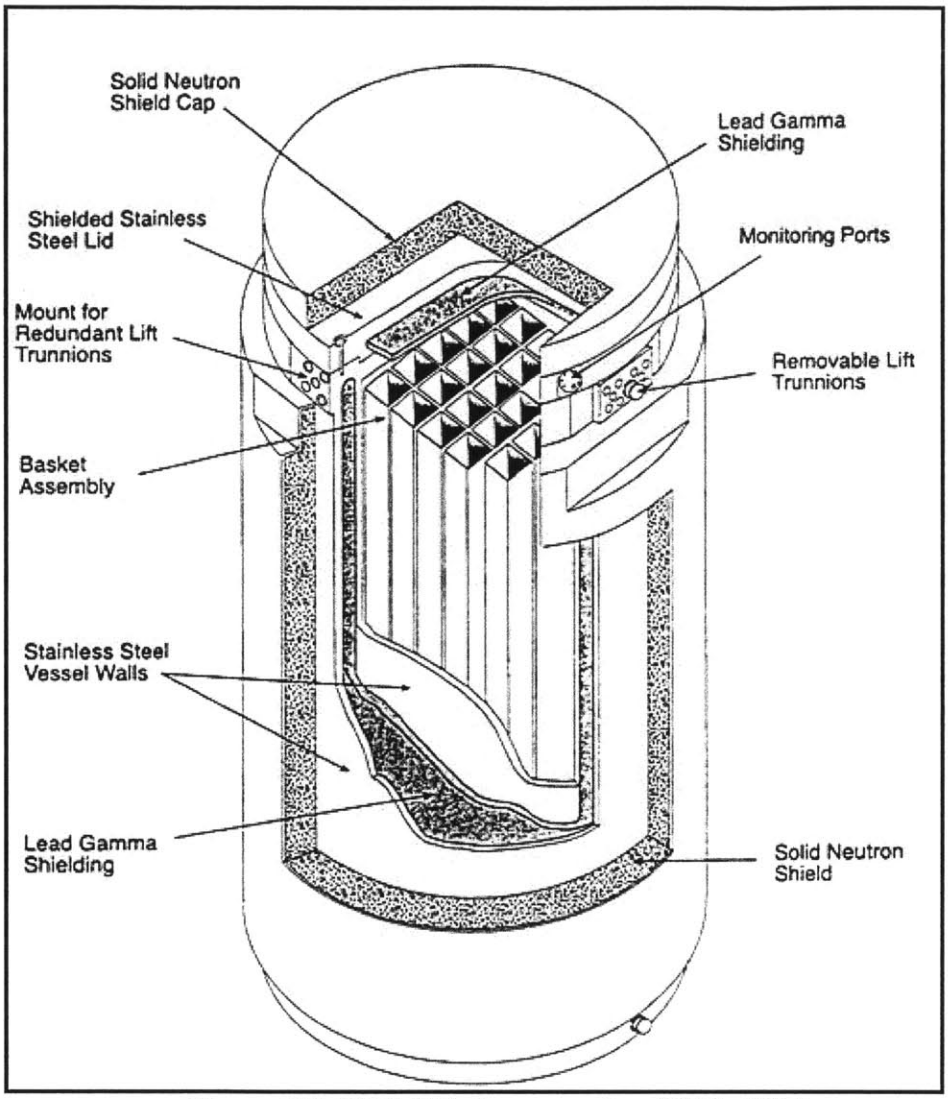

Figure 2.8- NAC S/T storage system [NEI, 1998]

2.C.2. NAC UMS

The NAC Universal MPC System, or UMS (illustrated in Figure 2.9), contains a welded transportable storage canister (TSC), vertical concrete storage cask (VCC), and a transfer cask. The transfer cask is used for lowering the TSC into the spent fuel pool, after which the TSC is transferred through the bottom of the transfer cask into the VCC, as shown in Figure 2.10 [Dry Casks, 2013].

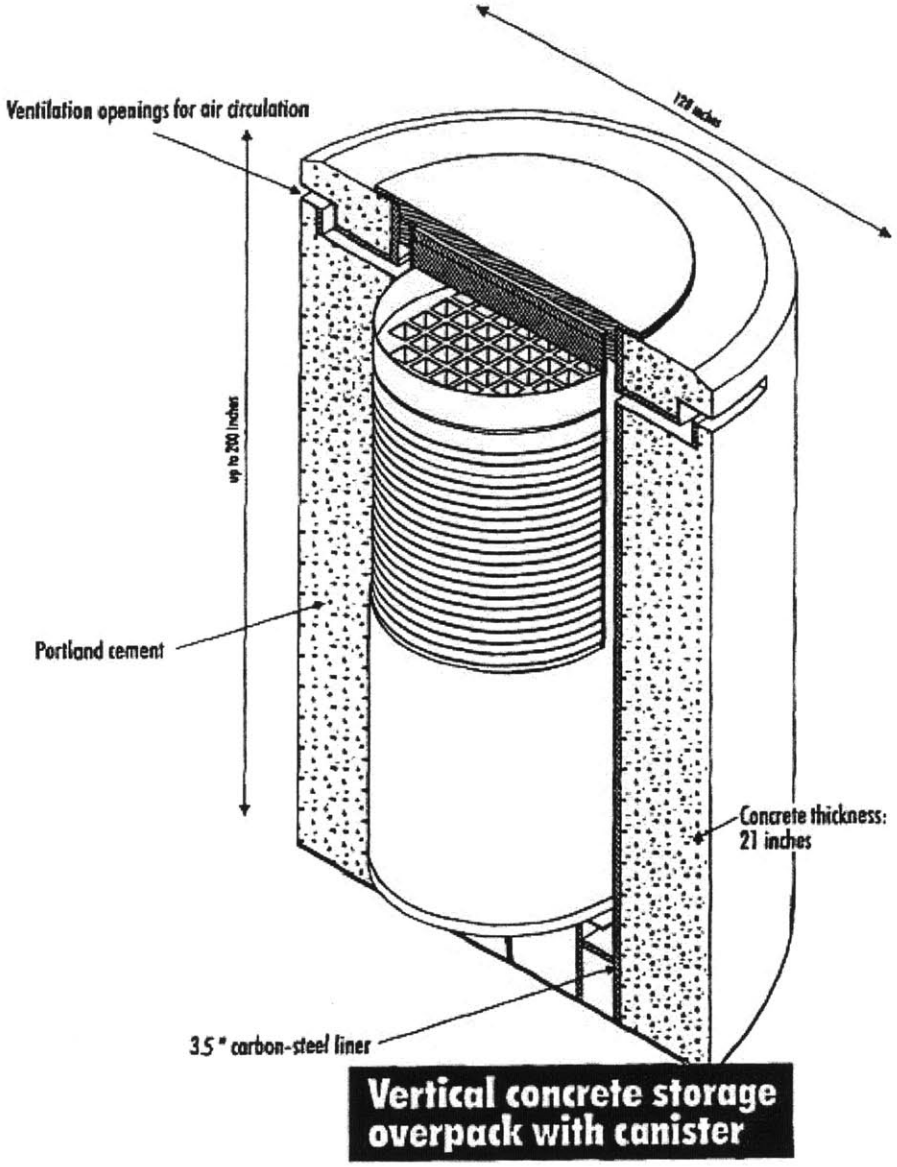

Figure 2.9- NAC-UMS [Wacid, 2003]

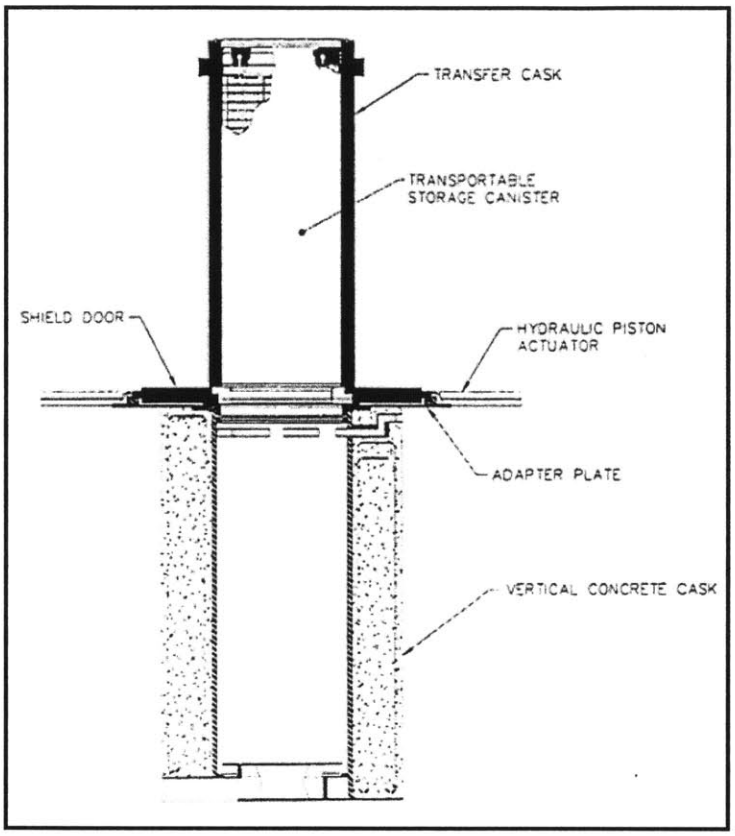

Figure 2.10 - Transfer of a recently loaded NAC-UMS TSC from its Transfer Cask to its VCC [NEI, 1998]

The TSC holds 24 PWR or 56 BWR assemblies. The TSC for PWR assembly storage comes in three different lengths, and in two different lengths for BWR assembly storage. It consists of a cylindrical shell with a shield lid, structural lid, bottom plate, port covers, and fuel basket. The basket consists of a series of stainless steel and carbon steel support disks, as well as Boral sheets for criticality control. Aluminum disks for heat transfer are placed between the support disks, and are the primary means of heat transfer from the TSC internals to its outer wall.

The VCC overpack provides structural support, radiation shielding, partial environmental protection, and allows for the cooling of the TSC by natural convection. It consists of a steel liner surrounded by a thick layer of concrete. A carbon steel lid is bolted on top of the cask, providing axial gamma-ray shielding [EPRI, 2010].

2.C.3. NAC MPC

The NAC MPC is known as a "sister-system" to the older UMS. It too is composed of a transportable storage canister (TSC), a transfer cask, and a vertical concrete cask (VCC). As of March 2009, it was used only at the decommissioned Connecticut Yankee and Yankee Rowe ISFSIs [StoreFUEL, 2009]. It includes a cylindrical fuel basket that can hold as many as 36 fuel assemblies for Yankee Class fuel and up to 26 assemblies for Connecticut Yankee fuel, both of which were PWRs. Like the TSC of the UMS, the TSC consists of a right circular cylindrical stainless steel shell with a welded bottom plate, shield lid, structural lid, and port covers. As with the UMS, the bolted VCC serves as the canister's overpack, providing structural support, shielding, partial environmental protection, and allows for cooling by natural convection. The exterior of NAC MPCs can be seen in Figure 2.1.

2.C.4. MAGNASTOR

The NAC MAGNASTOR, illustrated in Figure 2.11, is the newest NAC storage system, with a Certificate of Compliance issued in 2009. It is a DPC-based system which can hold 37 PWR or 87 BWR assemblies. Like the NAC UMS and MPC, it consists of a welded TSC, a concrete storage cask, and a transfer cask [EPRI, 2010].

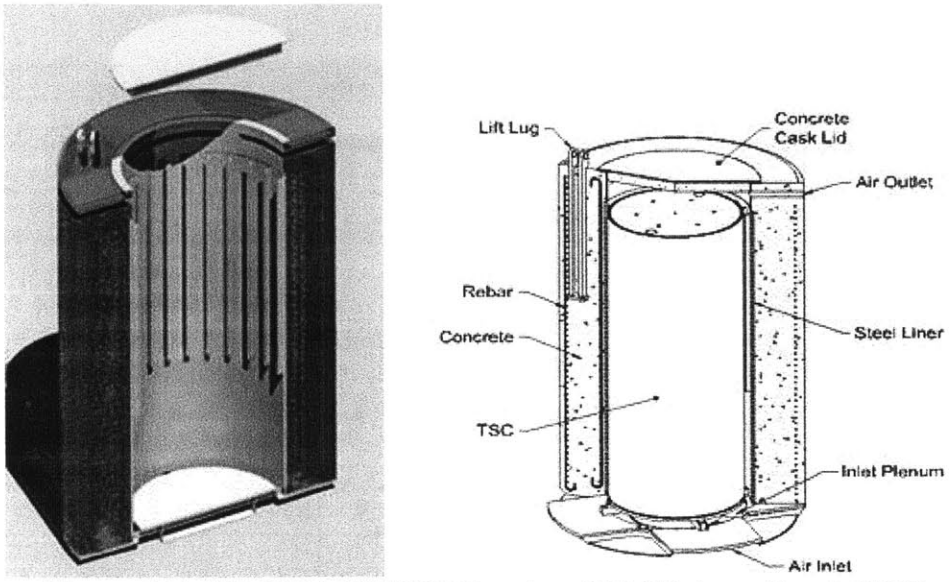

Figure 2.11- NAC MAGNASTOR system [NAC International, 2013]

2.D. Other Vendors

While Transnuclear, Holtec, and NAC are responsible for producing the vast majority of dry storage systems in the US, there are several other vendors that produce dry storage systems as well. The remaining canister vendors will be described briefly below, though further information on each can be found in the EPRI Industry Spent Fuel Storage Handbook [EPRI, 2010].

BNG (British Nuclear Group) Fuel Solutions, sometimes shortened as BFS or BFS/ES (purchased by EnergySolutions in 2006) manufactured the FuelSolutions VSC-24 and W-150. The VSC-24 is a welded canister with a bolted overpack that holds 24 PWR assemblies. While this canister is no longer made, VSC-24's do store SNF at Palisades, Point Beach, and Arkansas Nuclear One (see Figure B.13 in Appendix B for a schematic of a VSC-24). General Nuclear Systems Inc., a subsidiary of the German GNB (Gesellscaft fuer Nuklear-Behaelter), produced the CASTOR (Cast Iron Cask for Storage and Transport of Radioactive Material [Bare and Torgerson, 2001]) V/21 and X/33, vertical cast iron casks designed to vertically hold 21 and 33

PWR assemblies respectively, with a nickel coating on the inner surface and an epoxy resin coating and heat conduction fins on the outer surface. A drawing of each can be seen in Figures B.14 and B.15 in Appendix B. The NuPac (Nuclear Packaging, Inc.) 125-B system was made specifically for the purpose of transporting nuclear reactor core debris from Three Mile Island to Idaho, where it is now stored at INTEC (Idaho Nuclear Technology and Engineering Center) in above-ground dry storage. Perhaps one of the most unique dry storage systems in the US is the MVDS (Modular Vault Dry Store) [Roberts, 1998] produced by Foster Wheeler Energy Applications. The MVDS, an image of which is shown in Figure 2.12, consists of an enclosed concrete vault with 32 PWR or 150 BWR storage positions which hold one assembly each in an individual fuel storage container (FSC). The MVDS also consists of a transfer cask reception bay, charge face structure, large foundation, and neutron source storage wells [EPRI, 2010].

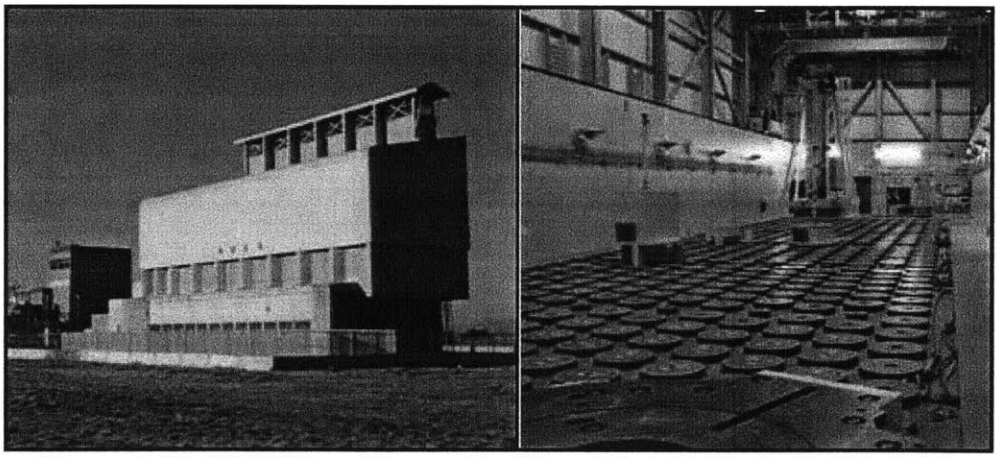

Figure 2.12- MVDS Dry Storage Facility at Fort St. Vrain [DOE, 2009]

3. Welds

3.A. Importance of Welds

The welding of used fuel storage canisters results in the most vulnerable areas for stress corrosion cracking and is therefore vitally important to the study of canister failure by SCC. The

area most vulnerable to SCC is known as the heat affected zone, or HAZ. The HAZ is the region adjacent to a weld in which the stainless steel was not melted but was subjected to severely elevated temperatures for a brief time. Depending on the details of the welding procedure, the HAZ may have been exposed to sufficient heat to bring about phase transformations, recrystallization, grain growth, and precipitate coarsening that may result in embrittlement and/or a reduction in resistance to localized corrosion [Black, Kohser, and DeGarmo, 2008]. Furthermore, the heat from the weld allows chromium to migrate from within grains and precipitate as chromium carbides at the grain boundaries, leaving the region immediately adjacent to the grain boundary depleted in chromium. This process is called sensitization, and it depletes the steel of chromium available in the grains to provide a passive film, leaving the steel in the HAZ especially susceptible to intergranular attack.

Furthermore, the expansion and contraction experienced from the weld process along with local constraint creates high and variable residual stresses throughout the weld region. In most welding applications, these residual stresses would be relieved by a post-weld heat treatment (PWHT). However, these stresses are left untreated in used fuel storage canisters as applying a PWHT would also serve to increase sensitization and leave the canisters even more susceptible to corrosion. This combination of high residual stresses and susceptible material makes the HAZ the most susceptible area to stress corrosion cracking [Itzhak and Eliezer, 1983]. An image displaying the location of the HAZ as well as the regions within it can be seen in Figure 3.1.

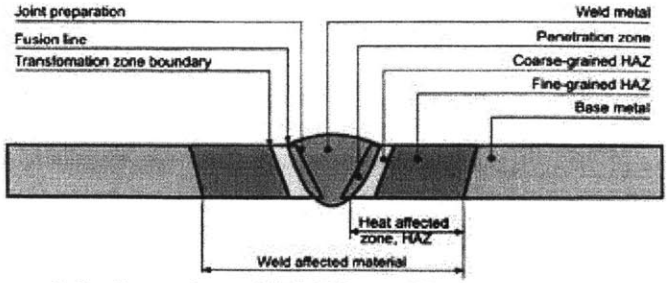

Figure 3.1 - Location of HAZ in weld zone [Weman, 2003]

A primary goal in the investigation of the effect of residual stress on canister material is to gather as much information as possible on the canister welds in order determine which welds in particular are of greatest interest to the failure of canister material by SCC. An interrelated goal is to understand and predict the residual stress distribution in the canister material, as well as to be able to compare past residual stress measurements of similar welds.

It will be shown that even the subtle details of the welding process are greatly influential on the resultant residual stress distribution, and therefore also in the identification of which welds and areas of the canister are of greatest interest. For this reason, it is prudent to investigate the various categories, classifications, and specifications of welds used in canister fabrication.

3.B. Weld Classification

3.B.1. Welding Process

There are a large number of welding processes, separated into categories such as arc welding, oxyfuel gas welding, resistance welding, and solid-state welding, to name a few. As will be discussed, the weld processes of greatest interest for used fuel storage canisters are submerged arc welding (SAW) and tungsten inert gas welding (TIG).

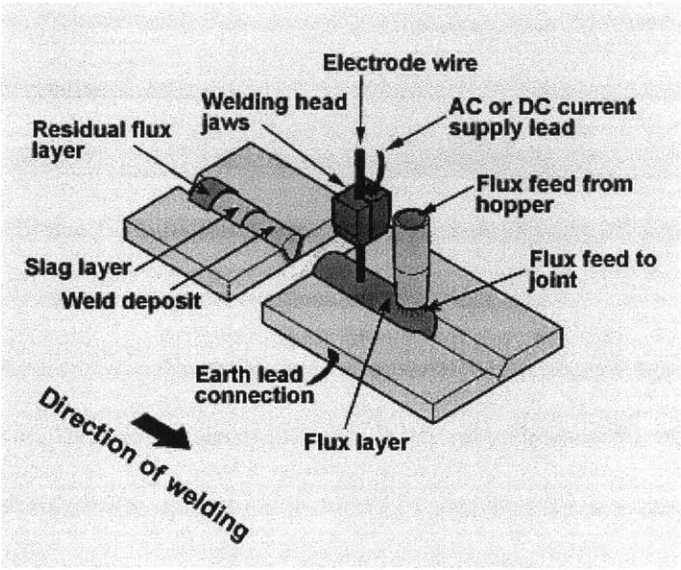

Figure 3.2 - Submerged Arc welding diagram [Submerged Arc Welding, 2003]

Submerged arc welding gets its name from the molten weld and arc zone being "submerged" by a granular fusible flux (a schematic of which can be seen above in Figure 3.2). This granular fusible flux consists of either lime, silica, manganese oxide, calcium fluoride, or other compounds, which becomes conductive when molten, providing a path for the current to pass between the electrode and the work piece. By covering the molten weld and arc zone, it protects the weld from atmospheric contamination, as well as covering the splatter, sparks, and fumes that are normally a part of shielded metal arc welding [Rainwater, 2008]. It uses a continuously fed consumable solid or tubular electrode with either AC or DC current, and is known for its ability to deposit large amounts of weld metal quickly and consistently. While traditionally submerged arc welding is process that must be performed on a flat surface, circumferential joints can be rotated under a fixed welding head to deposit a single pass or multiple passes [Submerged Arc Welding, 2003].

.

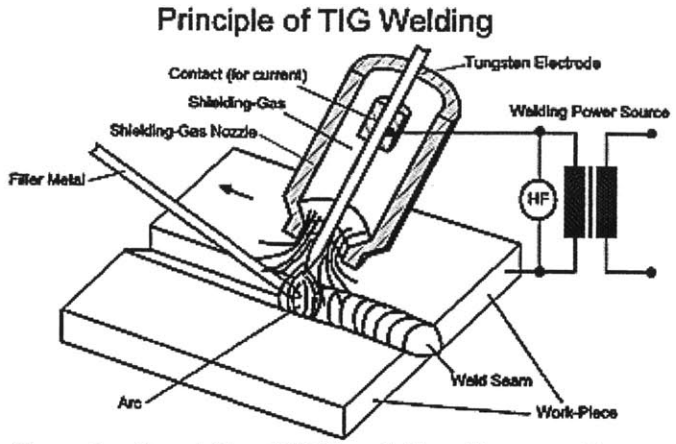

Figure 3.3- Tungsten Inert Gas (TIG) welding diagram [Azom.com, 2013]

Tungsten inert gas welding, also known as gas tungsten arc welding (GTAW) is also an arc welding process, but uses a non-consumable tungsten electrode to provide the arc, and an inert shielding gas such as argon or helium for protection from atmospheric contamination. A consumable filler rod provides weld metal. The operator has greater control over a TIG weld than in shielded metal arc welding, allowing for stronger and higher quality welds. It also has the benefit of leaving no slag behind, and can provide precise control of welding variables such as heat input. It is, however, a more difficult and slower welding technique. A schematic of the Tungsten inert gas welding process can be seen in Figure 3.3.

3.B.2. Weld Category (Location)

The American Society of Mechanical Engineers Boiler and Pressure Vessel Code (ASME B&PV) categorizes the locations of pressure vessel welds with the letters A-D, as shown in Figure 3.4 below. Before continuing further, it should be mentioned that some of the more widely followed codes and standards regulating used fuel storage systems, such as the ASME B&PV, are covered in Appendix C. As is described in further detail in Appendix C, the NRC accepts the use of ASME Code Section III, to the extent practical, for spent fuel storage systems.

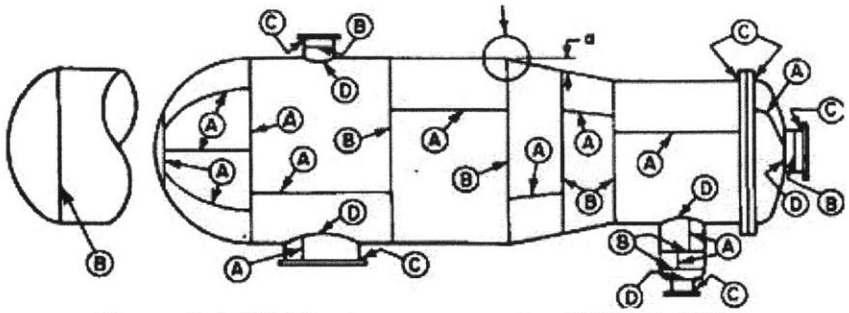

Figure 3.4- Weld category examples [ASME, 2007]

Figure 3.4 shows the ASME B&PV categories of welds. These categories correspond to the location of a weld on a pressure vessel. Category A includes all longitudinal (axial) welds in shells and nozzles. Category B includes all circumferential welds in shells and nozzles. Category C includes flange welds, tubesheet welds, and flat head welds. Category D includes nozzle attachment welds. As will be shown, welds on a typical canister shell include Categories A, B, and C. Category A and B welds are more commonly referred to as axial and circumferential welds respectively, and will be referred to as such for the remainder of this thesis.

3.B.3. Weld Type (Joint Geometry)

Weld type, also known as joint geometry, describes the geometry of the base metal and weld metal at a joint. A list of weld types can be seen below in Figure 3.5.

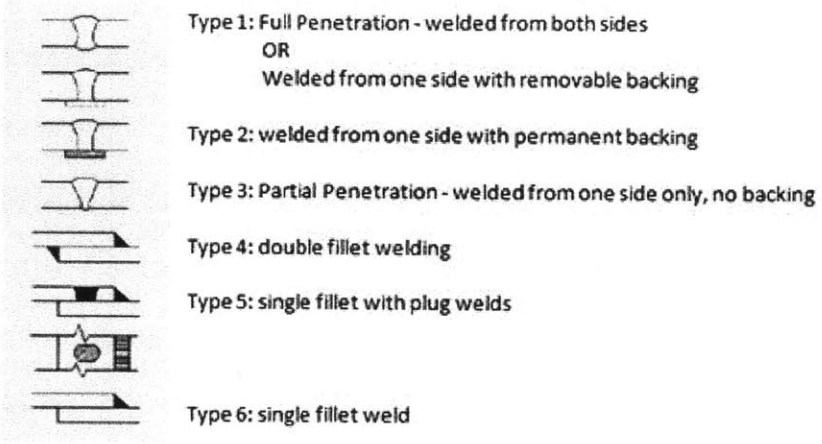

Figure 3.5 - Weld Types

The weld type is often dependent on the type of joint. A list of joints is can be seen in Figure 3.6. As will be covered in the residual stress section of this thesis, a difference between joints (particularly between a Single-V and Double-V joint) is very important in determining through-wall residual stress distributions. ASME Section III Subsection NB states that (with minor exceptions) Categories A, B and C weld joints shall be full penetration butt joints. Further information on this is provided in Appendix C.

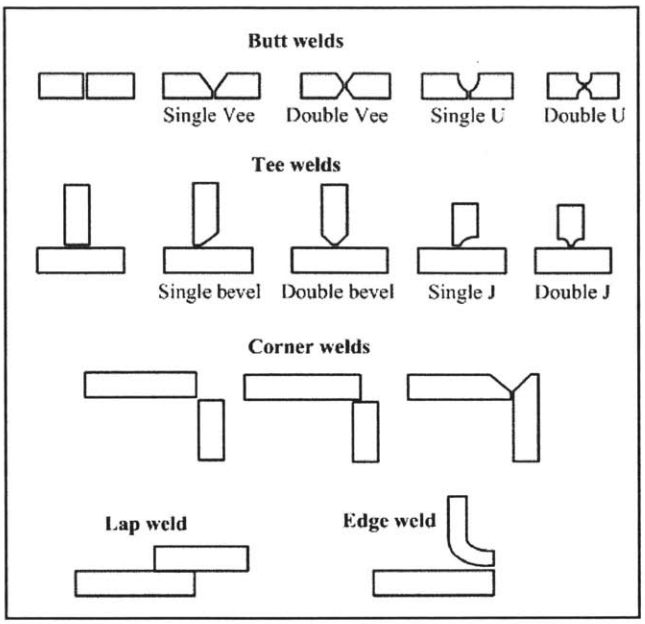

Figure 3.6 - Weld Joints [Kopeliovich, 2012]

3.B.4. Weld Treatment

After welding, a weld can be left in the as-welded condition, or have one of several treatments applied. These treatments include the previously discussed post-weld heat treatment often used to relieve stresses in welds (though these will not be discussed in detail here, as PWHT is not used in canister welds). Weld surface treatments, however, can be used on canister material. These may serve to smooth the surface of the as-welded piece, or manipulate the stress state. Examples of weld treatments include grinding the surface of a weld flush with the base material, burr grinding, TIG dressing, shot peening, and low plasticity burnishing. Several of these treatment possibilities are illustrated in Figure 3.7.

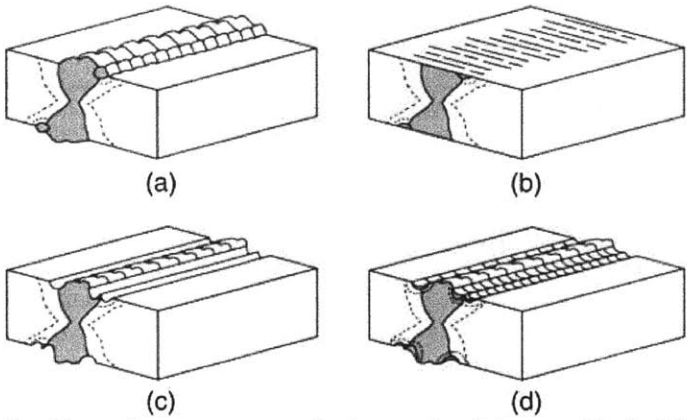

Figure 3.7- Weld details and treatment techniques for (a) as welded, (b) ground flush, (c) burr ground, and (d) TIG dressed. Dark area is the weld, area within the dashed lines is the HAZ [Weigand and Berman, 2012]

After communications with one major vendor and the fabricator for another major vendor, it was learned that the most common treatment applied to canister welds is surface grinding. Canisters typically have their welds ground flush in order to remove stress concentrators from the surface as well as to smooth the surface of the canister for insertion into the overpack.

3.C. Used Fuel Storage Canister Welds

The process of investigating and predicting the residual stress state of canister welds is made much more difficult by the fact that so little information on the welding of used fuel storage canisters is publicly available. The details of each canister's welds are contained within the Welding Procedure Specifications, or WPS, written by the canister's vendor or fabricator and kept as proprietary information. Further complicating this is the fact that each vendor can hire several different fabricators for a single canister design, and each fabricator (while obligated to adhere to ASME BPVC Sections III and IX as well as AWS Standards D1.1 and D1.6) can choose their procedure as long as the resulting properties conform to the appropriate codes and standards. Often, some of the weld parameters in question are not recorded during fabrication, or

even measured. As a result, no specific record exists of many of the weld factors in question. Useful canister weld specifics are therefore extremely difficult to come by. What little information that is publicly available as well as what was learned from canister vendors and fabricators that may and be divulged publicly is included below.

One of the more detailed sources available on used fuel canister welds is *A Pilot Probabilistic Risk Assessment of a Dry Cask Storage System* [NRC, 2007], which uses the Holtec HI-STORM 100 as its example. This document describes the Holtec MPC as an austenitic stainless steel cylindrical shell, constructed with one circumferential and four axial seam welds. The two axial welds on each side of the MPC are slightly offset at the circumferential weld, as shown below in Figure 3.8 (the weld locations are also represented on a three-dimensional diagram of a Holtec HI-STORM 100 in Figure 3.9). The shell is next welded to a 6.35cm (2.5in) thick baseplate. These welds are all full-penetration, submerged arc welds. After welding, they undergo dye penetrant (PT) and radiographic examinations but are not given a post-weld heat treatment. Once the canister is loaded with used fuel, the lid is welded to the shell. This weld is 1.90cm (0.75in) thick, and undergoes PT examinations. A redundant lid seal is created by placing a closure ring on the MPC lid and welding to the shell and lid, as shown at the top of Figure 3.8. Vent and drain ports (used for draining the canister of water, hydrostatic testing, and then filling the canister with helium) are closed with welded cover plates. The vent and drain cover plate welds as well as the lid's outer ring welds are TIG rather than SAW welds.

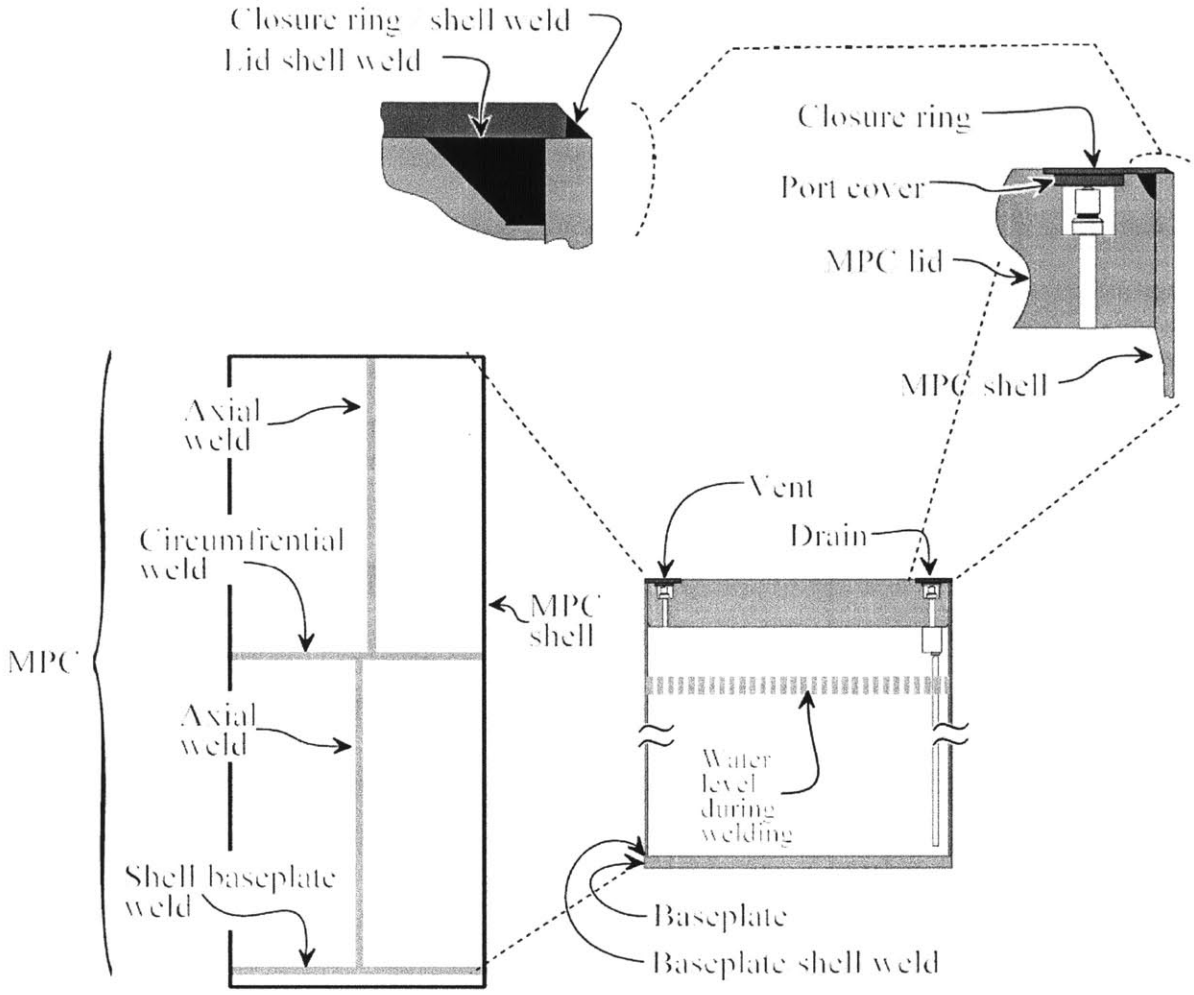

Figure 3.8- Weld locations on a Holtec HI-STORM 100 MPC (see Figure 3.9 for a clearer representation of the welds) [NRC, 2007]

The report indicates that the NRC did not consider the MPC lid welds in the MPC failure assessments for their dry cask storage system Probabilistic Risk Assessment (PRA) for the following reasons:

1. "The TIG process used on the lid produces is expected to produce [sic] a much tougher weld than the submerged arc (SA) weld used in the shell of the MPC."
2. "The redundancy of the lid design requires at least two welds to fail in order to compromise MPC confinement."

3. "The applied stresses at these locations are less than the stresses in the MPC shell for all events analyzed."

The failure mechanisms considered in [NRC, 2007] for the MPC under mechanical and thermal loads included weld fracture, creep rupture, and an exceeded load limit. As for corrosion, the report briefly indicates that the MPC is made entirely from austenitic stainless steel types 304, 316, 304L, or 316L, and that because these grades are corrosion resistant in high-humidity and industrial environments, that coastal and industrial atmospheres should have no effect on the confinement ability of the MPC. It should be noted that this report, completed in June of 2006, was written at a time when the completion of a long-term repository for used fuel appeared imminent, and that the expectation was that used fuel storage canisters would have to endure environmental corrosion for a much shorter period than is currently expected.

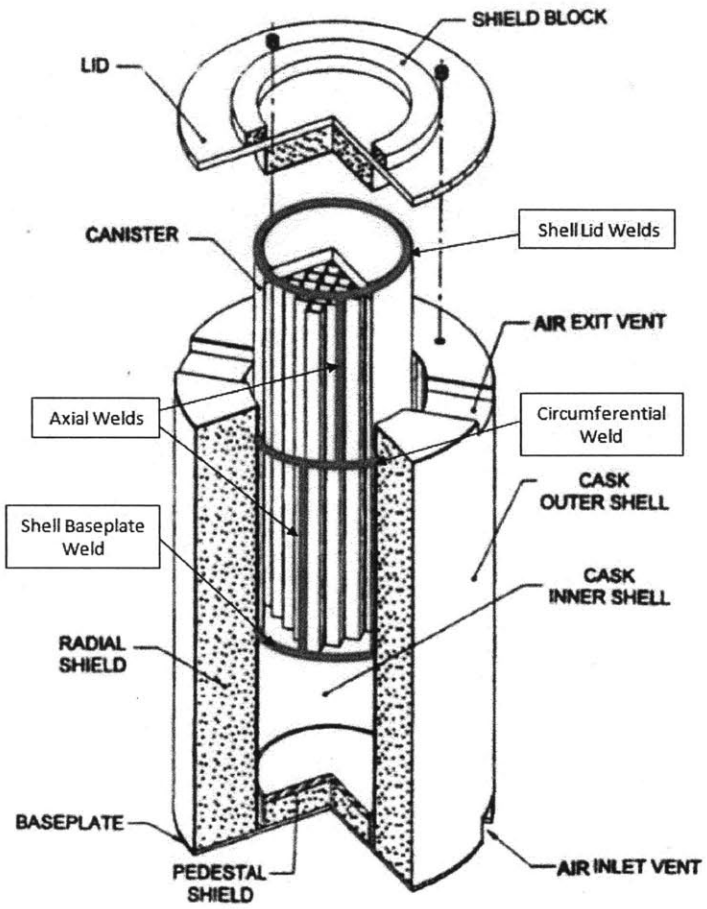

Figure 3.9 - Weld Locations on One Side of a Holtec MPC within a HI-STORM 100 overpack

A document from Japan's CRIEPI (Central Research Institute of Electric Power Industry), also makes reference to redundant lids being the typical design in used fuel canisters (as shown in Figure 3.10), though no mention is made of any canister designs in particular [Saegusa et al., 2008].

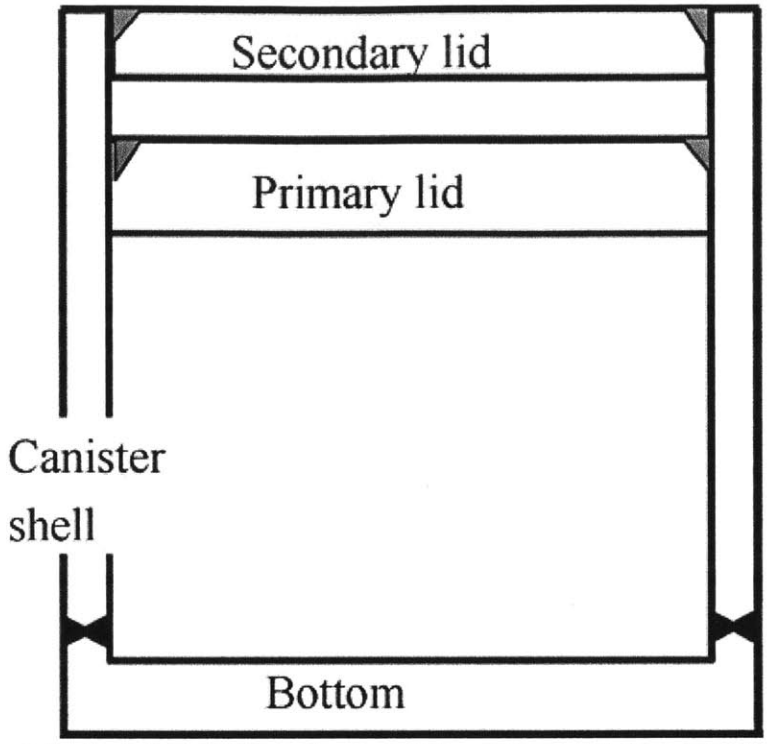

Figure 3.10 - Used fuel canister with redundant lid welds and full penetration canister shell welds [Saegusa et al., 2008].

These few sources, along with conversations with those from the Electric Power Research Institute (EPRI), the NRC, vendors, and fabricators have indicated that the weld configuration specified in [NRC, 2007] is typical of thin-walled canister-based dry storage systems for each of the major three vendors, with the only major difference being the number of axial welds. Also in these conversations, including conference calls with the EPRI Extended Storage Collaboration Program (ESCP), it was decided for the aforementioned reasons that the welds of greatest concern for SCC vulnerability were the axial and circumferential shell welds. These welds, if breached, would compromise the integrity of the canister allowing for potential release of radioactive material to the environment.

Another area of the canister under consideration is where the fuel assembly baskets are welded to the inner surface. In conversations with a prominent canister vendor's fabricator, it

was learned that these welds are often TIG, and there was a discussion as to whether the HAZ from these welds would reach and adversely affect the outer surface of the canister. However, it was decided that for the time being, experimentation will focus on the circumferential and axial shell welds.

4. Residual Stress

Tensile stress is one of the three requirements for a material to fail by stress corrosion cracking. This stress can be either applied or residual, so long as it exceeds a minimum threshold of tensile stress for a given material and environment.

The only significant applied stress on a used fuel canister comes from internal canister pressure. There is an initial pressure from the backfilled helium in a newly filled canister, though the reduction of canister temperature over time will serve to decrease this pressure [Rigby, 2010].

However, other time-dependent variables such as the amount of water vapor within the canister and gaseous radioactive decay products (assuming cladding failure) can increase or decrease canister pressure depending on the circumstances. One worst case calculation, which assumed only circumstances that increase pressure, yielded internal pressures that peaked at 0.35MPa [ASTM, 2008]. For a 177.8cm (70in) diameter canister with 1.27cm (0.5in) thickness (therefore qualifying as a thin walled pressure vessel), this results in a hoop stress of approximately 50MPa and an axial stress of approximately 25MPa. While this stress is not insignificant, the literature review of residual stress distributions in Section 4.C. shows that that the difference in residual stress readings at a given point can vary by up to 50MPa between measurement techniques (see Figure 4.12 for example). Therefore, the worst case scenario for canister applied stress is within the margin of error for measuring canister residual stresses.

Rather than applied stress, residual stress is likely to be the primary contributor of tensile stress in used fuel storage canisters. In fact, it will be shown that effect residual stress can be so great, that even subtle differences in a residual stress distribution can have a major impact on the life prediction of used fuel storage canister material.

A previous study of SCC in austenitic stainless steels for dry cask storage utilized U-bend specimens [Mintz et al., 2012]. These tests, while useful in their own right, purposefully induced tensile stresses in order to force SCC, but failed to accurately represent the stress distribution throughout the HAZ of a real canister weld. Having an accurate characterization of the residual stress distribution throughout the material is vital for an accurate assessment of expected canister life. The reason, as will be discussed in greater detail in Section 5, is that once initiated, a crack relies on tensile stress to drive it through the thickness of a material. If the residual stress begins on the outer surface as highly tensile, but further into the material's thickness it becomes less tensile or even compressive, it is possible that crack arrest may occur. It is therefore of great importance that the stress distribution through the canister wall's thickness be known, as well as the uncertainty in this distribution, in order to model crack initiation and propagation including uncertainty.

As mentioned previously, welded canister mock-ups are being fabricated in order to take high-resolution residual stress measurements of authentic canister material. In the meantime, it is useful to study the factors affecting residual stress in welded stainless steels, as well as to compile a literature review of published residual stress measurements on similar welded stainless steel samples. This will serve to build a foundation for interpreting future residual stress measurements, allow one to make a preliminary prediction of the time necessary for SCC to propagate through a canister wall, as well as to provide a starting point in the search for solutions

to problem of canister residual stress, should our measurements prove that one is necessary to extend used fuel canister lifetime.

4.A. Factors Contributing to Residual Stress

As was discussed in Section 3 of this thesis, the canister welds are of greatest interest for SCC because the sensitized HAZ and with its untreated residual stresses form the most susceptible area for crack initiation and propagation. It should be noted that while sensitization plays a role in crack initiation, it does not play a major role in crack propagation, given that the growth of chloride-induced stress corrosion cracks in austenitic stainless steel is transgranular [Jones, 1996]. It should also be mentioned that while the HAZ is the most likely location for failure by SCC, it is entirely possible for SCC to occur in areas away from the canister welds. As for the welds themselves, there exists a significant amount of delta ferrite in the weld deposits which reduces susceptibility to cracking, making the weld metal an unlikely location for failure by SCC to occur [Davis, 2006]. With this in mind, the HAZ of canister welds will be the focus here.

Because discussing the axial and hoop stresses of both circumferential and axial canister welds (see Figure 3.9) can be disorienting, we will additionally rely upon the coordinate system defined in Figure 4.1 below. In Figure 4.1, both circumferential and axial welds are simplified to a single straight weld in a plate. Because of the large ratio of diameter to thickness in used fuel storage canisters, this is a reasonable approximation for both weld categories. The direction parallel to any given weld in question will be x, the direction perpendicular to the weld but parallel with the surface will be y, and the direction perpendicular to the surface (into the material thickness) will be z, as is shown below. Therefore, stresses oriented parallel to the direction of the weld will be signified σ_x, which will represent the axial stresses in axial welds

and hoop stresses in circumferential welds. σ_y will represent stresses oriented perpendicular to the direction of welding but parallel to the surface (hoop stresses in axial welds and axial stresses in circumferential welds). No σ_z will be discussed, because it will be assumed for this application that the stresses in the z direction are negligible in both magnitude and effect on crack propagation relative to those in the x and y directions.

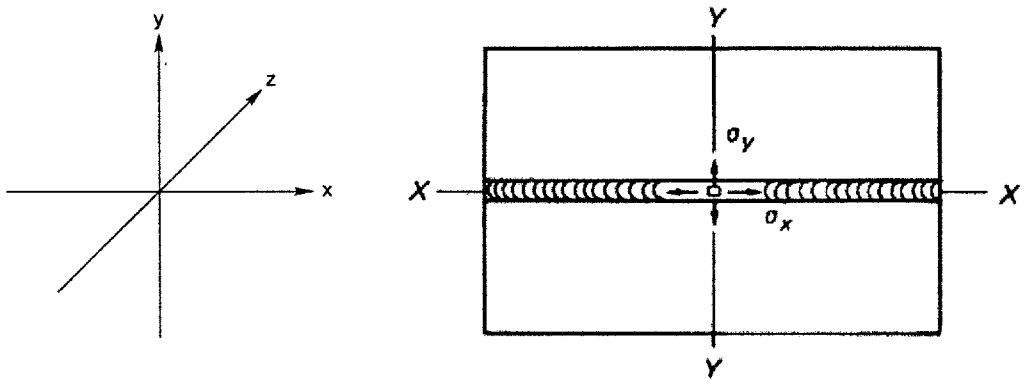

Figure 4.1 – Residual Stress Coordinate System [Masubuchi, 2011]

There are many factors which influence the residual stress distributions found in welded stainless steels. A list summarizing some of the most influential factors can be seen in Table 4.1. Many of these factors are variables of the welding process, described in greater detail in Section 3.

Table 4.1 - Factors Contributing to the Residual Stress within Welded Stainless Steels

Factor	Description
Sample Thickness	Thicker welds result in stresses of greater magnitude
Sample Diameter	Samples with greater diameter behave more like flat plates and less like pipes
Sample Restraint	Can affect how the material responds to the expansion and contraction of the welding process
Steel Type / Mechanical Properties	Aside from influencing how the material responds to compression/expansion, mechanical properties can vary throughout the HAZ, making it difficult to model accurately with finite element analysis
Weld Type (joint geometry)	The through-wall residual stress distributions of Double-V vs. Single-V welds differ greatly from one another
Weld Category (location)	Axial stresses are generally greater than hoop stresses in axial welds, and hoop stresses are generally greater than axial stress in circumferential welds ($\lvert\sigma_x\rvert > \lvert\sigma_y\rvert$)
Weld Sequence	Starting and ending positions of a weld have much more varied residual stresses than other positions
Weld surface treatment	Depending on the treatment, can have a wide range of effects, often difficult to quantify
Other WPS variables	Miscellaneous welding variables contained within a WPS such as preheat temperature, interpass temperature, and number of passes all play a role
Base metal history	Preparation of the base material can leave residual stresses behind that are often ignored

One of the most influential factors is geometry. From Table A.3 of Appendix A, we see that thin-walled canisters have a thickness between 1.27cm and 1.59cm (1/2in and 5/8in), an outer diameter between 152.4cm and 177.8cm (60in and 70in), and a height most typically between 406.4cm and 508.0cm (160in and 200in). The thickness of a weld, and therefore the volume of the weld, is hugely influential on residual stress. A thicker weld will have the effects of expansion and contraction magnified by the greater volume of weld metal, often resulting in a greater magnitude of residual stress, either tensile or compressive. The diameter of a pipe or

canister matters as well: locally, large diameter pipe welds are more geometrically similar to flat plate welds than to small diameter pipe welds. Sample geometry often determines restraint as well. Whereas a flat, unrestrained plate is free to expand or contract in all directions, the edges of the plates used to make a cylinder are welded to one another, restricting the amount of expansion/contraction allowed in the hoop orientation. This is a form of global constraint, whereas the welding process itself is a form of local restraint, producing local stresses in the vicinity of the weld. Global restraint, however, is a restraint of the entire system that results in a uniform stress in addition to local stresses. In this regard, the order that these welds are completed is very important: because the lidless cylindrical shell is most often constructed before a baseplate is welded on, there is much greater restriction for expansion/contraction in the hoop direction. This global restraint can result in a baseline hoop tensile stress experienced throughout the material, in addition to any local stresses. The geometry of this arrangement and constraint can be seen below in Figure 4.2.

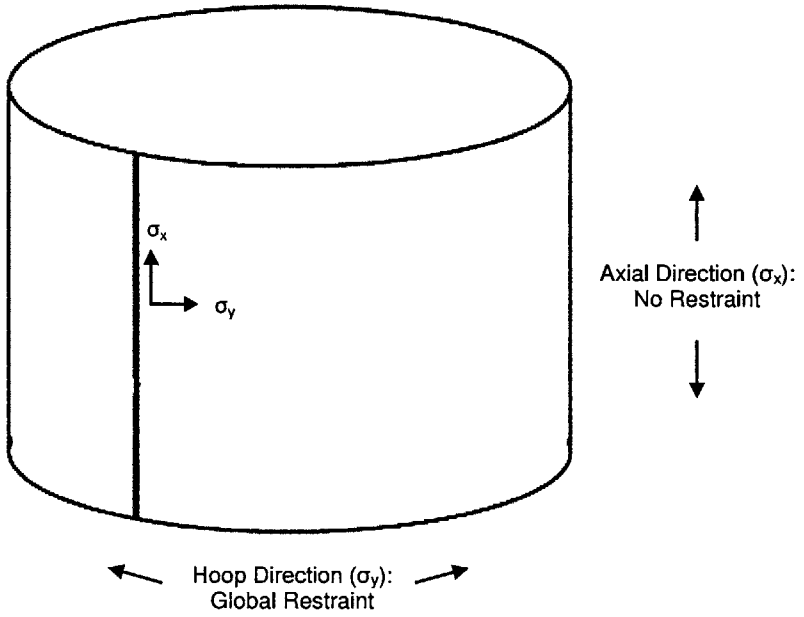

Figure 4.2 - Global Restraint in the hoop direction (in this case σ_y) of a welded hollow shell, with the axial direction (σ_x) unrestrained, representative of the initial stages of canister fabrication

The type of steel and its mechanical properties such as yield strength, ultimate strength, and fracture toughness can influence how a sample responds to welding. In general, a more ductile steel that work hardens less will have lower residual stresses when welded than a less ductile steel that work hardens more. However, steels with higher yield strengths can often support higher residual stresses. Distribution of microstructure is also of great importance. When steel is welded, the area of the HAZ closest to the weld can experience phase transformation in complex and difficult-to-predict patterns. This can complicate the residual stress distribution in this region, as this microstructural transformation can be accompanied by grain growth and changes in yield strength as a result of work hardening, all of which can be extremely difficult to model accurately.

As will be shown in this section, particularly in the work of Deng, Murakawa, and Liang, the yield strength of the base and weld metal can have a significant impact on through-wall

residual stress. The cyclic thermal loads of welding can plastically deform the material, work hardening it, and thus increasing yield strength and decreasing ductility [Deng, Murakawa, and Liang, 2008]. This localized strengthening can also be due to changes in microstructural distribution as well as the Hall-Petch grain size effect [Boyce, Reu, and Robino, 2006]. It has been shown that in thicker, austenitic multi-pass welds that the cooling of subsequent passes results in significant increases in yield strength with great variation throughout the weld deposit [Brooks and Lippold, 1996].

Weld type (joint geometry) plays a significant role in the distribution of stress through the thickness of a material. A Single-V weld (a type of partial-penetration weld), with the majority of weld metal on one side of the thickness, will have the majority of the expansion and contraction from the weld metal on that side of the thickness as well, and will therefore be likely to experience greater tensile stress on the side with more weld metal. Conversely, a Double-V weld (a type of full-penetration weld) will have large concentrations of weld metal on both sides of the thickness, and is therefore likely to have localized maxima in tensile stress near both the inner and outer surfaces, with a localized minimum of tensile stress (possibly compressive stress) in the center.

Weld location matters as well. A baseplate weld will obviously vary from the circumferential and axial weld, but axial and circumferential welds will vary from one another as well. Both welds will see greater tensile stress in the σ_x orientation than σ_y: an axial weld would experience the majority of its contraction in the axial direction, and is therefore more likely to see the greatest tensile stresses in the axial direction. Likewise, a circumferential weld will experience the majority of its contraction around the circumference of the cylinder, and is therefore most likely to see the greatest tensile stresses in the hoop direction. Essentially, the

greatest tensile stresses are most often seen in parallel orientation to the weld (σ_x). This is supported by the results of [Ogawa et al., 2008], [Deng, Murakawa, and Liang, 2008], [Dong, Zhang, and Rawls, 2003], and [George, Smith, and Bouchard, 2000].

As will be shown in greater detail in [Teng, Chang, and Tseng, 2003] the weld sequence plays a role in the residual stress. Locations where the welding process begin and end have noticeably different residual stress profiles than do intermediate locations along the weld.

Surface treatments have the potential to greatly affect residual stress. The effect can be one of increasing tensile or compressive stress depending on the type of treatment. Surface grinding has been shown to produce levels of surface compression nearly identical to that of shot peening [Prevey, 1996]. In one study in which grinding was performed on a variety of steel specimens, both austenitic (Faced Centered Cubic or FCC crystal structure) and ferritc (Body Centered Cubic or BCC crystal structure), X-ray Diffraction (XRD) measurements showed that compressive stresses were present on the surface, with both normal and shear stresses decreasing absolutely with increasing depth [Hauk, Oudelhoven, and Vaessen, 1982]. It has also been suggested with limited experiments on T-shaped specimens under cyclic bending deformation that burr grinding may extended crack initiation life of materials subjected to low cycle fatigue, though it was concluded that more data is needed [Tateishi, Hanji, and Hanibuchi, 2009]. In yet another investigation, it was shown with XRD that a ground SAE 1045 steel sample experienced greatly compressive residual stresses on the surface, as is shown below in Figure 4.3 [Iancu et al., 1990]. In addition to this, grinding can reduce stress concentration effects. However, there is not a consensus that surface grinding results in compressive stresses in all circumstances. Some sources claim that grinding can leave tensile residual stress due to the heat produced during the process [Cheng et al., 2003].

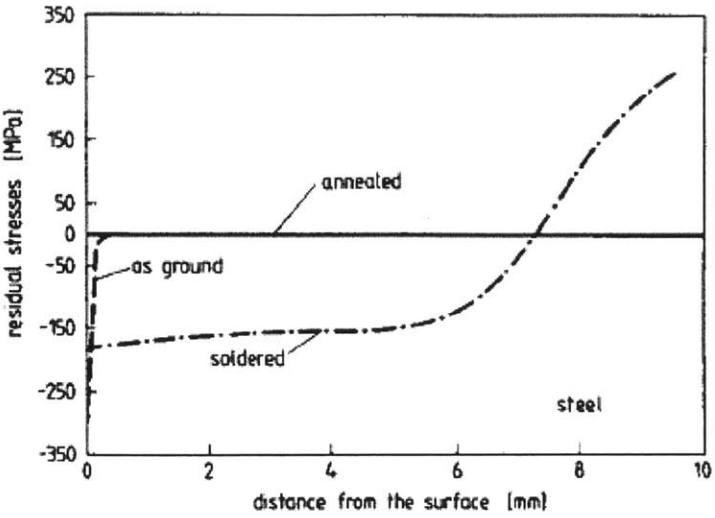

Figure 4.3 - Effect of grinding on residual stress of SAE 1045 carbon steel (note the "as ground" line) [Iancu et al., 1990]

Because of the range of complex effects that heat input can have on the residual stress state of a weld, the welding process specifications are very important to the residual stress profile. Several of these factors have already been discussed, such as welding process, joint design, weld sequence, and surface treatment. Other factors such as interpass temperature (the temperature that the weld must cool to before another pass can be completed), welding current, and weld speed are highly influential in determining the thermal transient that the base metal is subjected to, and are therefore also highly influential in determining the resultant residual stress state.

Taking all of these factors into consideration may still be insufficient to predict the residual stress state of a material. For instance, often ignored from residual stress assessments is a material's history, assuming that before welding and fabrication that it is free of stress. On the contrary, these materials have likely already endured a number of mechanical processes that have left a footprint of residual stresses behind. For instance, the steel plate used to make the cylindrical shell of used fuels storage canisters is rolled flat, which typically results in tensile

stresses near the plate edges and compressive stress in the interior. The plate is then cut into the proper dimensions, which alters the original residual stress state, as well as inducing new additional residual stresses near the cut edge, particularly in cases of thermal cutting [Dong and Brust, 2000]. Next, the plate is rolled into a cylinder, which is likely to leave the outer surface in tension and the inner surface in compression. After welding, the shell is often straightened, adjusted, or rolled once more to ensure a round shape. Depending on the specifics of this process, additional stresses, compressive and tensile, can be induced. The steel plate's processing history must also be considered for a complete picture of the residual stress state in used fuel canister material.

4.B. Residual Stress Measurement Techniques

There are a large number of techniques for measuring residual stress. Some are destructive (techniques which alter or destroy the sample from the material being analyzed) and some are non-destructive. In addition to these measurement techniques, there are finite element models, which seek to construct a computerized model of a component in order to predict the expected residual stresses based on thermal and mechanical simulation. This section will focus on several of the more complex and/or commonly used techniques, which are identified in the literature review of Section 4.C., as well as in the planned measurements identified in Section 7. Figure 4.4 plots the depth of penetration (the depth 'z' into the weld from the surface) vs. spatial resolution for several common residual stress measurement techniques.

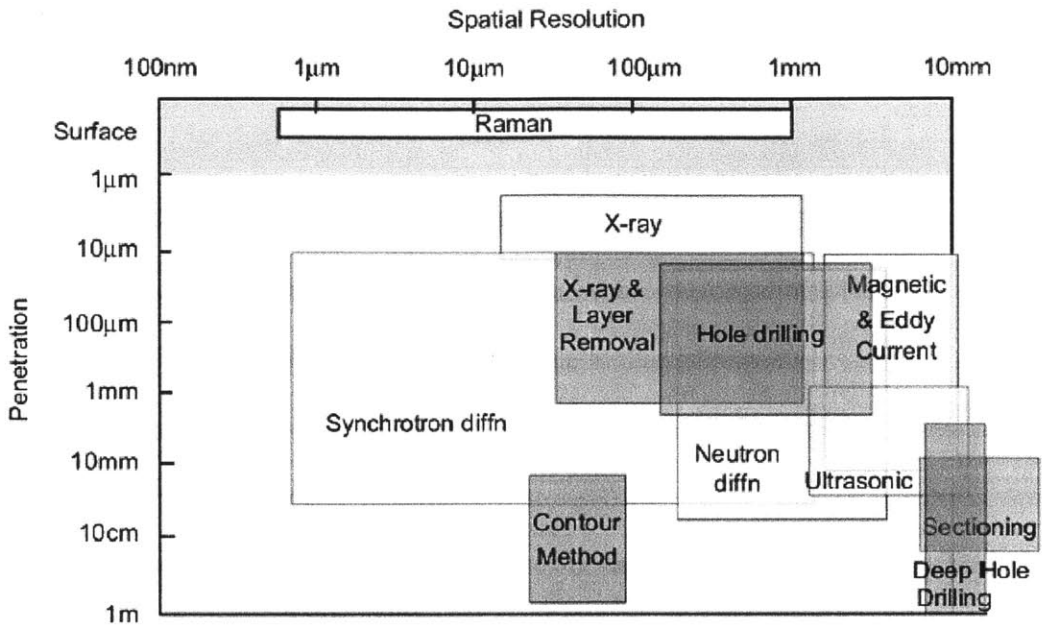

Figure 4.4 - Residual stress measurement techniques by spatial resolution and depth of penetration, with destructive techniques shaded in grey [Withers et al., 2008]

Although these techniques are referred to here as stress measurements, it should be noted that because stress is an extrinsic property, it cannot be externally measured. Instead, some intrinsic property (normally strain or some form of displacement) must be measured in order to calculate the associated stress. Strain gauges, for instance, measure the strain at a position of a material under stress. This directly observable data can then be used to calculate the stress present. Each measurement technique below takes a different approach to measuring intrinsic properties, such as strain, to derive the associated stress from their measurements.

4.B.1. X-Ray Diffraction (XRD)

X-Ray Diffraction (XRD) is a method of residual stress measurement that uses x-rays to measure surface strain at the atomic level, and from it calculates the residual stress. It is one of the most commonly used methods of surface residual stress measurement, offering a high-resolution, close to 10μm in certain applications [Withers et al., 2008].

Diffraction occurs when a set of plane waves encounter a plane of regularly spaced particles whose spacing is of comparable magnitude to the waves' wavelength. In the case of XRD, the waves are x-rays, and the plane of particles is the polished surface of a material, with atoms arranged in a regularly spaced lattice. When waves interact with two different planes of atoms, the set of waves that reflect off deeper plane travels further than the waves that reflect off the top plane, and as a result the reflected beam experiences interference, constructive or destructive, from the phase-shifted waves. When the incident x-rays are angled properly with the sample, the result is constructive interference. From the angle θ that results in constructive interference, Bragg's law can be applied to determine the spacing between the planes [Callister, 2007].

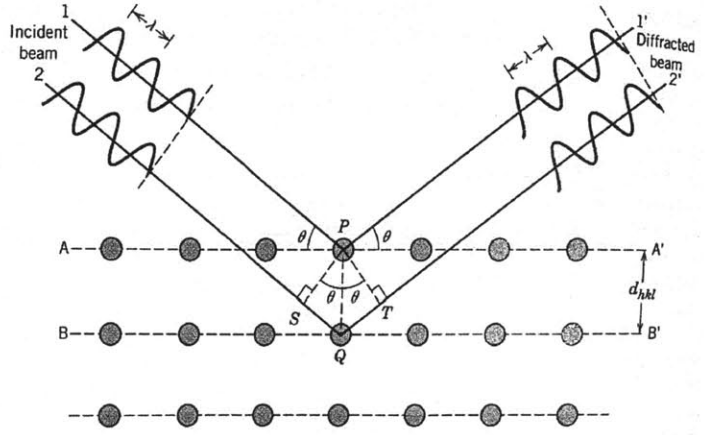

Figure 4.5 - Diffraction of X-rays by planes of atoms [Callister, 2007]

Bragg's Law:

$$n\lambda = d_{hkl}sin\theta + d_{hkl}sin\theta = 2d_{hkl}sin\theta \quad (1)$$

$$d_{hkl} = \frac{a}{\sqrt{h^2+k^2+l^2}} * \quad (2)$$

*For cubic crystals only (Austenite is FCC and Ferrite is BCC, both cubic)

a = lattice parameter (unit cell edge length)

λ = x-ray wavelength

θ = diffraction angle

d = lattice spacing of crystal planes

hkl = Miller indices, specifying the orientations of planes for a crystal structure. They are used in all crystallographic planes other than hexagonal crystal systems [Callister, 2007]

A tensile stress in the horizontal direction of the sample in Figure 4.5 would result in a Poisson's ratio contraction, decreasing the distance 'd' between planes. This change in the lattice spacing changes the angle at which the waves constructively interfere, also known as the diffraction peak. By measuring the change in the angular position of the diffraction peak for at least two orientations of the sample, the stress at that position can be calculated [Prevey, 1986].

While x-ray diffraction has many benefits as a residual stress measurement technique, it does have several significant drawbacks. In addition to it being somewhat expensive, and only working with polycrystalline samples of fine grain size, its major drawback is that it can only measure the residual stresses on the surface. Only a layer less than roughly 25μm (0.001in) from the surface is measured [Prevey, 1986]. For measurements at multiple depths, material must be physically removed, which depending on the process can alter the residual stress state being measured. This is most often accomplished with electropolishing, the "only viable means of removing material without inducing residual stresses" [Lambda Technologies, 2012]. Electropolishing is more of a precision material removal technique, and is better suited to minor removal of material (its depths can be measured to a precision of 2μm). Because it is not suited to penetrate deeply into the depths of a material, other techniques for reaching greater depths are employed, which can alter the stress state. For this reason, other techniques are used for

measuring residual stresses into the depth of a material. However, XRD remains one of the most frequently used and reliable techniques for measuring near-surface residual stresses.

4.B.2. Deep Hole Drilling

Deep Hole Drilling, or DHD, is one of the more common techniques used to measure residual stress in steels of relatively large thickness. DHD is based around the idea of drilling a hole through a sample, and measuring the diameter of the hole at various depths to determine whether the hole widened or shrunk when the material around the hole is removed. It is a practical means of measuring residual stresses up to 0.7-1.0m deep in steels, whereas nondestructive measurements, such as neutron diffraction, are limited in depth of penetration, cost, and availability [Kingston, 2004].

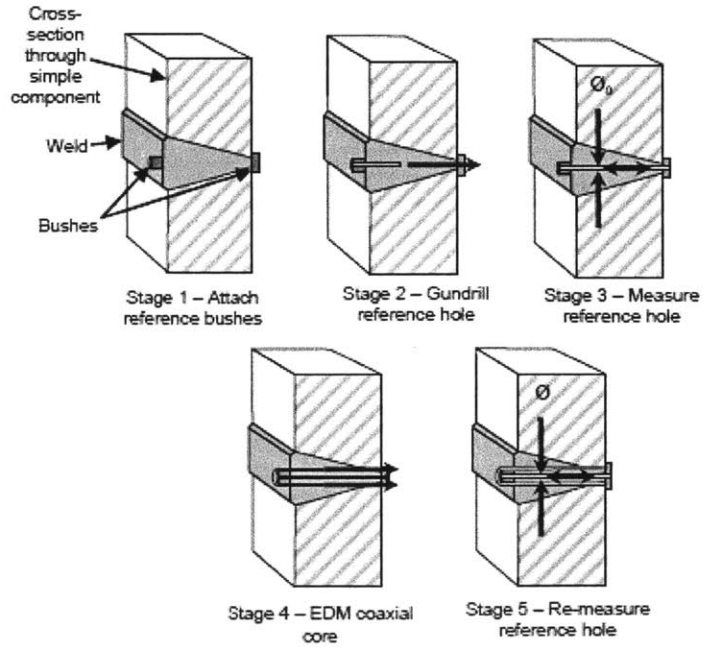

Figure 4.6 - Five steps of the Deep Hole Drilling procedure [Ogawa et al., 2008]

The DHD procedure can be broken down into five steps, shown in Figure 4.6 above. First, "reference bushes" (more commonly referred to as "drill bushings") are glued to either side of the specimen, and serve as guides for the drilling shaft. Next, a reference hole is drilled through the bushes and through the sample piece. This hole is typically 1.5mm – 3mm in diameter and can be drilled in a number of ways, with gun-drilling being the most commonly used method [Mahmoudi et al., 2009]. Next, the diameter of the reference hole is carefully measured using an air probe. The diameter is measured at many angular positions (often every 22.5°) and at many depth levels (often every 0.2mm) [Ogawa et al., 2008]. This set of measurements represents the diameter when stresses are present. To relieve these stresses, a cylinder (or core) of material surrounding the reference hole is removed from the larger sample. Typically 5mm beyond the diameter of the reference hole, a cut is made using wire EDM (Electrical Discharge Machining, which is discussed in greater detail in the following section). Once the reference hole and surrounding material are removed from the sample, the reference hole diameter is re-measured, through the entire thickness including the reference bushes. It is assumed that after core removal by EDM that no stresses remain in the reference hole. The difference between the measured diameters before and after the core was removed with EDM is therefore assumed to be representative of the original stresses, which allows these original stresses to be calculated. Ogawa et al. reported that for steel, the nominal accuracy of DHD is about ±30MPa.

There are several drawbacks to DHD. It is best used for measuring residual stresses in materials of moderate thickness, and is not recommended for use in components of less than 10mm thickness [VEQTER, 2013] (however, considering that the typical canister wall thickness is between 12.7mm-15.9mm, DHD is marginally applicable for canister residual stress

measurement). Further, the method is semi-invasive, which leaves the material being measured with a hole that will need filling, or requires a mock-up to be made if drilling the actual component of interest is not an option.

4.B.3. Contour Method

The contour method of residual stress measurement is one of the newer methods available for measuring residual stress [Pagliaro, 2008]. It is a destructive technique that sections the material in the area of interest, perpendicular to the stress orientation of interest, leaving the cut face free to release its stress and deform from a flat face to a contour that is a measure of the 2D strain field. The contoured surface is measured and modeled, and the stresses that would be necessary to force the contoured surface back to its original flat shape are then calculated. These calculated stresses are equivalent to the pre-cut stresses that created the contour. The contour method is illustrated in Figure 4.7.

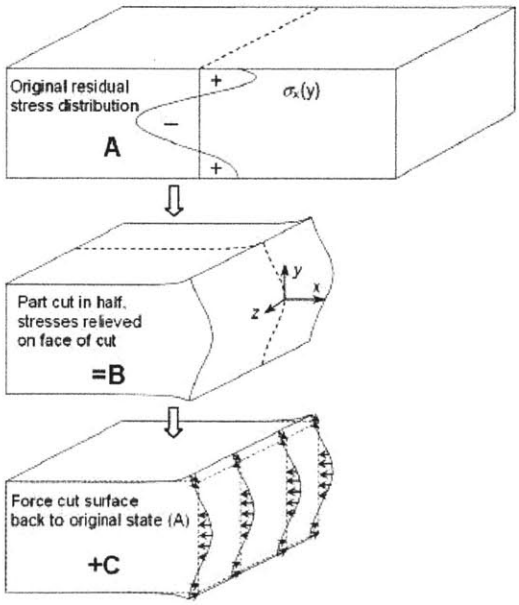

Figure 4.7 - Three steps of the Contour Method of Residual Stress Measurement [Pagliaro, 2008]

The contour method can be broken down into the following steps:

1. **Make the Cut.** Because the subtleties of the cut surface are so important, the cut must be as clean as possible. For this reason, wire EDM is most often used to cut the samples. Wire EDM uses an electrically charged wire to vaporize the immediately surrounding material and is "stress free" [Prime, 2001]. During this process the wire slices through the material, without ever actually making contact with it. If executed properly, the process induces virtually no parasitic stresses to the material.

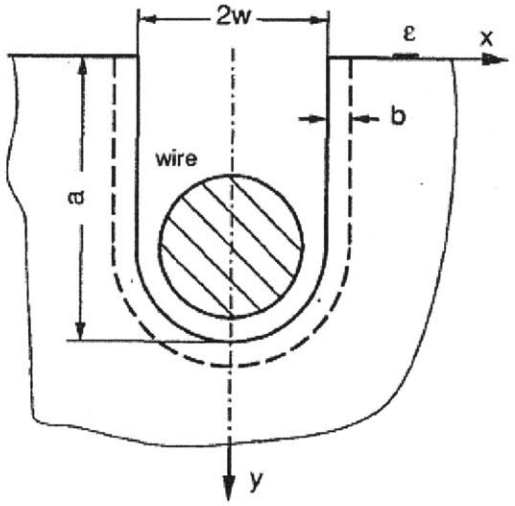

Figure 4.8 - Wire EDM making a cut through a material with a depth of 'a' and width of '2w' [Cheng et al., 1994]

2. **Measure the Material.** After cutting the piece, the residual stresses in the material are free to relax at the cut surface by expanding or contracting. To measure this resultant contour, a device called a Contour Measuring Machine is utilized. A Contour Measuring Machine (CMM) is the simplest and most widely available means of measuring the contour of the newly cut surface. A CMM utilizes a touch trigger probe in a precision x,y coordinate system, in order to measure the curvature of the surface and map it in three dimensions (see Figures 4.9 and 4.10). CMMs are generally precise to within several micrometers [LANL, 2012].

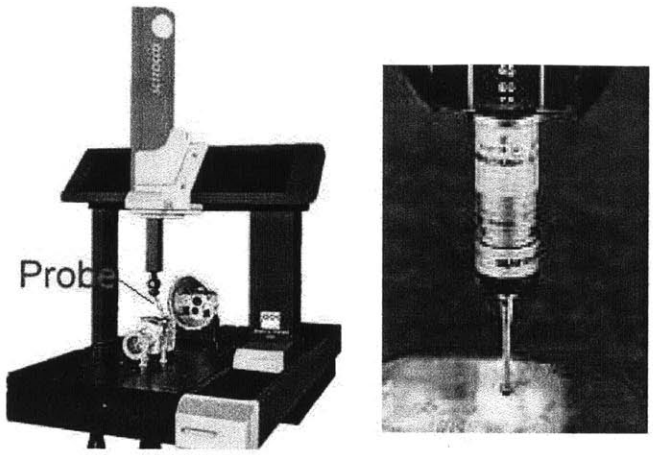

Figure 4.9 – Contour Measurement Machine (CMM) with probe tip for measuring [LANL, 2012]

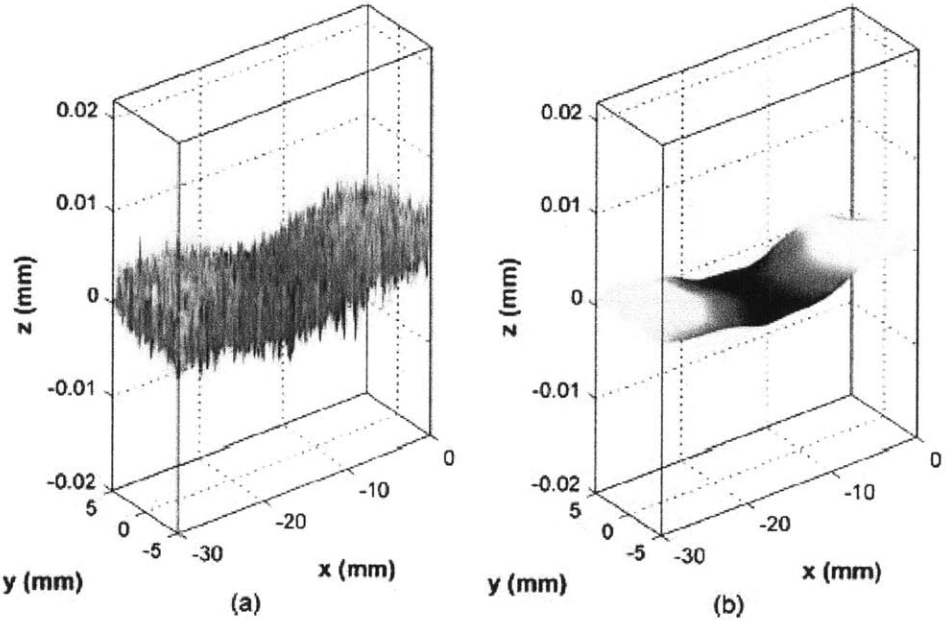

Figure 4.10 - Example of a CMM output: a) data from the measured contour and b) corresponding smoothed spline fit [Pagliaro et al., 2010]

3. **Calculate the Stress**. With the CMM's three dimensional output, a 3D finite element model of the cut part is built. Then, the opposite of the measured contour is taken as a displacement boundary condition and applied to the edge of the model. It is applied in

the normal direction only, leaving all other directions unrestrained. The post-process finite element results give the original stresses along the cut surface.

Typically, the CMM is used on both contoured faces on either side a single cut, as averaging the two can eliminate asymmetric errors caused by uneven cutting (see Figure 4.11). Symmetric errors, however, cannot be averaged out. These can be caused from local cutting irregularities (wire breakage), change in the width of cut (can occur in heterogeneous materials), and wire vibration (can be avoided using the appropriate settings).

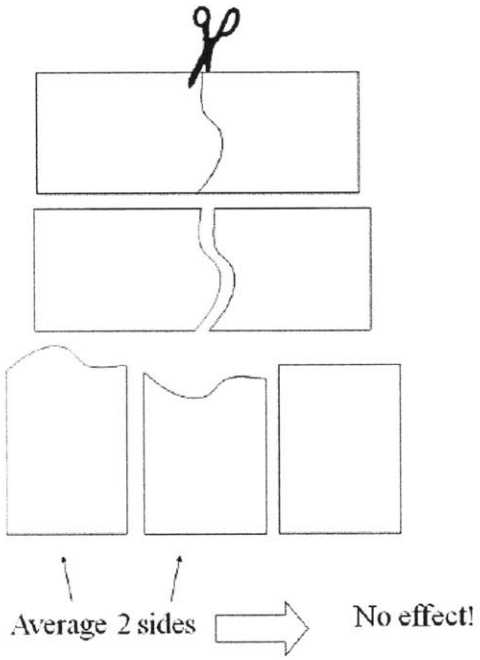

Figure 4.11 - Correcting for a crooked cut by averaging the two contours [Prime and Kastengren, 2011]

There are a few drawbacks to the contour method. Being a destructive method means that one must cut through and remove the area of the sample being measured. Also, because it is relatively new, there is a much smaller body of literature on contour measurements than other measurement techniques. Work is still being done validating contour measurements against other methods of residual stress measurement. One example comparing the residual stress

results obtained using the contour method to those obtained using neutron diffraction is shown in Figure 4.12 [Withers et al., 2008]. Also, because EDM cuts can flare near the edges, the stress values obtained close to the edges of an EDM cut are generally not reported, though there are several examples of good edge results, such as [Johnson, 2008] and [Evans et al., 2007]. There are also a number of specific issues that are still being considered when making use of the contour method. For instance, the importance of material plasticity is yet to be quantified [Withers et al., 2008]. Furthermore, components must be small enough to fit within the EDM and CMM to be measured. Despite these drawbacks, the contour method is a promising and affordable method of taking residual stress measurements deep into a material's thickness with high spatial resolution.

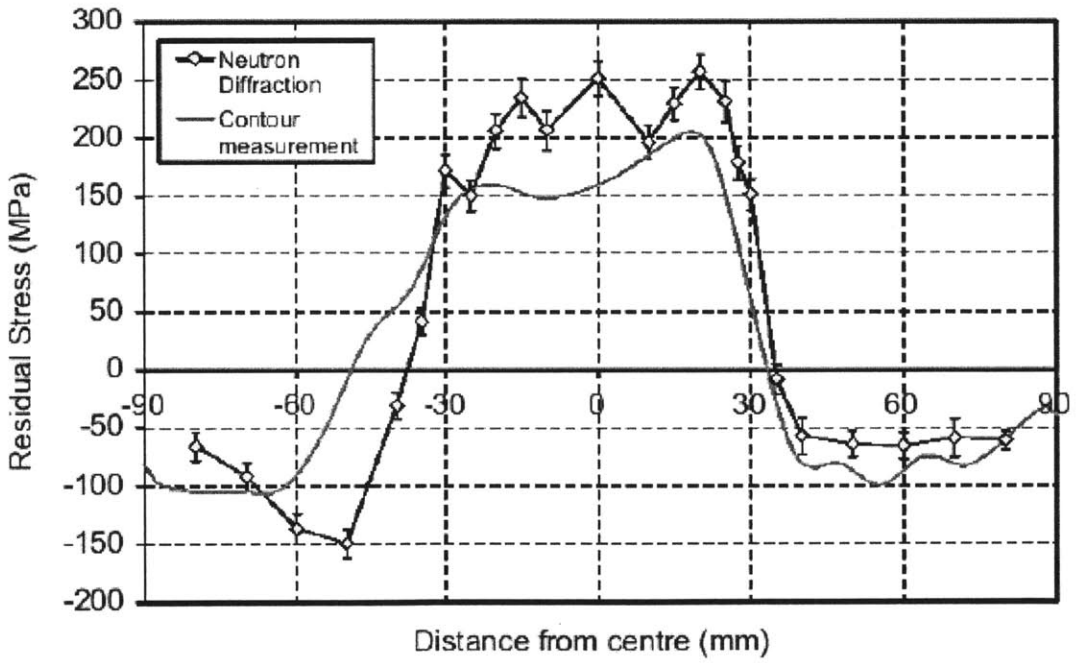

Figure 4.12 - Comparing the results of contour measurement and neutron diffraction for measuring the stresses perpendicular to a weld (σ_y) [Withers et al., 2008]

4.C. Previous Studies of Weld Residual Stress

The welded stainless steel examples cited in this literature review all vary from the used fuel storage canister shell welds in some way, so as a reminder of what this thesis is comparing them to, the known specifications for a typical used fuel storage canister and its welds of greatest interest are listed here:

- Thickness: either 1.27cm or 1.59cm (1/2in or 5/8in)
- Outer Diameter: between 1.5m and 1.8m (60in - 70in)
- Height: between 3m and 5m (120in - 200in)
- Material: austenitic stainless steel of types 304, 304L, 316, or 316L
- Welds of greatest interest: the axial and circumferential shell welds
    - Joint Geometry: full penetration double-V
    - Welding process: submerged arc

4.C.1. Kosaki, 2002

The only study of residual stress measurement taken on used fuel storage canister welds found by this author was in a paper from CRIEPI published only in Japanese [Kosaki, 2002]. Kosaki took a full-scale model canister and measured the residual stress into the thickness of canister lid weld using X-Ray Diffraction, as well as with the stain gauge method (the strain gauge method most commonly uses a bonded metallic strain gauge, a device whose electrical resistance varies with strain, to measure strain at various locations on a material's surface which can then be used to calculate stress) [Strain Gauge Measurement, 1998]. Stresses were measured from the canister outer surface inward toward the center of the canister lid, at the position labeled "No.1" in Figure 4.13 below. From the figure, it is clear that XRD measurements were taken far into the material's thickness, however no explanation is offered as to whether this was done with

electrochemical polishing or with another method that could have altered the stresses that were measured.

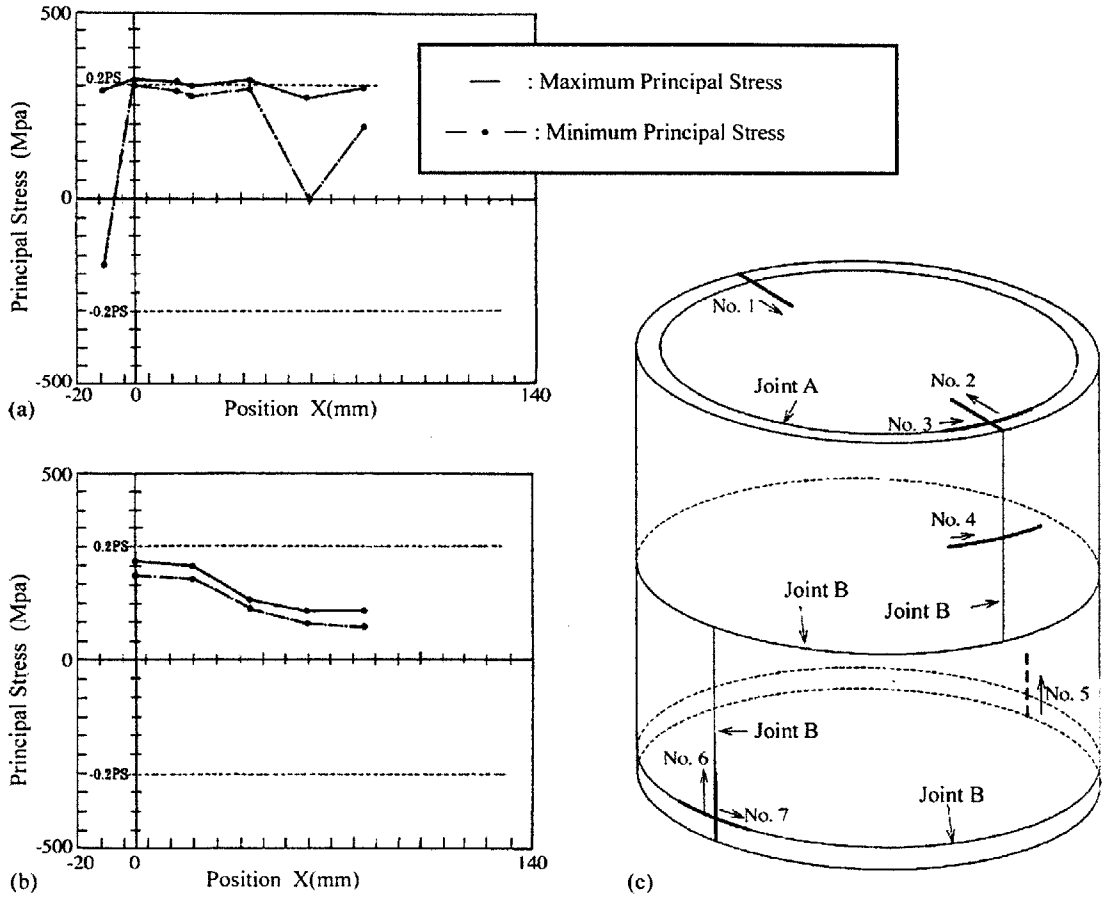

Figure 4.13 - Residual stress of used fuel canister lid. (a) is XRD from position No. 1, (b) is the results of the strain gauge method from position No. 1, and (c) shows the geometry of the specimen with the location of position No. 1 labeled. The "Principal Stress" being measured is hoop stress of a circumferential weld (σ_x in Figure 4.1). [Kosaki, 2008]

The document describes the canister as being made in the same manner as an actual used fuel canister. It is made of 304 and 304L with a wall thickness of 15mm, a diameter of 1.300m, a height of 1.200m, a lid thickness of 40mm, and a canister baseplate thickness of 40mm. The welds are identified as automatic TIG welds.

The stresses begin as highly tensile near the surface, identified in the figure above as approximately 350MPa, with 300MPa identified as 0.2PS. PS, or proof stress, is most often used for ductile materials such as aluminum alloys (though not typically for steels) in which no well-defined yield point between elastic and plastic regions exists, and instead the two gradually transition into one another. 0.2PS, or 0.2% proof stress, is often used in place of yield stress for such materials, and is defined as the stress at which a definite deformation has occurred, where 0.2% strain remains upon unloading [Campbell, 2011]. It is usually referred to as 0.2% yield stress in the US. As can be seen from (a) in Figure 4.13, the XRD measurements indicate that 0.2PS is reached, and that plastic deformation has likely occurred at the weld and as far as 45mm into the depth of the lid.

While the results of this study are very useful in that they provide insight into the stress state of a model canister, the weld examined is a lid weld. As was mentioned in Section 3, the lid welds are of lesser interest than the circumferential and axial shell welds, as the TIG process creates a stronger weld than does SAW, and the lid typically is sealed redundantly such that two welds would have to fail to compromise the containment.

4.C.2. Ogawa et al., 2008

Ogawa, Chidwick, Kingston, Dennis, Bray, and Yanagida carried out a program of residual stress measurements and modeling for the circumferential weld of a Type 316F austenitic stainless steel pipe. The pipe had an outer diameter of 369mm (14.5in) and a wall thickness of 40mm (1.5in). The weld was a Single-V joint configuration, with nickel-based Alloy 82 weld metal. The weld was deposited using the TIG process with a total of 25 passes, with each pass beginning and ending at the "zero degree" position labeled in Figure 4.14.

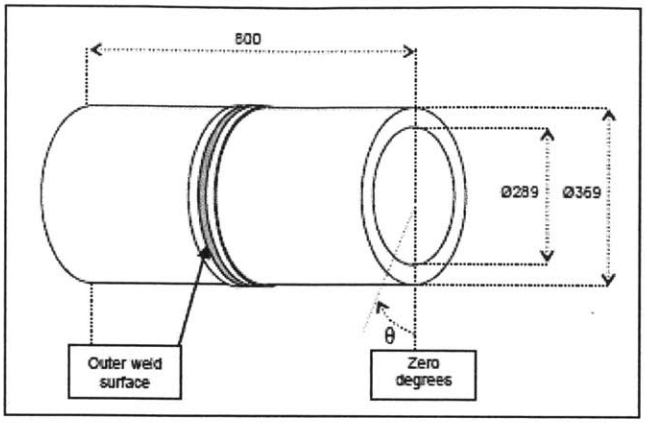

Figure 4.14 - Welded Pipe, dimensions in mm [Ogawa et al., 2008]

Residual stress measurements of this pipe were taken using deep hole drilling. The hole was made using gun-drilling, with EDM used to remove the hole. Three measurements were taken with the gun-drilling occurring from the outer diameter inward, and three measurements were taken with the gun-drilling occurring from the inner diameter outward.

In addition to the DHD measurements, finite element models were made to predict the residual stress. The Frazer-Nash Consultancy (FNC) used ABAQUS 6.6 to produce three axisymmetric models with isotropic, non-linear kinematic, and mixed mode isotropic/kinematic hardening material models [Bray and Dennis, 2006]. The simulations mapped the residual stresses in three dimensions to compare with the measured hoop and axial residual stresses.

The set of residual stress fields predicted by the axisymmetric FNC models were then used by the University of Bristol (UoB) to perform virtual DHD, also done using ABAQUS 6.6. The through wall residual stresses of this model were then overlaid with those predicted by FNC as well as with the actual DHD measurements. The results can be seen in Figures 4.15 - 4.18 below.

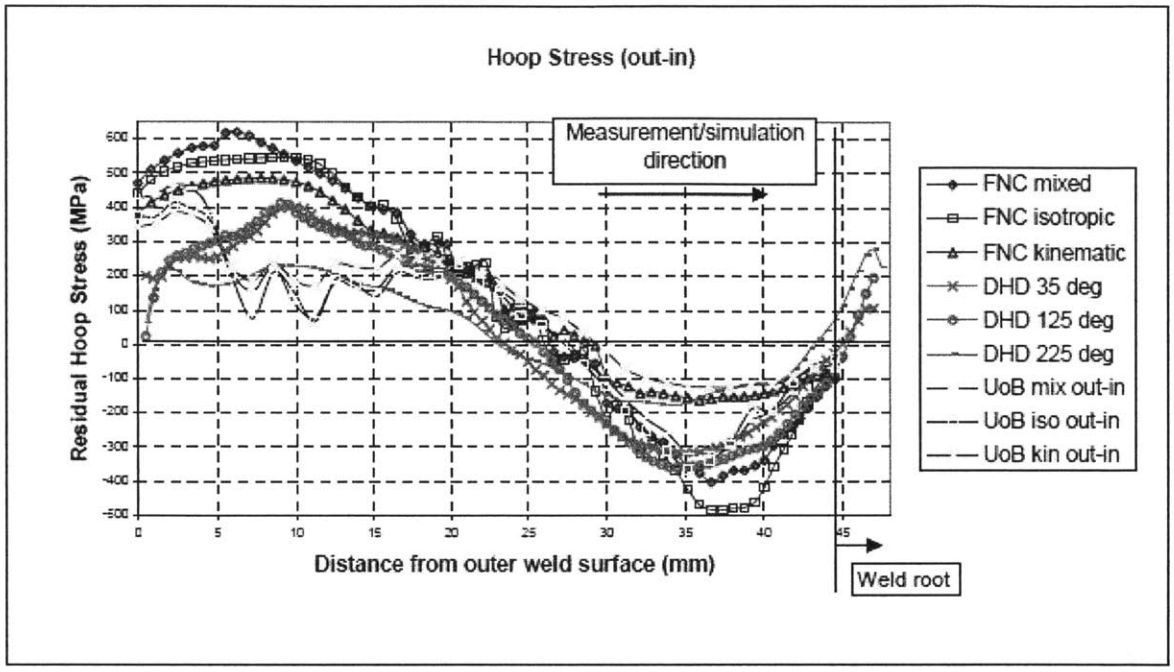

Figure 4.15 - Hoop stress measured from the outer surface inward (σ_x as a function of z) [Ogawa et al., 2008]

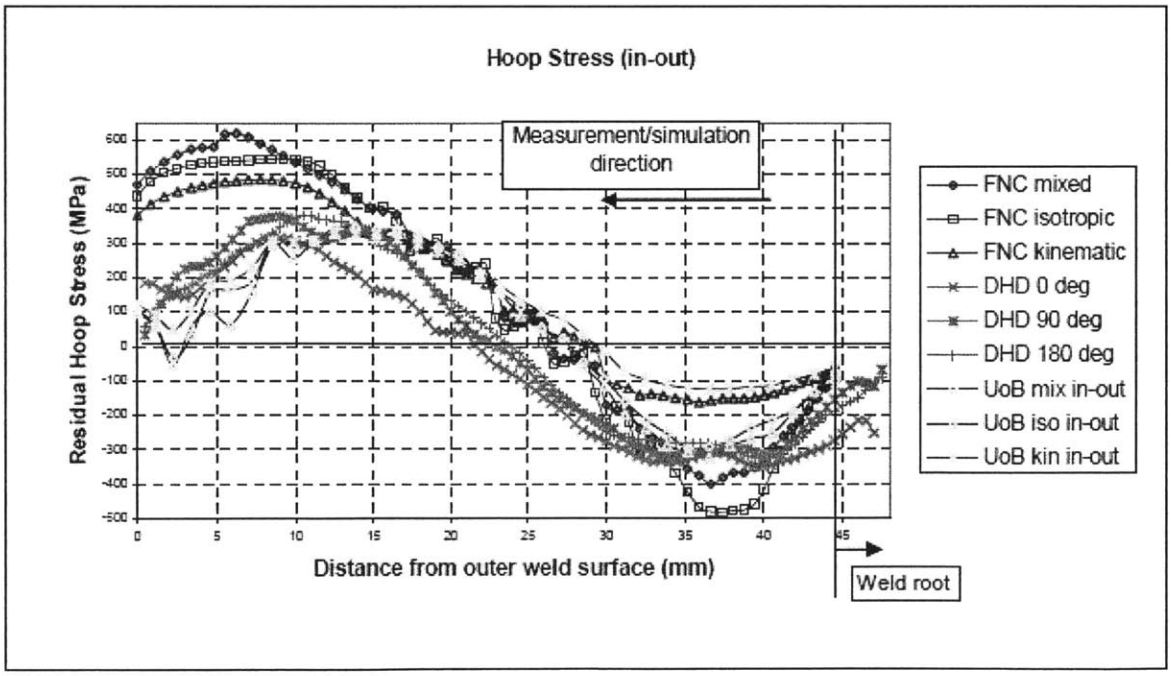

Figure 4.16 - Hoop stress measured from the inner surface outward (σ_x as a function of z) [Ogawa et al., 2008]

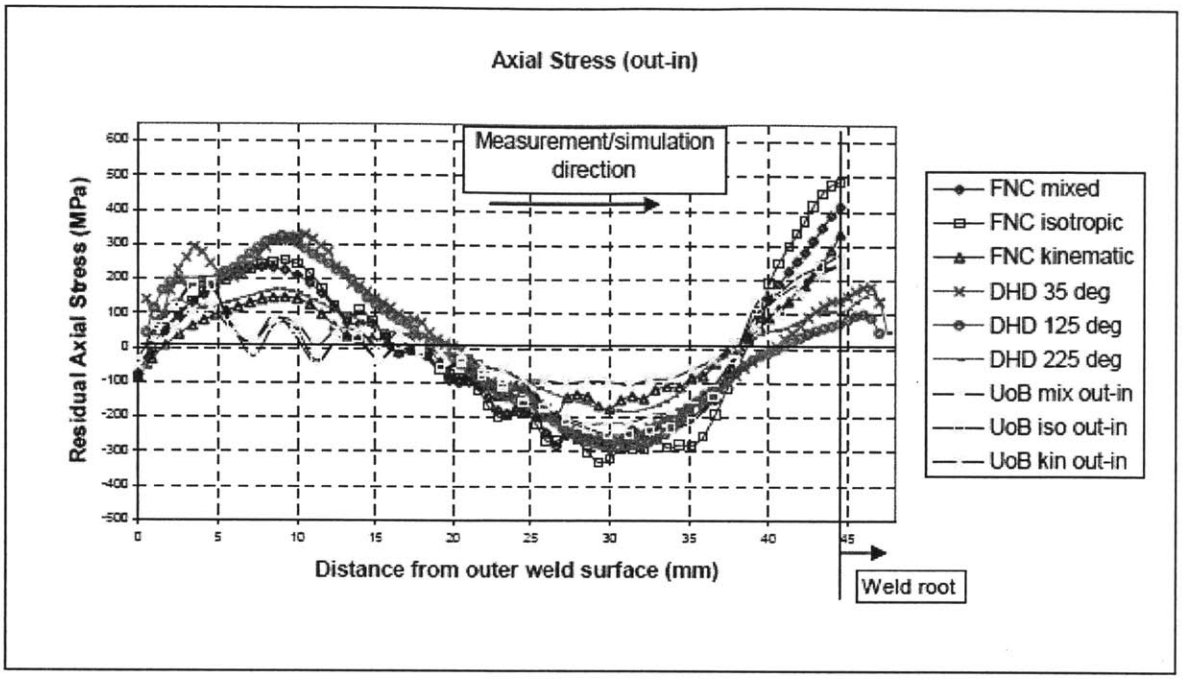

Figure 4.17 - Axial stress measured from the outer surface inward (σ_y as a function of z) [Ogawa et al., 2008]

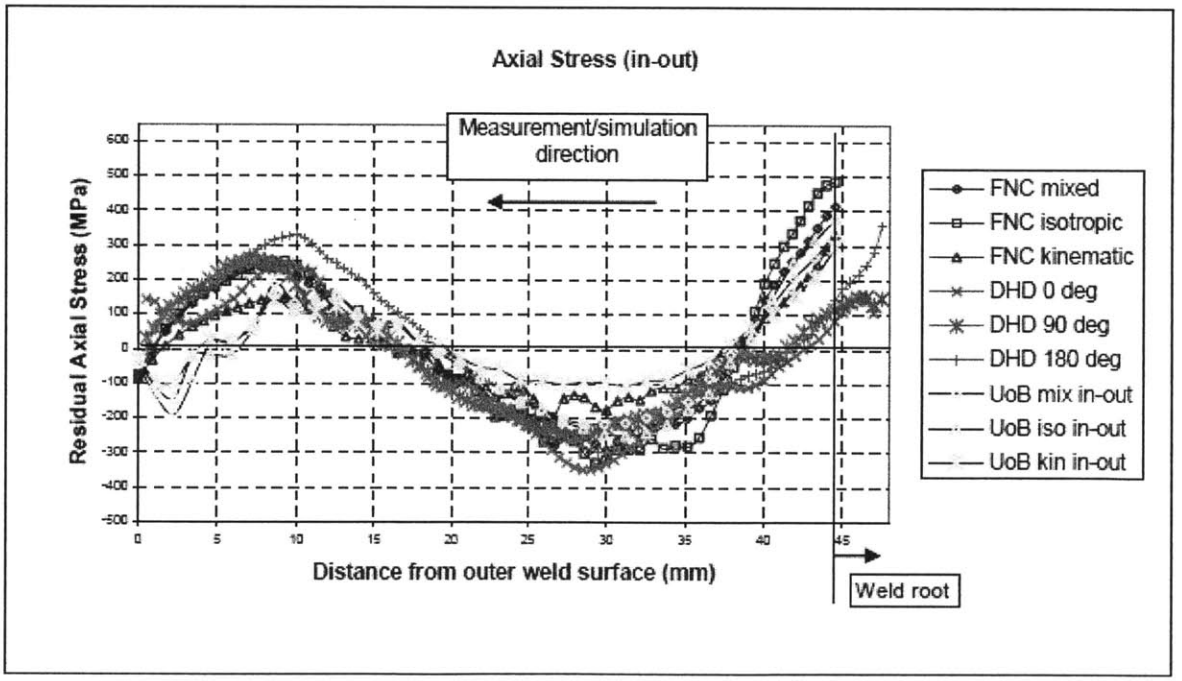

Figure 4.18 - Axial stress measured from the inner surface outward (σ_y as a function of z) [Ogawa et al., 2008]

For hoop stress (σ_x), the DHD for all six locations measured showed the same trend of tensile stress at the outer surface, increasing to approximately 350MPa at 10mm depth, then decreasing to approximately -325MPa at 34mm, before increasing once more towards the inner surface. For axial stress (σ_y), the DHD measurements showed a similar trend of tensile stress at the outer surface, increasing to approximately 250MPa at 10mm depth, then decreasing to approximately -250MPa at 28mm before increasing once more towards the inner surface. It was noted that the hoop and axial shear stresses were not included in the figure as they were negligible in most cases, and in the other cases were small compared with the hoop and axial stresses.

The results of this analysis are very significant. Firstly, the residual stress distribution for single-V circumferential welds for contains a region of compressive stresses for every scenario, independent of stress orientation or drilling direction. Tensile stresses occurred near the outer surface where the majority of weld metal is located, and decreased into compression further into the thickness of the material before returning to near-zero or tensile. Also, it can be seen that the hoop stress (σ_x) was more extreme than the axial stress (σ_y) for these circumferential welds. It is expected that the magnitude of stresses oriented parallel with the weld direction would be greater, given that the cumulative length of weld metal in that direction provides much greater potential for expansion/contraction. Furthermore, while the hoop stresses (σ_x) returned to near-zero towards the inner surface, the axial stresses (σ_y) instead became highly tensile, at a location with a presumably small amount of weld metal and therefore little potential for contraction.

As for the effect of the measurement location, while some variance existed there was no clear, consistent pattern observed. The zero degree location, where the weld began and ended, did not appear to have significantly altered residual stresses relative to the other locations. The

decreased magnitude of the 225 degree measurements in Figures 4.15 and 4.17 were considered by Ogawa et al. to be due to either a variation with angular position within the pipe itself or an anomaly.

As for the effect of the gun-drilling/EDM direction, the DHD hoop stresses (σ_x) were tensile in the weld root for those that were drilled from the outside in, but were compressive for those drilled from the inside out. The DHD axial stresses (σ_y) did not have such a noticeable difference for those drilled from the outer or inner surface.

As for consistency of the models with the DHD measurements, while following the same general trends and patterns, there was a wide range between the stresses measured with DHD and the stresses predicted in the models. For hoop stress (σ_x), the models overestimate the maximum tensile stresses observed by DHD by 200-300MPa, while disagreeing amongst themselves as to the maximum compressive stresses. For axial stress (σ_y), the models were more consistent with the actual DHD measurements, but seemed to overestimate the tensile stress near the inner surface by 200-300MPa. This shows that while models can be useful for predicting residual stress trends, actual measurements are needed for any amount confidence in the accuracy of the stress magnitude.

Compared to a typical used fuel storage canister, this pipe had a much smaller diameter with greater wall thickness, and, in all likelihood, a greater number of passes. This is likely to result in residual stresses of greater magnitude. Furthermore, the large number of passes are likely to work harden the material, increasing yield stress which in turn increases residual stress. That being said, many useful insights can be gained from these measurements. It appears that tensile stress peaks just into the surface of where the majority of weld metal resides. The same could be expected of canisters, but with a double-V weld it would suggest that a similar tensile

peak could be seen near both the inner and outer surfaces. Also, it appears that these stresses can decrease to zero or become compressive further into the material's thickness where less weld metal is present. This is highly significant when considering the propagation of cracks through a used fuel canister, as the presence of compressive stress or even sufficiently low tensile stress could slow crack growth substantially. Also, while the thickness and number of passes likely makes the magnitude of the stresses observed here greater than those that would be expected in a canister, it provides a ballpark for the magnitude of stresses in an austenitic circumferential weld.

4.C.3. Deng, Murakawa, and Liang, 2008

Dean Deng, Hidekazu Murakawa, and Wei Liang utilized the strain gauge method and the finite element method (FEM) to investigate the weld residual stress distribution in an austenitic stainless steel pipe [Deng, Murakawa, and Liang, 2008]. This paper also placed particular emphasis on the influence of yield strength of the weld metal on residual stress.

The material investigated was Type 304 stainless steel pipe with an outer diameter (OD) of 216.3mm (8.5in), wall thickness of 23mm (0.9in), and 800mm (31.5in) in length. Prior to welding, the pipe was subjected to a solution heat treatment process (the procedure specifications of which were not mentioned), which has the effect of taking chromium carbides that have precipitated at grain boundaries, and allowing them to dissolve back into solution in the austenite. After the heat treatment, during which "significant deformation" occurred, the pipe was straightened by mechanical methods.

Once heat treated and straightened, the pipe was welded circumferentially using the gas tungsten arc (GTA) welding method Y308L filler metal. The weld was a single-V type with 14 passes. The interpass temperature was given as approximately 50°C, with temperature measurement on both the inside and outside surface using K type thermocouples. The welding

conditions are given in Table 4.2, and a schematic of the pipe weld with passes and thermocouple locations can be seen in Figure 4.19.

Table 4.2 - Welding condition for each pass [Deng, Murakawa, and Liang, 2008]

Pass Number	Welding Current (A)	Arc Voltage (V)	Welding Speed (mm/min)	Nominal Heat Input (kJ/mm)
1	140.0	9.5	70.0	1.14
2-3	150.0	9.5	80.0	1.07
4-5	190.0	10.0	80.0	1.43
6-14	275.0	14.7	80.0	3.03

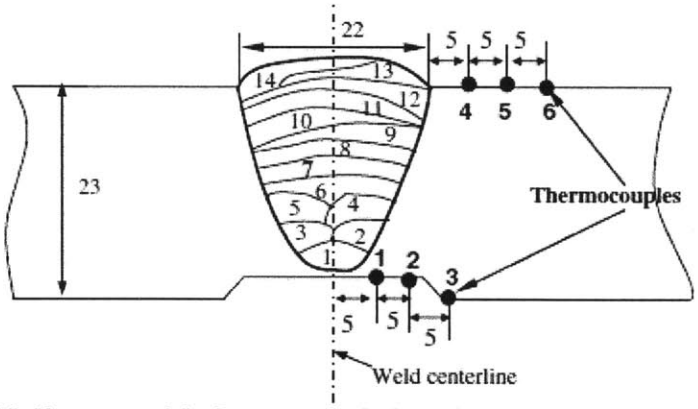

Figure 4.19- Weld diagram with thermocouple locations [Deng, Murakawa, and Liang, 2008]

After welding, electrical-resistance strain gauges were used on the outer and inner surfaces of the welded pipe to measure surface stresses, and finite element analysis was used to predict the through-wall stresses. The equations used to calculate surface stress from strain are given below for hoop and axial strain [Deng and Murakawa, 2006]:

$$\sigma_H = -E(\epsilon_H - \nu\epsilon_A)/(1-\nu^2) \tag{3}$$

$$\sigma_A = -E(\epsilon_A - \nu\epsilon_H)/(1-\nu^2) \tag{4}$$

where ϵ_H is the released strain component in the circumferential (hoop) direction, $\epsilon_A$is the realeased strain component in the axial direction, E is Young's modulus (198.5GPa at room temperature) and ν is Poisson's ratio (0.3).

The model employed a "thermal elastic plastic finite element computational procedure" based on ABAQUS Code. It should be noted that the model did not take into account initial residual stresses, which were likely present from the heat treatment process and cold work. FEM analysis was performed for three separate cases to investigate the effects of yield strength and work hardening on residual stress:

- Case A: The mechanical properties of the weld metal were equal to those of the base metal
- Case B: The yield strength of the weld metal was greater than that of the base metal, but did not consider the work hardening effect of the weld metal (it was considered for both weld and base metal in all other cases)
- Case C: The yield strength of the weld metal was greater than that of the base metal, but did consider the work hardening effect of the weld metal

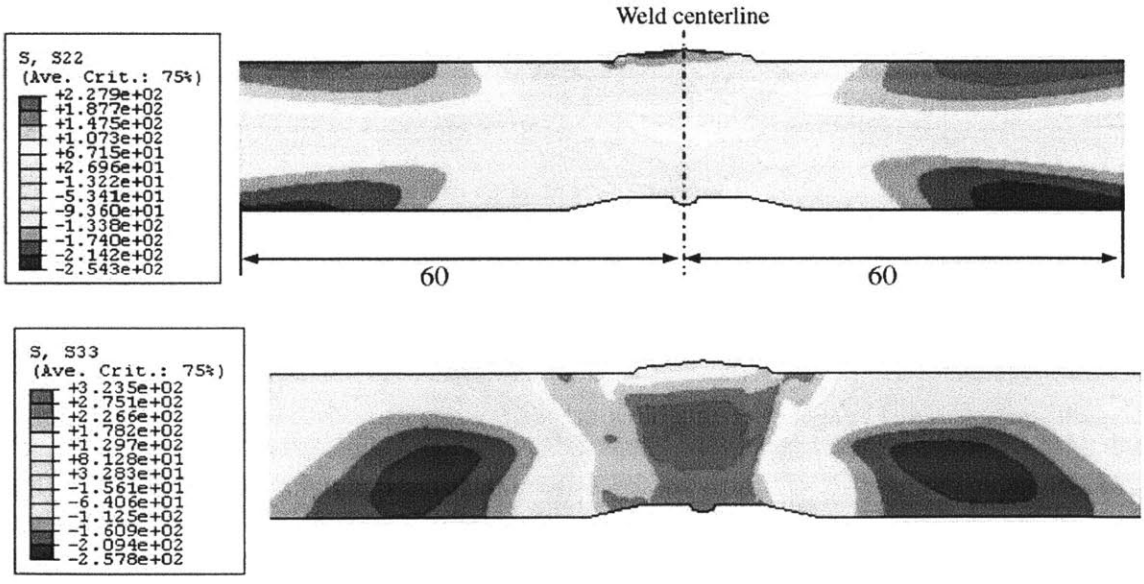

Figure 4.20- FEM axial, σ_y, stress distribution (top) and hoop, σ_x, stress distribution (bottom) for Case A [Deng, Murakawa, and Liang, 2008]

Figure 4.20 shows the axial and hoop stress (σ_y and σ_x respectively) distributions for Case A. The distributions are asymmetric as a result of the sequential welding process shown in Figure 4.19. It can be seen that a large tensile hoop stress (σ_x) exists in the center of the weld, which fades rather quickly to a compressive stress to the sides of the weld. This is very interesting, as pitting and crack initiation are most likely to occur in the HAZ, just to the sides of the weld. If the HAZ is located over these pockets of compression, it could be excellent news for crack propagation. The axial stresses (σ_y) show a large bending moment, which is expected given the shape of the single-V weld deposit, with the majority of weld metal and therefore contraction on the outer surface.

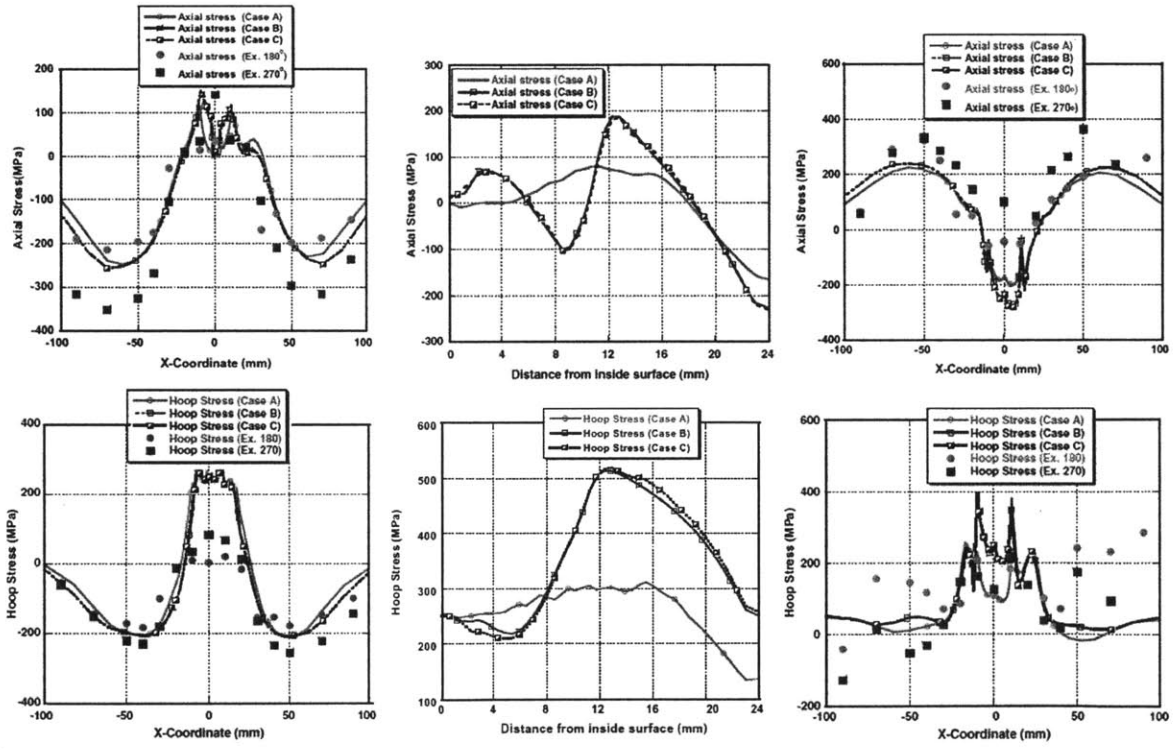

Figure 4.21 - Axial stress (σ_y, top row) and hoop stress (σ_x, bottom row) for inner surface (left column), through-wall along the weld centerline from inside to outside (center column)*, and outer surface (right column) [Deng, Murakawa, and Liang, 2008]

*Note for comparison purposes that the two through-wall figures go from the inside surface to the outside surface, the opposite direction of the Figures 4.15 - 4.18 of [Ogawa et al., 2008]

Figure 4.21 overlays the three FEM cases with the strain gauge results for inner and outer surfaces, both axial and hoop. Generally, the models seem to agree with the strain gauge results (to within about 100MPa). This seems to indicate that the initial stresses of the heat treatment and cold working (those ignored by the model) were mostly inconsequential in comparison to the weld residual stresses. As for the through-wall stresses, the discrepancy between the three different cases is dramatic. It can be seen that while the work hardening effect of the weld metal (the difference between Cases B and C) had little to no consequence on residual stress, that the yield strength of the weld metal was hugely influential on the model's assessment of both the axial and hoop stress. When the yield strength of the weld and base metal were equal (Case A) both axial and hoop stresses changed little throughout the depth of the weld. However, when the weld metal yield strength was greater than that of the base metal (Cases B and C) the residual stresses were much more extreme; the axial stress (σ_y) went from tensile on the inner surface to compressive, then tensile, and then sharply compressive again on the outer surface. The hoop stress (σ_x) meanwhile reached 500MPa at the center of the thickness, 200MPa greater than when the yield strengths were equal. The effect was much greater towards the outer surface, which again is expected as that is where the majority of the weld metal is located. This goes to show that while the work hardening effect is not greatly significant, the relative yield strengths of the weld and base metals can be highly influential in determining the residual stress state of a weld. It should be noted that residual stresses in the base material (and therefore the HAZ) are not expected to be affected as strongly by the weld metal's higher yield strength as is the weld metal itself (this can be seen in the much lower residual tensile hoop stresses to the side of the weld deposit in Figure 4.20). That being said, should a canister be welded with a filler metal of much

greater yield strength than the base metal, the residual stresses are likely to be much greater because of it.

4.C.4. Dong, Zhang, and Rawls, 2003

P. Dong and J. Zhang of Battelle along with G. Rawls of Westinghouse performed finite element analysis on a 1.59cm (5/8in), "K" configuration (similar to double-V), submerged arc, circumferential weld in a steel storage tank. The weld metal was identified as E6010 with the base metal identified as A285. A285 is a ferritic steel, unlike the austenitic stainless steel used for fuel storage canisters. It should be noted that the room temperature yield strength of the base and weld material are quite different from one another, (33.7ksi for A285 and 56.2ksi for E6010 according to [Matweb.com, 2013]) which was shown in the case of Deng, Murakawa, and Liang to result in a much more varied distribution with higher tensile stresses within the weld metal.

The tank's radius to thickness ratio was 816 to 1, implying a diameter of 25.9m (85ft). Because of the large diameter, it is expected that the circumferential weld will behave similarly to an axial weld locally, depending on the restraint conditions during welding. A total length of 1.02m (40in) was chosen for the model, in order to fully contain the residual stress distributions within the finite element model. The weld geometry is shown in Figure 4.22 with the welding parameters in Table 4.3.

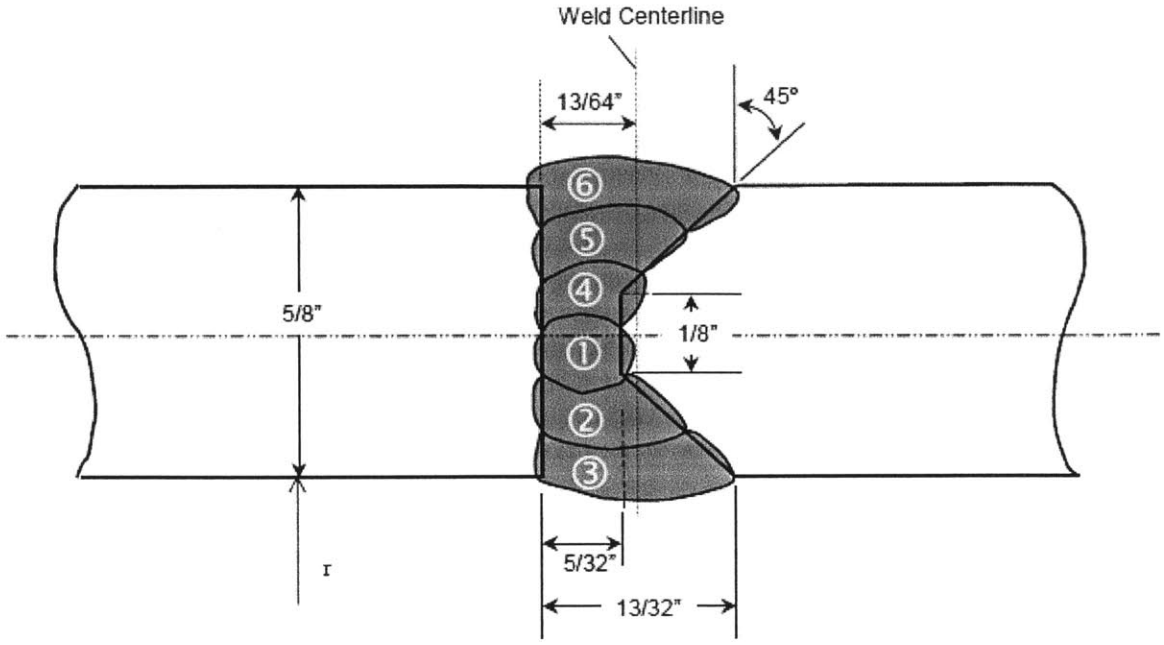

Figure 4.22 - Geometry and weld-pass profiles for a butt-girth weld [Dong, Zhang, and Rawls, 2003]

Table 4.3 - Welding parameters for residual stress modeling [Dong, Zhang, and Rawls, 2003]

Current (A)	Voltage (V)	Welding Speed	Electrode Size	Inter-pass Temperature (°C)	Number of Passes
197.5	24.0	0.318cm/s (0.125in/s)	0.476cm (3/16in)	10 (50°F)	6

Residual stress was calculated using a finite element model which performed thermo-mechanical residual stress analysis, taking into account the welding parameters of Table 4.3, joint detail, weld pass deposition sequence, and temperature-dependent properties. The results can be seen in Figures 4.23-4.26 below.

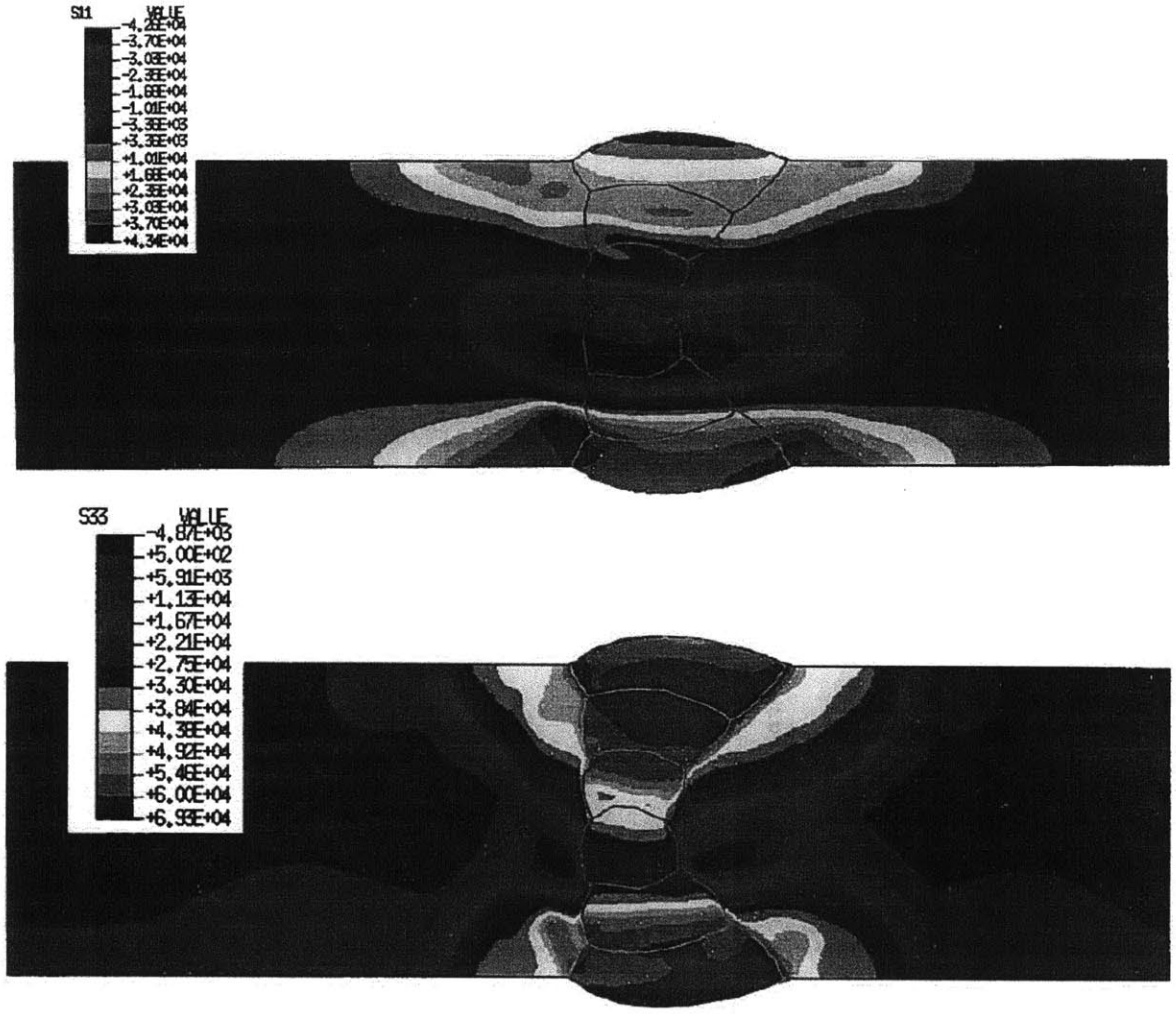

Figure 4.23 - Predicted weld residual stress distributions for axial (σ_y, top) and hoop (σ_x, bottom) stress in psi [Dong, Zhang, and Rawls, 2003]

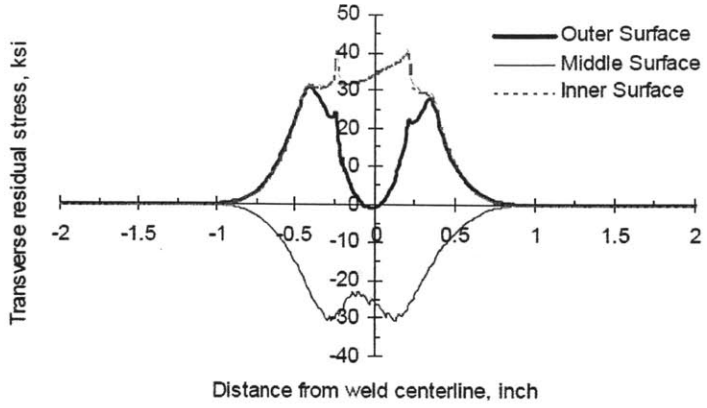

(a)

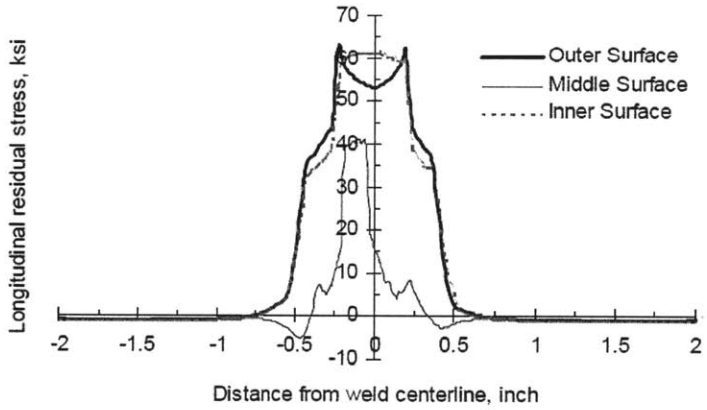

(b)

Figure 4.24- Residual stress distribution at the inner, middle and outer surfaces for axial (transverse, σ_y) stress (a), and hoop (longitudinal, σ_x) stress (b) [Dong, Zhang, and Rawls, 2003]

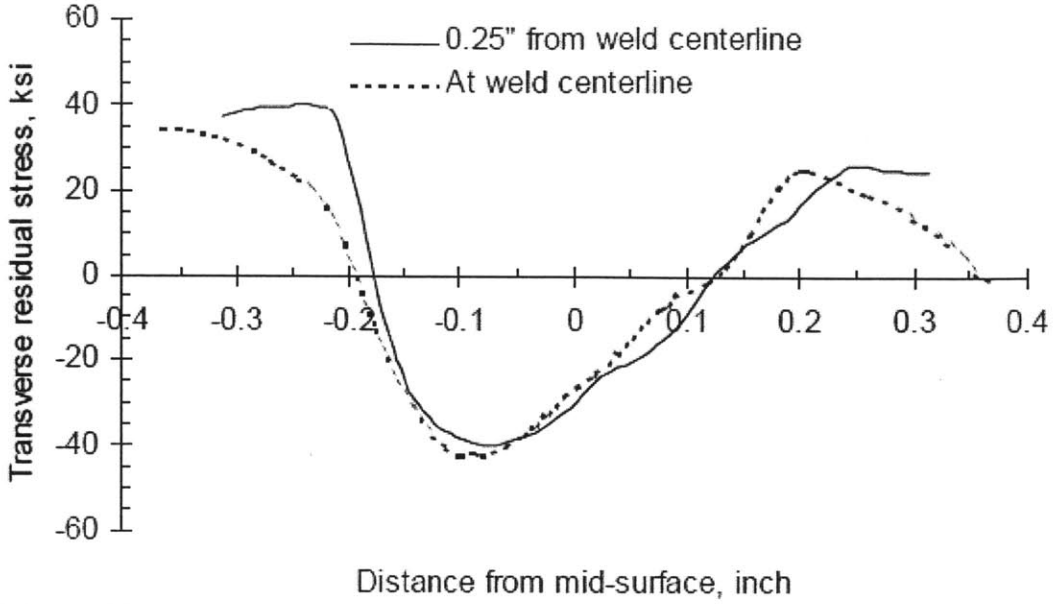

Figure 4.25 - Axial (σ_y) residual stress distribution [Dong, Zhang, and Rawls, 2003]

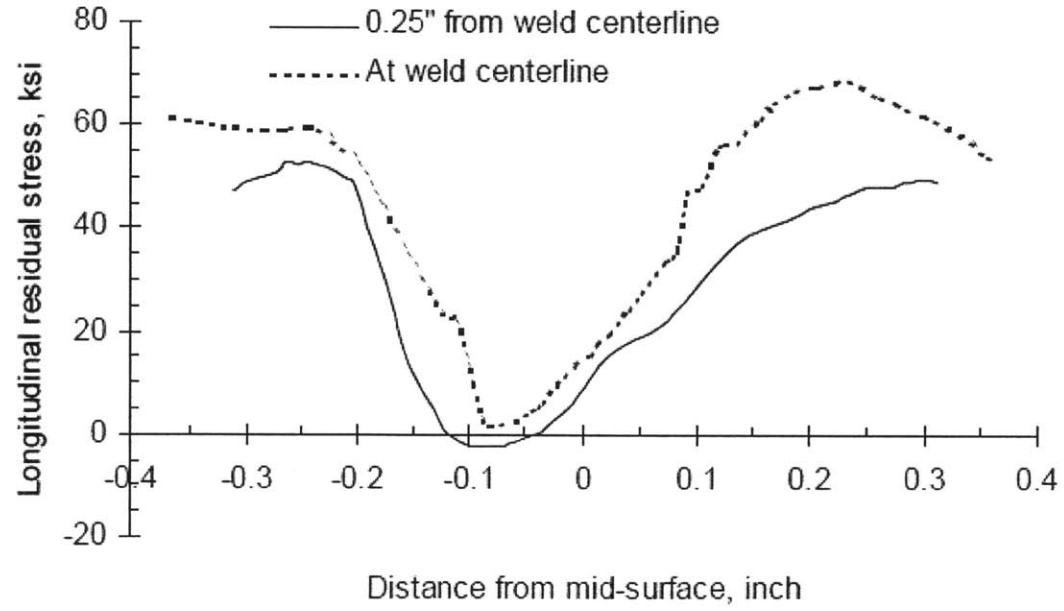

Figure 4.26- Hoop (σ_x) residual stress distribution ([Dong, Zhang, and Rawls, 2003]

From can be seen from Figure 4.25 that axial stress (σ_y) begins as tensile, goes compressive in the center of the thickness, and then returns tensile again. Hoop stress (σ_x)

meanwhile follows a similar pattern, but is more highly tensile, and falls only to near-zero stress before becoming highly tensile again.

One of the more interesting features of Figures 4.23, 4.25 and 4.26 is that they offer a look at how the residual stress state 0.64cm (0.25in) from the weld centerline compares with that at the weld centerline. In this weld, which is 1.59cm (0.625in) thick, 0.64cm from the weld centerline is likely somewhere near the fusion zone of weld and base metal or just into the course-grained region of the HAZ. Since cracks are most likely to initiate in the HAZ, insight into how stresses behave in the region beside the weld is very useful. Not only does it show what the residual stress state looks like in this particular case, but it also offers a basis for making engineering guesses as to what could be expected to the side of the weld centerline in literature where only centerline residual stress distribution is reported. In Figure 4.24, the "middle surface" also shows what the residual stress state is within the thickness of the material, both in the center and to the sides of the weld metal. While the axial stress (σ_y) is compressive for nearly an inch on either side of the centerline within the material thickness, the hoop stress (σ_x) appears to go compressive only for a small area around 1.27cm (0.5in) from either side of the weld centerline. In Figures 4.25 and 4.26, the model for the area 0.64cm (0.25in) away from the weld predicts that the stress is less tensile throughout the thickness in the hoop (σ_x) direction, but actually slightly more tensile in the axial (σ_y) direction. However, these differences between the 0.64cm (0.25in) model and centerline model are very slight as overall the two models are very close together. This indicates that the residual stress does not change dramatically from the centerline outward, as least to within 0.64cm (0.25in).

Perhaps the most interesting aspect of this example is that while the base material and diameter are different than in used fuel storage canisters, the geometry and process are very

similar to what is expected of used fuel storage canister welds: 1.59cm (5/8in), "K" configuration (similar to double-V), circumferential, submerged arc welded, with 6 passes (roughly the number expected in used fuel storage canister welds). This implies that even if the ferrite base metal experiences a different magnitude of residual stress than austenite, the shape of these residual stress distributions likely remain a good example of the relative symmetry of residual stress that can be expected in a canister weld.

4.C.5. George, Smith, and Bouchard, 2000

D. George, D.J. Smith, and P.J. Bouchard used DHD and Finite Element simulations on the HAZ of a butt-welded stainless steel pipe, 35mm (1.38in) thick and 432mm (17in) in diameter. The weld was a single-V, as shown in Figure 4.27d. The pipe was made of AISI type 316H, welded using a standard manual metal arc (MMA) weld procedure with over 30 passes.

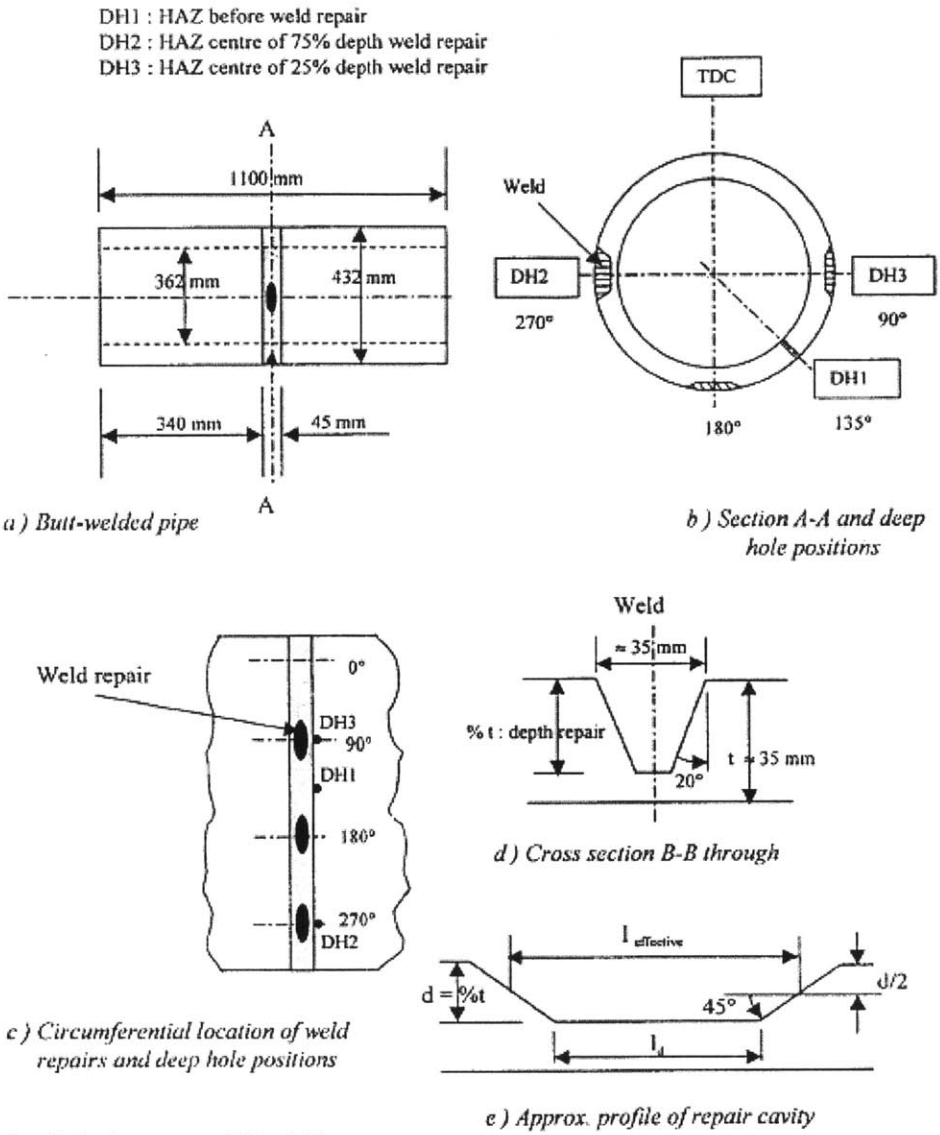

Figure 4.27 - Test component layout [George, Smith, and Bouchard, 2000]

Aside from mapping the original residual stress distribution, an additional goal of this paper was to determine the effects of weld repair on residual stress. The weld repairs were done by excavating weld metal with a hand grinder to depths of either 25% or 75% thickness at three

locations around the circumference, labeled DH1, DH2, and DH3 (see Figure 4.27b and 4.27c). These cavities were then filled with Type 316L using the same MMA weld process.

DHD was accomplished with a gun-drilled 3.175mm diameter hole, with measurements taken at 0.2mm intervals using an air probe. The gun-drilled hole was then was removed by sectioning out a 20mm diameter column of material around the hole with EDM. DHD was first administered on the pristine DH1 position. After excavation and repair, DHD was then administered on positions DH2 and DH3. Each of these locations was then modeled with axisymmetric finite element analysis. The results of these measurements can be seen in Figure 4.28 below.

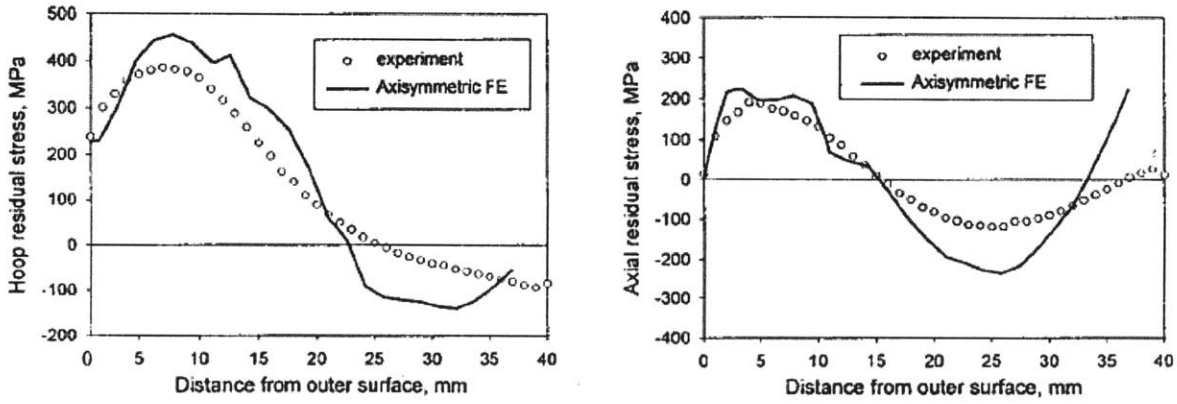

a) Hoop b) Axial

Figure 4.28 - Residual stress distribution in the HAZ (no weld excavation or repair) for σ_x (hoop, on the left) and σ_y (axial, on the right) [George, Smith, and Bouchard, 2000]

Figure 4.28 shows that these residual stresses were very similar to those in Figures 4.15-4.18 of Ogawa et al.'s welded pipe. The two pipes had very similar thickness and diameter, both were single-V, both made of 316 stainless steel, and both were measured with DHD and modeled with finite element analysis. Both have a hoop stress (σ_x) peaking near 400MPa, dipping compressive, and reducing in magnitude at the inner surface, as well as an axial stress (σ_y) peaking around 200MPa, dipping to about 200MPa compressive, and then returning tensile just

before the inner surface. Even the finite element models followed the same patterns, in that they both overshot the axial stress (σ_y) near the inner surface.

One major difference between the two, however, is that Ogawa et al. performed DHD in the weld metal (Alloy 86), whereas George, Smith, and Bouchard performed DHD in the HAZ (Type 316H). This indicates that residual stresses likely do not vary significantly from the weld metal to the HAZ, reinforcing the observations in Figures 4.25 and 4.26 that the residual stress distribution in the weld centerline and nearby base metal are very similar. It also shows that the residual stress of the alloy 82 weld metal used in [Ogawa et al., 2008] does not vary significantly from that of the Type 316 HAZ used in [George, Smith, and Bouchard, 2000].

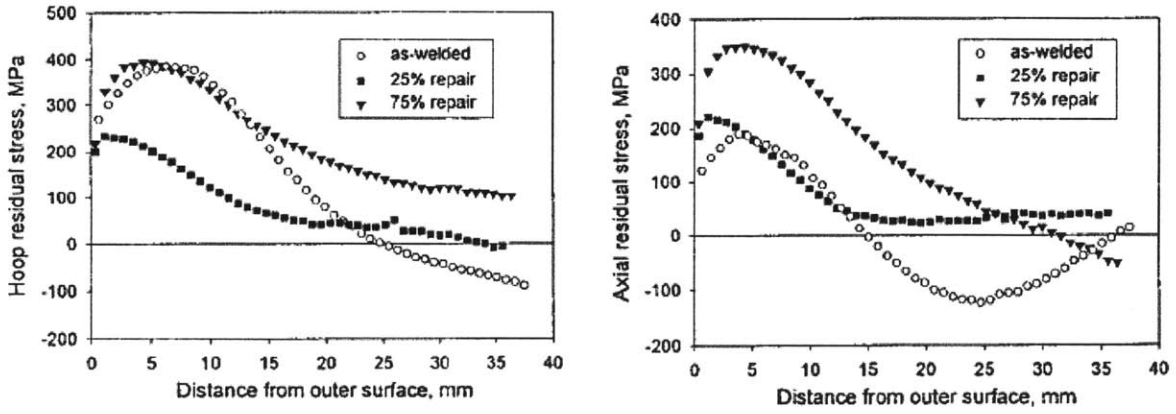

a) Hoop b) Axial

Figure 4.29 - Comparing DHD measured residual stress distributions in the HAZ for as-welded and repaired welds [George, Smith, and Bouchard, 2000]

Figure 4.29 shows that the weld repair made the residual stresses significantly more tensile, particularly beyond 15-20mm into the surface. As expected, the 75% repair saw the greatest increase in tensile stress. Surprisingly, the 25% repair actually became slightly less tensile in the hoop direction (σ_x) for the first 20mm of depth. Whereas the as-welded sample went compressive for both hoop and axial stress, both repair welds stayed tensile for nearly the

entire depth. This is highly significant if one is to consider weld repair as a potential solution to the problem of extending used fuel canister lifetime. Increasing the tensile stress deep into a weld would serve only to worsen the material's resistance to cracking in the long term, by eliminating its crack-resistant compressive stresses. One factor that was not mentioned, however, is the extent to which the hand grinder used for excavating the welds affected the residual stress state. It would be useful to be able to compare the residual stress measurements from the repaired weld to one that was excavated by hand grinding and left un-repaired.

4.C.6. Other Literature

There are a number of other useful documents on the subject of residual stress in stainless steel welds that, while less relevant to the welds of used fuel storage canisters, do provide unique and interesting insights for the purpose of better understanding or mitigating the problem of residual stress in used fuel storage canisters.

For example, Shirzadi, Bhadeshia, Karlsson, and Withers worked towards developing a stainless steel weld metal designed to mitigate residual stresses. A welding consumable was developed that solidified as delta ferrite, then transformed into austenite which then underwent a martensitic transformation upon cooling. The remnants of delta ferrite were not continuous, thereby leading to good toughness. The transformation plasticity associated with the formation of martensite under stress was shown to reduce distortion of the final weld. Moving forward, work is being done towards characterizing the residual stress state in weldments with the newly designed consumable [Shirzadi et al., 2009].

Gideon et al. used neutron diffraction to measure the residual stress in welded duplex stainless steel. Duplex steels, which combine two microstructures of steel (most typically austenite and ferrite) have the benefit of combing the favorable properties of each microstructure.

The result is a higher strength material that retains good weldability, toughness, and SCC resistance. In this paper, the material used was a 10mm thick, 200mm diameter duplex stainless steel linepipe (UNS 31803), primarily composed of ferrite mixed with austenite. The weld was a single-V, circumferential GTA weld with 5 passes. Magnetic Force Microscopy was used to determine the size, shape, and distribution of the ferrite and austenite throughout the sample, and neutron diffraction was used to measure the residual stresses (the locations of which can be seen in Figure 4.30). Combining the results of Magnetic Force Microscopy and neutron diffraction allowed Gideon et al. to determine the residual stresses for each microstructure throughout the weld. The results showed both austenite and ferrite to be under tensile stress in both the axial and hoop directions, with the highest stress being σ_x, parallel with the welding direction. These results can be seen in Figure 4.31, which displays the overall macroscopic residual stress (volume weighted for both microstructures, labeled as 'c' for both σ_y and σ_x) as well was the mean stress for each microstructure (labeled as 'a' for ferrite and 'b' for austenite). The austenite phase did show sections of compression in the transverse (axial, σ_y) direction. It was found that the highest ferrite phase stresses occurred in the mid-thickness of the plate [Gideon et al.].

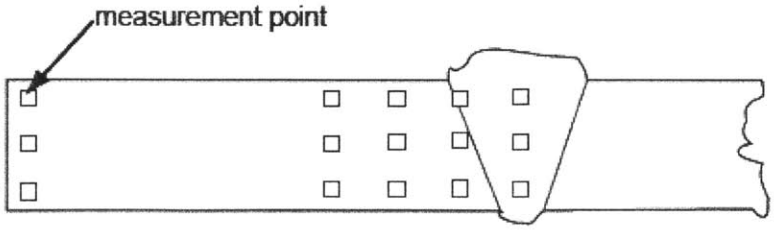

Figure 4.30 – Neutron diffraction residual stress measurement locations (results seen in Figure 4.31 below) [Gideon et al.]

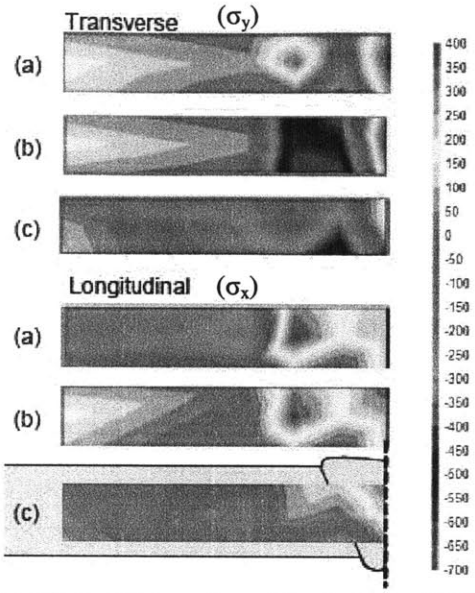

Figure 4.31 - Neutron Diffraction measured residual stress (MPa) for for (a) mean ferrite stress, (b) mean austenite stress, and (c) volume weighted macroscopic residual stress [Gideon et al.]

Teng, Chang, and Tseng completed a study on the effects of welding sequences on residual stress. Among other techniques, the finite element method was used to evaluate residual stresses for progressive welding, backstep welding, and symmetric welding in a thin-wall butt-weld. Each of these welding sequences is defined on the right side of Figure 4.32 below. On the left side of Figure 4.32 are the results of the FEM analysis on the hoop stress (σ_x) present for each of these welding sequences. It was shown that generally, the hoop residual stresses from symmetric welding were smaller than those from other welding sequences, but that local maxima of tensile stress occurred for both symmetric and backstep welding. These maxima appeared to occur not at the beginning or end of each ¼ length weld pass, but rather at the center of each (see Figure 4.32).

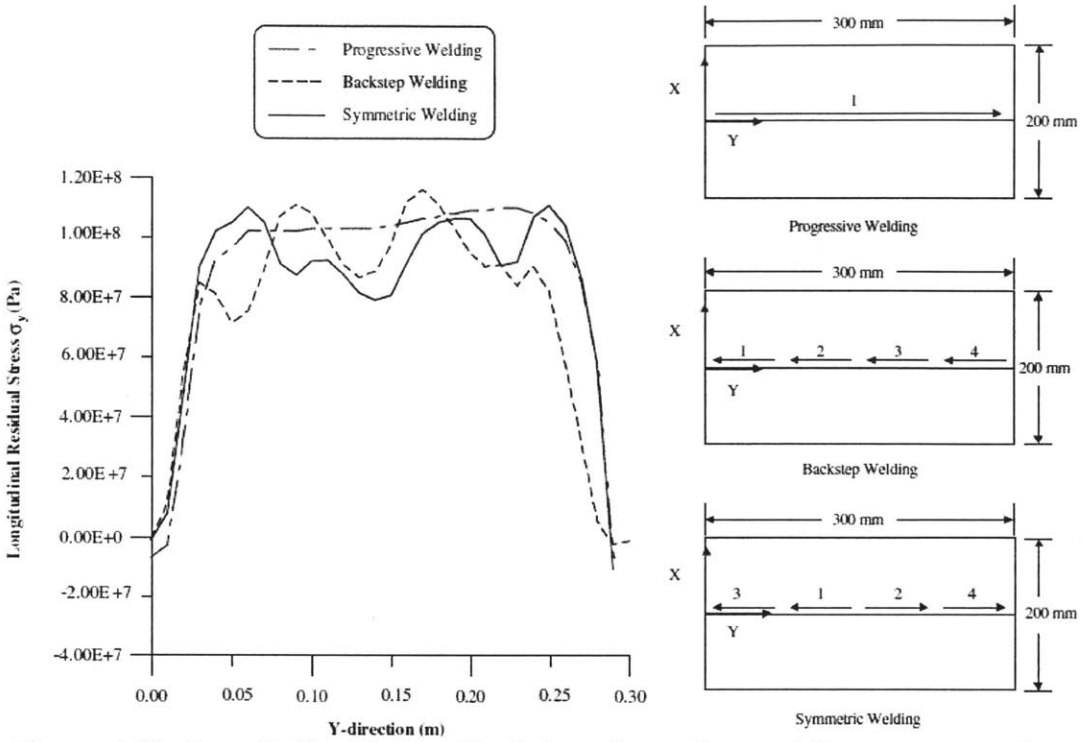

Figure 4.32 - Longitudinal (σ_x) residual stress for various welding sequences, shown at right [Teng, Chang, and Tseng, 2003]

Murugan et al. studied the temperature distribution and residual stresses from multipass welding in Type 304 and carbon steel with 6mm, 8mm, and 12mm thickness [Murugan et al., 2001]. The welds were manual metal arc, and XRD was used for residual stress measurements (near surface only). In order to allow residuals stress measurements to be taken between passes, it was necessary to allow the interpass temperature to be as low as room temperature, whereas it would normally be in the range of 175-200°C. It was noted that this may have resulted in slightly higher residual stresses. The results, organized by base metal type and thickness, can be seen in Figure 4.33. Unfortunately, stress orientation (whether the figure shows σ_x or σ_y) was not specified. It was shown that in general, carbon steel reached a higher peak temperature. It was also shown that with greater thickness, the peak temperature decreased, but residual stresses

were higher, indicating that the residual stress magnitude depends on more variables than simply the peak temperature.

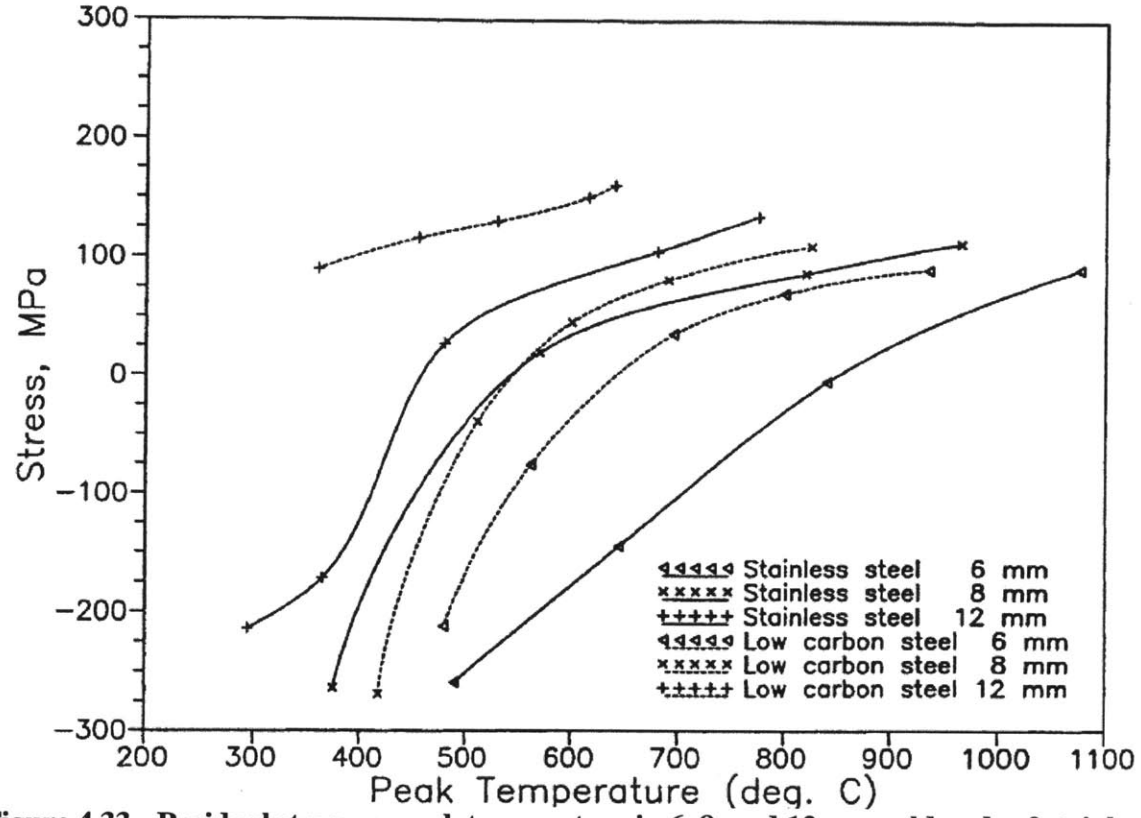

Figure 4.33 - Residual stress vs. peak temperature in 6, 8, and 12mm weld pads of stainless and carbon steel (stress orientation not specified) [Murugan et al., 2001]

4.C.7 – Summary of the Previous Studies of Weld Residual Stresses

A number of trends were observed in these studies of weld residual stresses. In [Ogawa et al., 2008] as well as in [George, Smith, and Bouchard, 2000], it was observed that for a single-V weld, both hoop and axial stresses experienced compressive stress near the inner surface. The fact that compressive stresses were seen in all orientations was highly significant because it was evidence that compressive stresses can exist in a weld, and that if a similar section of compression is found in canister welds, that crack growth could be slowed substantially. This was not observed in all of the literature, however. In the FEM analysis performed by Deng,

Murakawa, and Liang, for example, compressive axial stresses (σ_y) were predicted near the outer surface, but hoop stress (σ_x) was predicted to remain tensile throughout the material thickness.

Also shown in [Deng, Murakawa, and Liang, 2008] was the effect of work hardening and yield strength on weld residual stress. Work hardening was shown to have little impact on the residual stress state of the weld, however yield strength was shown to be highly influential. For a case in which the weld metal yield strength was greater than base metal yield strength, it was observed that residual stresses were much greater and more varied in both σ_x and σ_y orientations.

For welds that more closely matched symmetry of the double-V canister welds, the FEM analysis of [Dong, Zhang, and Rawls, 2003] on a "K" configuration weld showed approximately symmetric residual stress distributions for both axial and hoop stress. Axial stress (σ_y) went compressive in the center with tensile stresses near both surfaces, but hoop stress (σ_x) stayed near or above zero in the center of the thickness. While the material in use was ferritic stainless steel (rather than the austenitic stainless steel used in canisters), the dimensions and joint geometry were very close to that of typical canister material, and so the shape of these residual stress distributions is expected to closely match those in actual canister welds. Also seen in [Dong, Zhang, and Rawls, 2003] was the residual stress state 0.64cm (0.25in) from the weld center, which very closely matched the residual stress found in the center of the weld metal for both axial and hoop stress.

Kosaki took residual stress measurements in the lid of a used fuel canister. Stresses peaked around 350MPa, above 0.2% yield stress for the material [Kosaki, 2008]. However, it is unlikely that the lid weld would be the canister's weak point for failure by SCC because of the relative strength of the gas tungsten arc weld used, as well as the redundancy of lid welds.

Also observed was the level of consistency of residual stress measurement techniques with FEM analysis. Some found the range between FEM and DHD to be as large as 200-300MPa [Ogawa et al.]. Both strain gauges and FEM analysis were used in [Deng, Murakawa, and Liang, 2008], and were shown to vary by as much as 100-200MPa from one another.

Several other factors were observed as well. Weld repair (or possibly the hand grinding that preceded it) was shown to correlate with an increase in tensile stress, especially deeper into a material's thickness [George, Smith, and Bouchard, 2000]. The effect of weld sequence on hoop stress (σ_x) was observed, where it was seen that progressive welding (welding in which a single, long weld pass is chosen in favor of many short passes) generally resulted in lower tensile stress [Teng, Chang, and Tseng, 2003]. It was also shown that the magnitude of residual stress depends on more variables than simply the peak temperature in a weld [Murugan et al., 2001].

These observations were all taken into consideration for the prediction of the residual stress in a canister weld in Section 6 of this thesis.

5. Crack Propagation

As has been discussed, predicting the time to failure of used fuel storage canisters by SCC depends just as greatly on crack initiation as it does on crack growth. In fact, according to the US Nuclear Waste Technical Review Board, "A metal canister's corrosion lifetime for SCC corrosion can be estimated as the time needed for the canister temperature to decline to the point where condensation is possible, which can be above 100°C, plus the time for SCC corrosion to initiate, plus time needed for SCC corrosion to propagate through the canister wall thickness" [Rigby, 2010]. The final model for time to failure of used fuel storage canisters will likely follow this framework. However, for the sake of emphasizing the effect of residual stresses through the thickness of the canister wall, the focus here will be solely on the time needed for

SCC, once initiated, to propagate through the canister wall thickness for a single, constant environment.

5.A. Stress Intensity Factor

Under conditions conducive to SCC, an empirical linear relationship exists between applied stress and the log time to fracture by SCC for smooth austenitic stainless steel samples [Uhlig and Revie, 2008]. At the heart of this relation between stress and time to fracture is the stress state at the crack tip. Stress is greatest at the root of a pit or crack tip, greater than the applied or residual stress in the surrounding medium. The actual stress near the tip of a crack of length 'a' can be calculated in terms of the stress intensity factor, K. In its simplest form, the stress intensity factor is calculated as follows:

$$K_1 = \sigma\sqrt{\pi a} \tag{5}$$

where K_I is the stress intensity and 'a' is the crack depth. For the application of canister material, a more specific equation can be used (as will be shown in Section 5.A.2).

It should be noted that K_1 is only for plane strain (also known as Mode I loading) conditions, which is likely to be the primary loading mode for SCC in welds. Components undergoing SCC, in practice, likely experience the other two loading modes as well, Mode II and Mode III (also known as in-plane shear and out-of-plane shear) [Garverick, 1994]. A diagram of each of these three loading modes can be seen below in Figure 5.1.

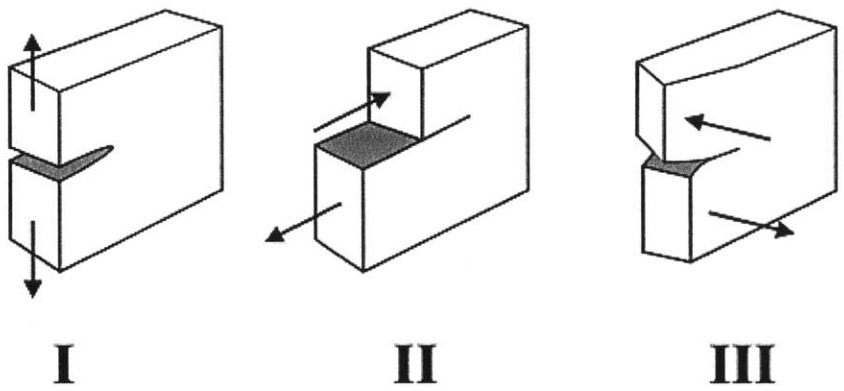

Figure 5.1 – Three loading modes: I (plane strain), II (in-plane shear), and III (out-of-plane shear) [University of Cambridge, 2013]

5.A.1. Effect of the Stress Intensity Factor on Crack Growth

The greater the stress intensity factor, the faster a crack propagates through a material. For an example of the how stress intensity factor behaves through the thickness of a material with a given residual stress distribution, see Figure 5.2 below.

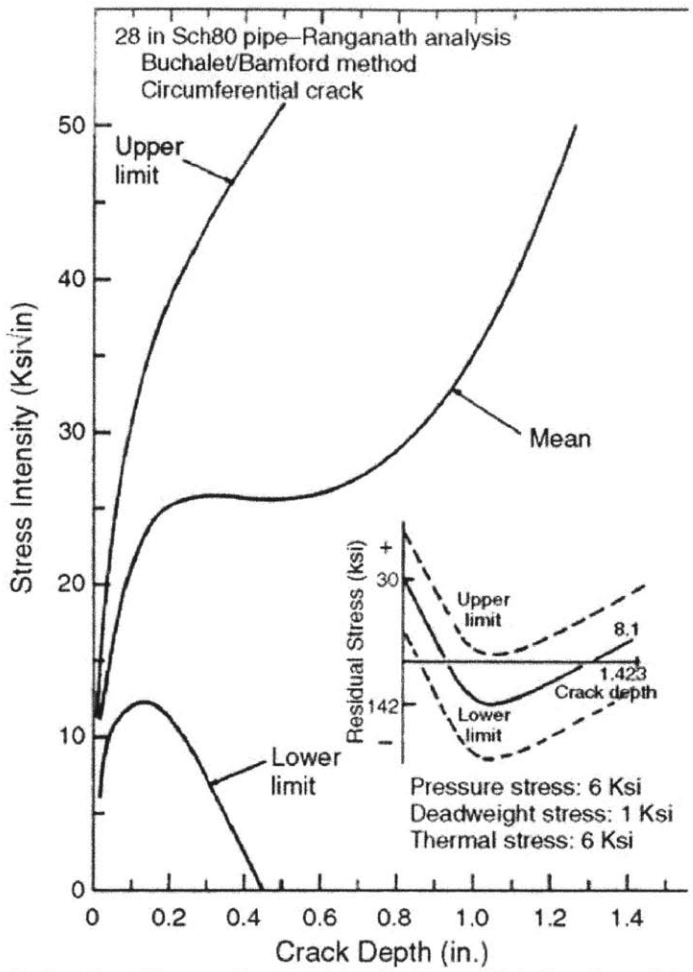

Figure 5.2 - K vs. crack depth with varying residual stress distributions [Andresen, 2008]

In this figure, stress intensity is plotted against crack depth for a steel pipe of 12.7mm thickness and 711mm diameter for three different residual stress distributions. It can be seen that for the upper limit residual stress distribution, stress intensity continues increasing sharply with crack depth. For the mean residual stress distribution, in which the middle portion experiences compressive residual stress, crack propagation is shown to plateau before increasing further (as for why it does not fall below zero, this is due to Andresen's use of the Buchalet and Bamford approach, in which K responds to the integrated area under a polynomial residual stress curve rather than its value at any given point). For the lower limit residual stress distribution, the stress

intensity drops to zero, signaling a cease in crack growth. From this figure it can be clearly seen how strongly a dip to low tensile stress or into compression can affect stress intensity through the thickness of a material.

Stress intensity does not need to reach as far as zero in order for crack growth to stop. There exists a nonzero threshold value of K_I, known as K_{ISCC}, that K_I must exceed in order for stress corrosion cracks to propagate. K_{ISCC} is defined as the crack intensity at which the measured SCC crack growth rate is essentially zero in short-time tests. [Uhlig and Revie, 2008]. If residual tensile stresses reach sufficiently low values, K_I will be lowered below the threshold value and crack propagation will cease.

In a paper by Brisson, Ballinger, and McIlree, the threshold value of K for K-driven crack growth in mill-annealed alloy 600 tubing in high temperature caustic was found to be approximately $4MPa\sqrt{m}$ [Brisson, Ballinger, and McIlree, 1998]. It should be noted that there have been papers that claimed much higher values of K_{ISCC} for chloride-assisted SCC in 304. However, this is likely due to the fact that values of K_{ISCC} can be extremely time-consuming to establish and often tests are not observed for enough time to be able to determine the true threshold value. They are found by conducting experiments at very low crack growth rates, and in some cases the claimed values indicate nothing more than the patience of the observer [Speidel, 1975]. For this reason, choosing a lower K_{ISCC} is a reasonable and more conservative approach.

For $K_I > K_{ISCC}$, there are three distinct regions of K_I within which the relationship between K and the log of the crack velocity, da/dt, changes. In region I, at low levels of K_I just above the threshold, crack growth rate is highly sensitive to K_I. The functional relationship in this region can often be approximated as an exponential (appearing linear in a log-linear plot,

such as Figure 5.3) [Speidel, 1975]. After K_I becomes large enough, crack growth enters region II. In region II, da/dt is independent of K_I but instead is highly sensitive to other corrosion variables such as pH, viscosity, and temperature (this is the region within which many of the crack growth measurements in Section 5.B. were taken). If K_I becomes large enough, without the component in question failing within regions I or II, it will enter region III where once again crack growth rate is highly sensitive to K_I [Uhlig and Revie, 2008].

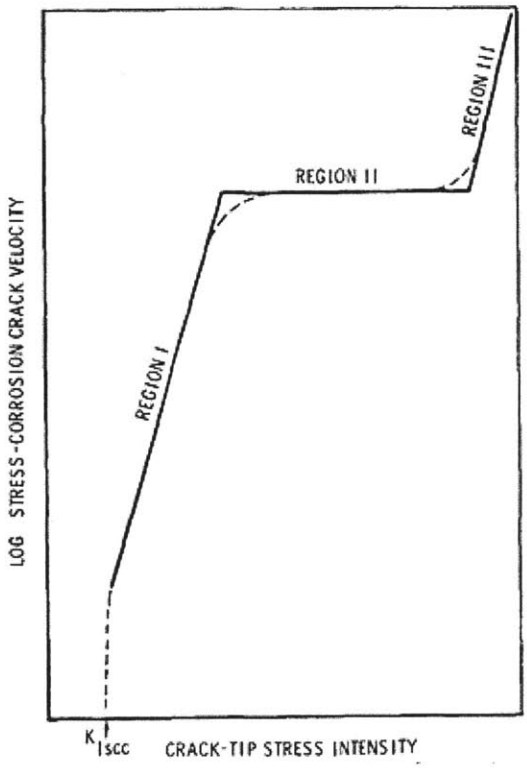

Figure 5.3 - Three regions of stress intensity's effect on crack velocity [Speidel, 1975]

The shape of da/dt vs. K relationship in Figure 5.3 is not immune the effects of the environment. With increasing relative humidity, region I expands by shifting to lower stress intensities, and region II is shifted to higher velocities [Uhlig and Revie, 2008]. Region III remains unaffected, and with increasing water vapor pressure, the region II's range of K_I values

can shrink. This can be observed in Figure 5.4 below. Figure 5.4a shows the expected effects of increasing vapor pressure, while Figure 5.4b shows the experimental evidence of such a shift. This information, while not exceedingly relevant for the sake of predicting residual stresses in a single, constant environment, may prove useful in future crack growth measurements once environmental factors are considered in the used fuel canister time to failure model.

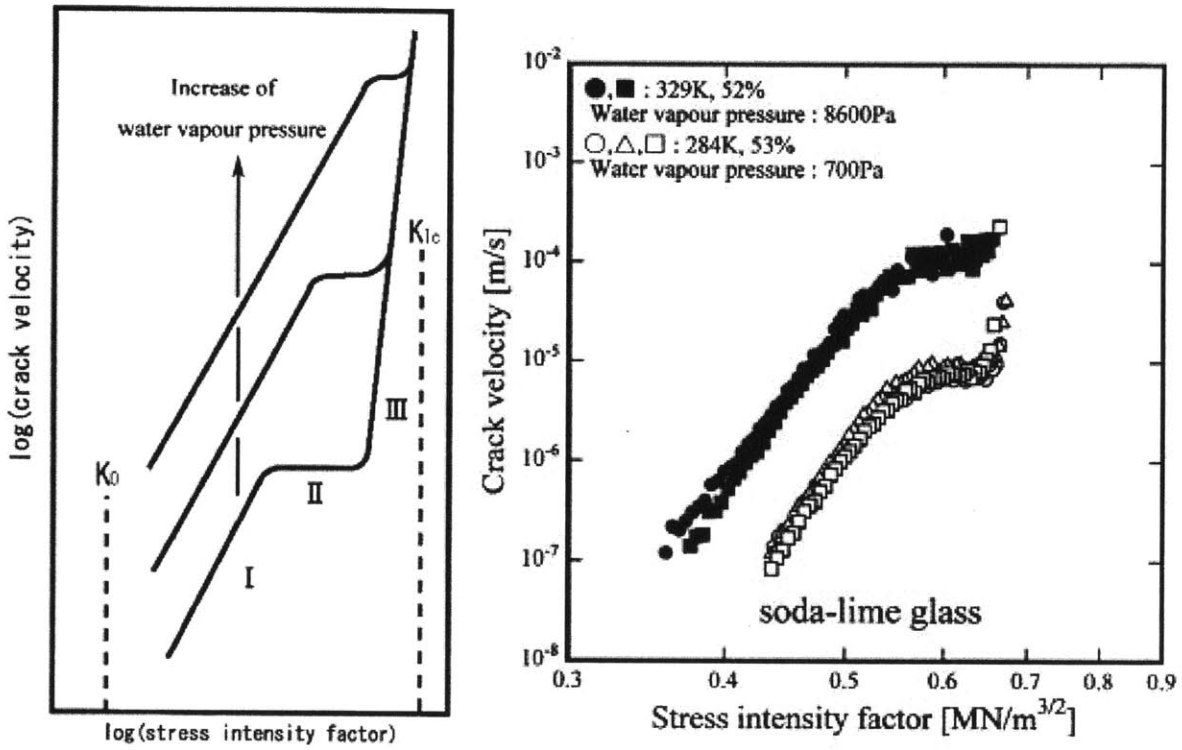

Figure 5.4- Effects of increased vapor pressure on the relationship between crack velocity and stress intensity factor – (a), schematic diagram [Atkinson, 1982], and (b) experimentally obtained results for soda-lime glass [Nara et al., 2012]

If it can be assumed that the stress is constant and on the order of the yield strength (which this thesis does not), then critical crack depth can be calculated from K_{ISCC}.

$$a_{cr} = 0.25\left(\frac{K_{ISCC}}{Y.S.}\right)^2 \quad (6)$$

where a_{cr} is the critical crack depth, beyond which the component will fail [Uhlig and Revie, 2008]. Again, such a concept assumes that the stress will not go compressive or below the stress

intensity threshold beyond the critical crack depth, however this thesis has shown that in welded stainless steel applications such as the used fuel canister, this is a very real possibility.

5.A.2. Calculating the Stress Intensity Factor for Used Fuel Canister Material

Because the ratio of radius to thickness of canister material is so great in used fuel storage canisters, the curved surface can safely be approximated as a flat surface for the purpose of calculating stress intensity factors. A crack propagating inwards from the outer surface will then take a semi-elliptical shape, similar to that shown in Figure 5.5 below.

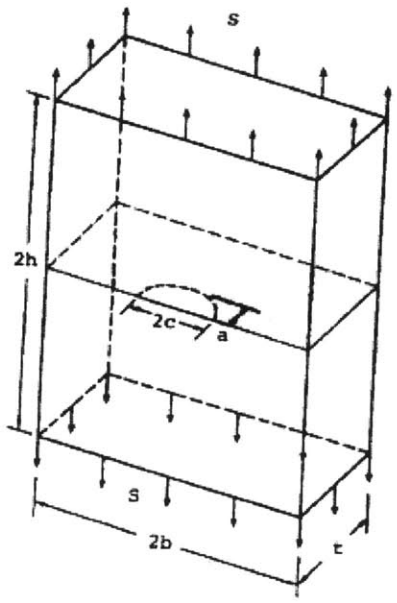

Figure 5.5- Semi-elliptical surface crack in a plate subjected to tension [Raju and Newman, 1979]

The stress intensity factor equation for cracks in three dimensional finite bodies is shown below [Lewis and Sines, 1983]:

$$K_1 = \sigma\sqrt{\frac{\pi a}{Q}}F(\frac{a}{t},\frac{a}{c},\frac{R}{t},\varphi,) \tag{7}$$

Q is the shape factor for the elliptical crack, a function of its width and depth:

$$Q = 1 + 1.464\left(\frac{a}{c}\right)^{1.65} \quad (8)$$

Equation 8 applies only when the crack is wider than it is deep (c > a). If the ellipse (crack) is deeper than it is wide (a > c), the a/c term is replaced with c/a. Further research may give greater insight into the exact shape of the average chloride-induced stress corrosion crack, though until that time the assumption will be made that the cracks are circular, such that a = c.

F, the boundary correction factor, accounts for the influence of the specimen's dimensions, and is a function of crack depth, crack length, hole radius (in certain applicable circumstances), plate thickness, and the parametric angle of the ellipse. Because of its dependence on many variables, F is often calculated for many scenarios using finite element analysis. As for the parametric angle of the ellipse, the stress intensity factor increases more rapidly near the intersection of the crack and the free surface (ϕ=0) than it does at the deepest point (ϕ= π/2). However, since the greatest concern is with crack propagation through the thickness rather than along its length, the focus here will be on boundary correction factors for ϕ= π/2.

Table 5.1 - Boundary Correction Factor for semi-elliptical surface cracks subjected to tension (v=0.3, a/c=1, φ =π/2) [Raju and Newman, 1979]

a/t	F
0.2	1.049
0.4	1.062
0.6	1.107
0.8	1.112

5.B. Crack Growth Rates

In order to build a model for canister lifetime, crack growth rate data will be needed. Once canister mock-up material is received, there will be experiments to obtain data for crack

growth rates on actual canister material in their actual environments, as well as in several lab-controlled accelerated corrosion settings. In the meantime, as was done with residual stresses, we can make use of the literature to obtain the best available approximations. There have been several papers that have investigated the crack growth rate of stainless steel due to chloride-induced SCC, which are discussed here.

5.B.1. Kosaki 2008

Kosaki obtained SCC propagation rates in 304, 304L, and 316LN for both natural exposure and in accelerated tests using three-point bend specimens as shown in Figure 5.6. The specimens measured 10mm x 15mm x 90mm, and were pre-cracked with either through cracks or half elliptical surface cracks. They were then loaded to either 0.4PS or 0.8PS, and subjected to a temperature of 60°C, 95% relative humidity, and a NaCl mist. The natural exposure tests were conducted at Miyakojima Island, a location known for its highly corrosive environment.

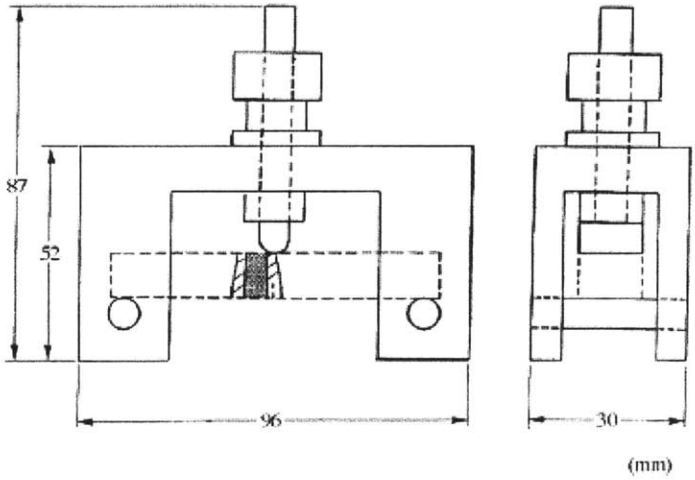

Figure 5.6- Three-point bend specimen and apparatus for accelerated SCC propagation tests [Kosaki, 2008]

The accelerated tests resulted in da/dt (also known as crack growth rate or CGR) values of 1.0×10^{-10}m/s to 3.5×10^{-9}m/s in the K range of 0.5-30MPa$\sqrt{m}$ for SCC propagation in Type

304 and Type 304L stainless steel. The natural exposure tests resulted in CGR values of 1.2×10^{-12} to 1.8×10^{-11} m/s in the K range of 0.6-9.0 MPa$\sqrt{m}$, roughly two orders of magnitude slower than the accelerated tests. To put these values in perspective, the natural exposure da/dt values roughly equate to 0.04-0.6mm/year, which would take about 25-375 years to penetrate 15mm, or slightly less to penetrate through 1.27cm (0.5in). Both the natural and accelerated conditions were independent of K, indicating that the observed crack growth likely occurred in region II [Kosaki, 2008].

5.B.2. Shirai et al. 2011

Shirai, Tani, Takeda, Wataru, and Saegusa measured crack growth rates under various conditions using four-point bend specimens in Type 304 stainless steel. The specimens measured 10mm x 20mm x 220mm, were polished with #600 polishing paper and cleaned ultrasonically with acetone. They were then sprayed with synthetic seawater with a pH of 8.2, heated to 80°C, and were subjected to a constant bending load (Figure 5.7). Crack growth was measured by Reverse Direct Current Potential Drop, in which the potential drop through the specimen is converted to crack depth data, assuming a half elliptical crack shape. It was shown that early crack growth occurred at a fast, constant rate, then transitioned to a slower, constant rate (see Figure 5.8).

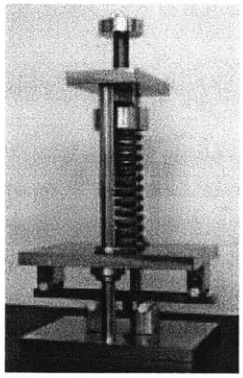

Figure 5.7- Constant load four-point bend specimen measured with RDCPD [Shirai et al., 2011]

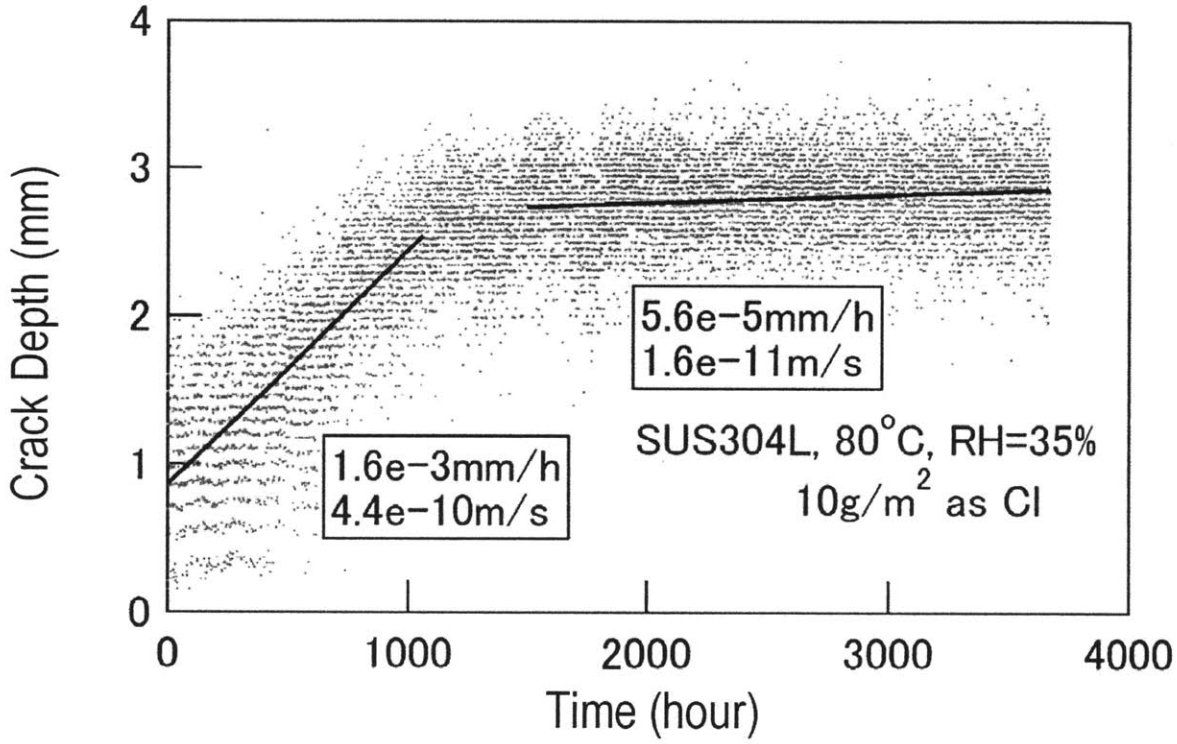

Figure 5.8 - Crack growth data for four-point bend test specimen [Shirai et al., 2011]

As is shown in Figure 5.8, the crack growth was measured as 4.4×10^{-10}m/s for the first 1500 hours, and then slowed to 1.6×10^{-11}m/s afterward. To simplify this, Shirai et al. assumed a certain initial crack size due to the initial fast crack propagation (simply taking the crack size at the end of the first 1500 hours as the initial crack size), and assumed the slow propagation rate

would hold through the rest of the wall. This through-wall CGR, (measured as $1.6x10^{-11}$m/s in the figure above) was "tentatively adopted" to be $1x10^{-11}$m/s [Shirai et al., 2011].

5.B.3. Tani et al. 2009

Tani et al. conducted crack growth rate tests for several austenitic stainless steels (including Type 304 and Type 316), as well as Type 312 duplex stainless steels, using a spring loaded specimen, similar to Shirai et al. 1/2T compact tension, or CT, specimens were used. Specimens were placed in the loading apparatus, as shown in Figure 5.9 below, and 20μL of synthetic seawater was injected into the machined notch. A load was then applied to give a stress intensity factor between 5MPa$\sqrt{m}$ and 30MPa$\sqrt{m}$. Specimens were held at 50°C and 80°C with a relative humidity of 35%. Crack length was measured using alternating DC potential drop. After testing, specimens were fractured by fatigue cycle, and the fractured surface was examined by SEM. Average crack length was measured, and along with the potential drop data, the CGR was calculated.

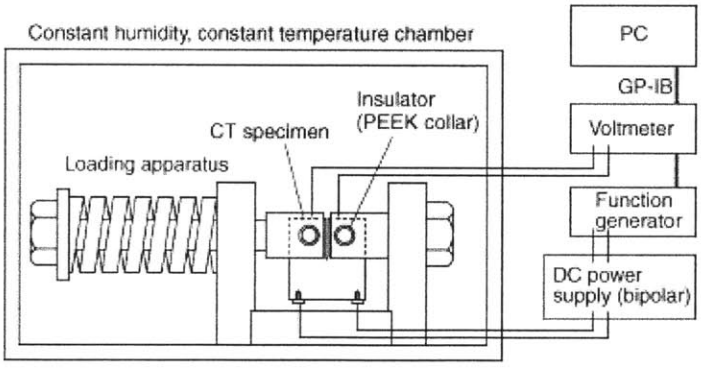

Figure 5.9- Experimental crack growth measurement apparatus [Tani et al., 2009]

The results of a crack growth rate test on a Type 316 CT specimen are shown in Figure 5.10 below. Crack growth rates of approximately $3x10^{-10}$m/s were obtained for K larger than 10MPa$\sqrt{m}$. No dependence of CGR on K was observed (see Figure 5.11). Crack growth rates

for samples at 50°C were found to be 400 times slower than for those held at 80°C. Also, for samples held at the same temperature, Type 316 showed a CGR 750 times faster than that of the duplex Type 312. These results were consistent with the results of a constant load test.

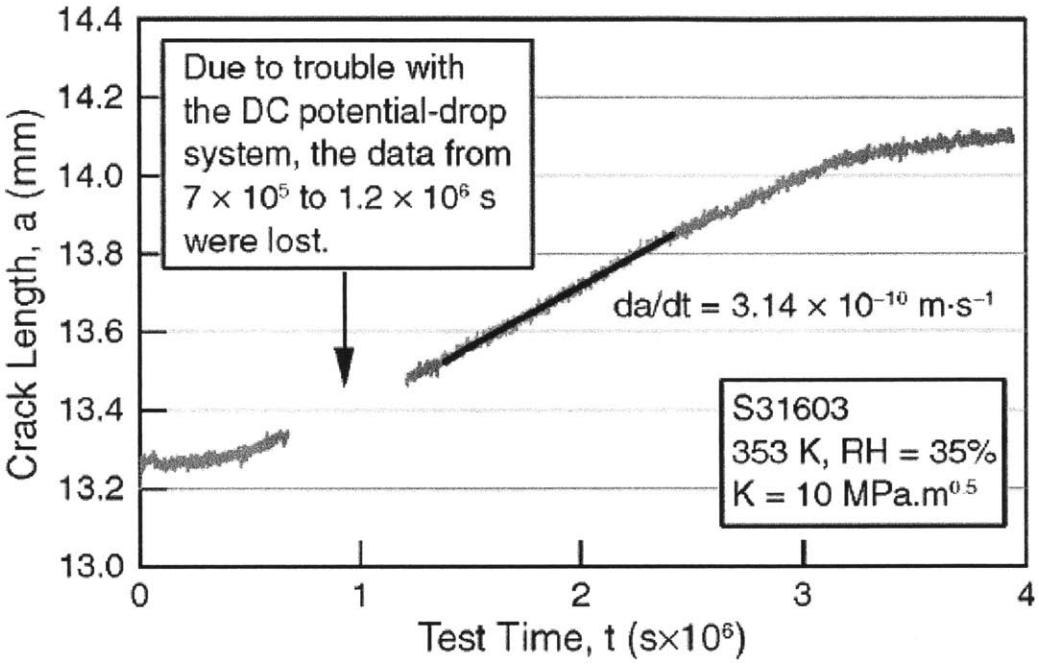

Figure 5.10- Crack length vs. time for a 316 stainless steel CT specimen held at 80°C with RH=35% [Tani et al., 2009]

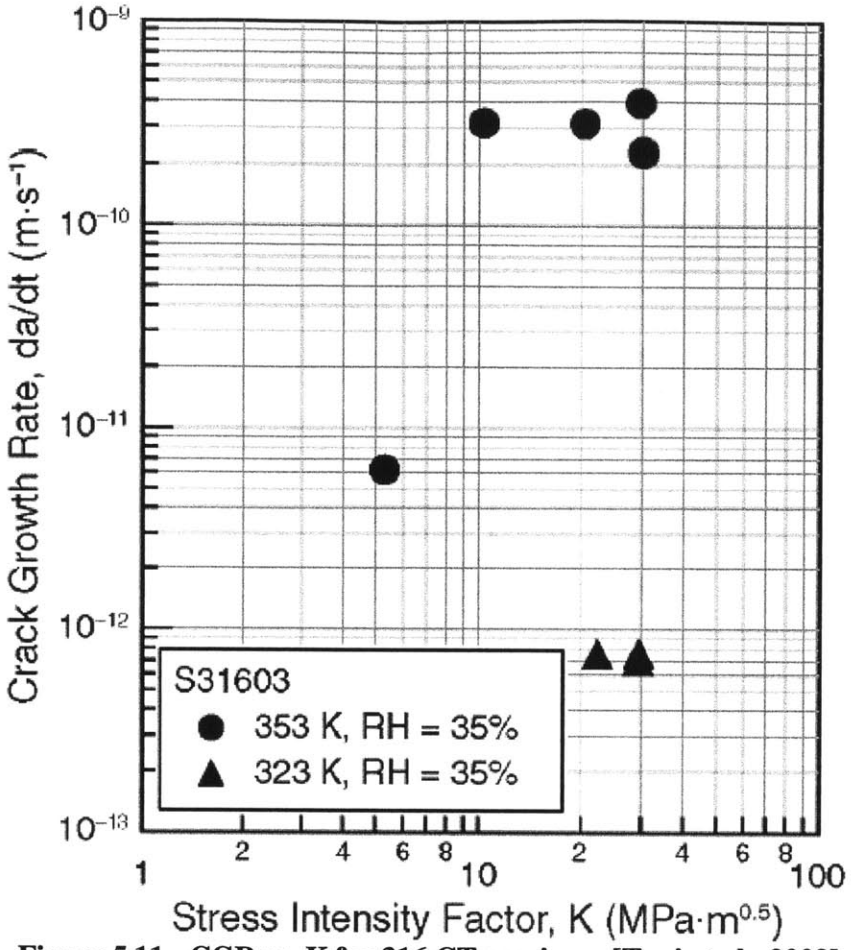

Figure 5.11 - CGR vs. K for 316 CT specimen [Tani et al., 2009]

5.B.4. Crack Growth Rate Summary

Table 5.2 contains a simplified summary of the CGR literature review. While the samples were of different dimensions, exposed to different temperatures and chemicals, comprised of slightly different materials, placed under different loads, in addition to number of other differences, they comprised the best available data for CGR data of Cl-SCC in austenitic stainless steel. Eventually, actual CGR data will be available, but for the time being, this will suffice to demonstrate the importance of the residual stress distribution in modeling canister lifetime.

Table 5.2 - Simplified summary of CGR literature review

	CGR (m/s)	Stress Intensity Range ($MPa\sqrt{m}$)
Kosaki et al. accelerated	$1.0x10^{-10}$ to $3.5x10^{-9}$	0.5 to 30
Kosaki et al. natural exposure	$1.2x10^{-12}$ to $1.8x10^{-11}$	0.6 to 9
Shirai et al.	$1x10^{-11}$	Not specified
Tani et al.	$3x10^{-11}$	> 10 (10-30?)

6. Results- Tentative Life Prediction Model

6.A. Estimated Residual Stress Profile

First, an estimate will be made for the residual stress distribution in the HAZ of a weld in used fuel canister material, with typical specifications as follows:

- 1.27cm (0.5in) thick
- 152.4cm - 177.8cm (60-70in) diameter
- Circumferential weld (for the reason that there is more literature on circumferential welds, and no reason to believe it will be any less susceptible to failure by SCC than axial welds, which given the large diameter should behave very similarly)
- Double-V
- Submerged Arc welded (likely 4-6 passes)
    - Specifications unknown (though likely tacked in place with TIG, then submerged arc welded for 4-6 passes. Each axial weld of the shell will likely be completed first, with the circumferential shell weld coming later to join the two shell halves in the center)

Using data from the residual stress literature review of Section 4 as a guide, a residual stress profile estimate for the hoop stress (chosen because hoop stresses are shown to be of greater magnitude than axial stresses in a circumferential weld and are therefore of greater interest) was chosen and is shown below in Figure 6.1. The justification for this estimate is as follows:

- At 1.27cm (0.5in) thick, the residual stress is likely to be smaller in magnitude than the 3.81cm (1.5in) welds of Ogawa et al. and the 2.23cm (0.9in) welds of Deng, Murakawa, and Liang. There is less weld metal, decreasing the magnitude of expansion/compression.
- For a double-V weld, the residual stress distribution is expected to be generally symmetric, as there would be roughly as much weld metal on the inner and outer surface, with a similar shape to the distribution of the ferritic weld of Dong, Zhang, and Rawls.
- Stresses should be slightly less in magnitude than those of Dong, Zhang and Rawls for the following reasons:
    - The yield strength of weld metal used by Dong, Zhang and Rawls is significantly greater than that of the base metal [matweb.com, 2013] which was shown in the case of Deng, Murakawa, and Liang to result in a much more varied distribution while allowing for higher tensile stresses.
    - The Type 304 stainless steel has a slightly lower yield strength than the 232MPa yield strength of the A285 used in that particular experiment. Otherwise, the two metals have generally similar mechanical properties [matweb.com, 2013].

- Because the canisters are fabricated from flat stainless steel plate which is then rolled into its circular shape, it is expected that the outer surface is in slight tension with the inner surface in slight compression prior to welding. This would suggest, all other factors being equal, that the outer half of the thickness would be slightly more tensile than the inner half
- It is expected that the surface of welds will be ground flush for the canister to fit smoothly in the surrounding overpack. This could result in a compressive layer on the outer surface, though as is shown in [Iancu et al., 1990] this layer will likely not penetrate further than a fraction of a millimeter. Because this model will focus solely on crack propagation rather than initiation, it will be assumed that the stress concentrator which initiates the crack has already penetrated through this compressive layer.
- Internal canister pressure from the helium backfill, gaseous fission products, and high internal temperature were shown to result in a potential maximum of 50MPa of additional hoop tensile stress. This conservative value is not likely to be approached in reality, though the baseline of hoop stress throughout the thickness will be raised due to its presence.
- While all of the many factors mentioned previously in this thesis are expected to play some role in the residual stress state of a canister weld, those discussed in this list are the most likely to influence the canister weld in a manner such that its residual stress distribution would differ significantly from the welds examined in the literature review.

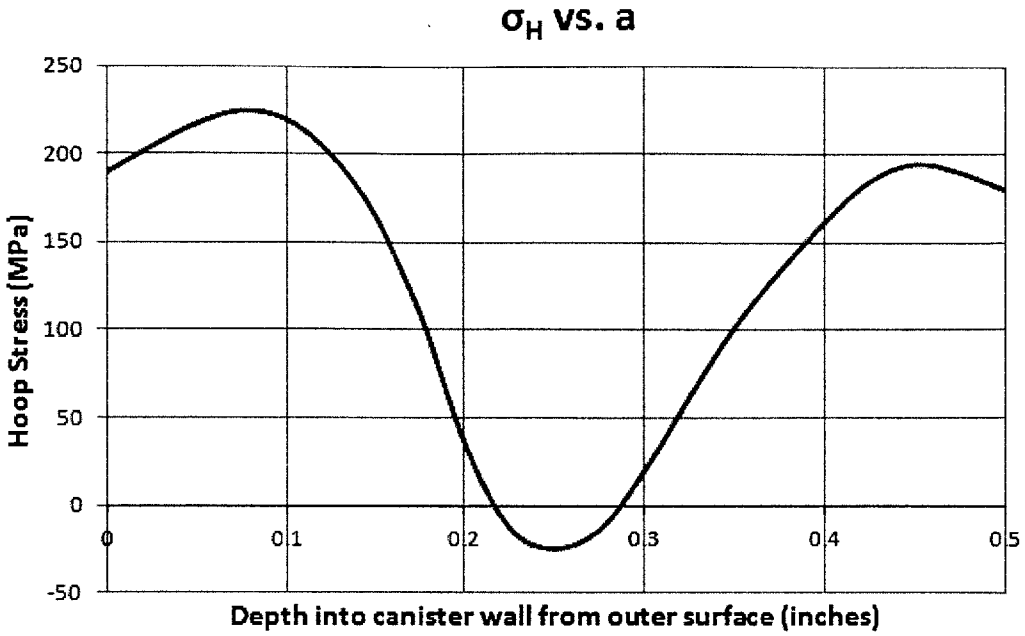

Figure 6.1 - Estimated residual stress distribution for hoop stress (σ_x) in the HAZ of a circumferential used fuel storage canister weld

The stress profile in Figure 6.1 was constructed by assigning a residual stress value every 0.635mm (0.025in) using the assertions listed above to estimate the hoop residual stress (σ_x) in the HAZ of a circumferential used fuel canister weld. It will be used in estimating the residual stress distribution's effect on time to failure predictions.

In order to showcase the dramatic effects of residual stress on time to failure, two other residual stress cases will be used along with this distribution. Because the estimated distribution goes compressive, the other two cases will showcase what can be expected if the residual stress distribution is more highly tensile. This would be similar to the finite element analysis of Deng, Murakawa and Liang as seen in Figures 4.20 and 4.21, in which the hoop stress within the weld metal remained highly tensile throughout the entire thickness. Based on the results of this investigation, it is expected that the residual stress in a double-V weld will not be as tensile as that example in particular, and that SCC is less likely to occur in the weld metal than it is to

occur in the HAZ. However, in order to explore the implications of this possibility as well as to demonstrate the importance of residual stress distributions on modeling time to failure, additional residual stress distributions will be included to compare the effects on time to failure of one residual stress profile that comes very close to the stress intensity threshold, and another that remains highly tensile throughout the material thickness.

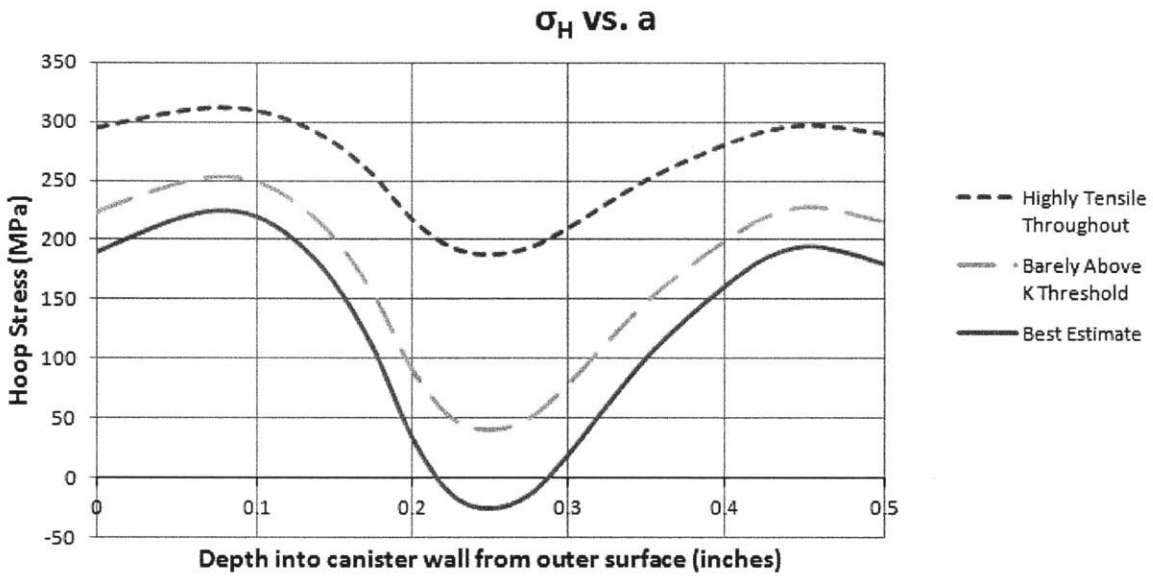

Figure 6.2 - Estimated residual stress distributions for hoop stress (σ_x) in a circumferential canister weld. Best estimate compared with two additional, more conservative, estimates

6.B. Estimated Stress Intensity

Stress intensity can be estimated using equations 7-8 as well as Table 5.1. Assuming a circular crack, such that a=c, the shape factor 'Q' is calculated to be 2.464. The boundary correction factors, F, are taken from Table 5.1, according to which value of a/t is closest for each data point (this is broken down in Table 6.1). Together with the residual stress values of Figure 6.2, this was used to assign an estimated stress intensity factor to each estimated data point.

Table 6.1- Range of a/t values which were assigned a respective boundary correction factor from Table 5.1

Range of a/t in residual stress estimate applied to each value of F	F	a/t at which this value of F was actually calculated
$0 < a/t \leq 0.3$	1.049	0.2
$0.3 < a/t \leq 0.5$	1.062	0.4
$0.5 < a/t \leq 0.7$	1.107	0.6
$0.7 < a/t < 1$	1.112	0.8

The threshold of stress intensity used here is that mentioned in Section 5.A.1. It was chosen as $4MPa\sqrt{m}$, serving as the value below which crack propagation is assumed to not exist. A graph of the stress intensity factors for each residual stress distribution is shown below in Figure 6.3. Notice how the "Barely Above K Threshold" distribution narrowly avoids falling below $4MPa\sqrt{m}$. If the residual stress of this distribution was slightly more compressive, crack arrest would occur. This is what is seen occurring with the "Best Estimate" distribution in which K falls below the K_{ISCC} value of $4MPa\sqrt{m}$, after which the crack no longer propagates. In reality, this would only mean that the stress-driven cracking mechanism would no longer be driving crack growth. Instead, it is likely that corrosive pitting would take over, though at roughly 20μm/year, this mechanism is orders of magnitude slower [Rigby, 2010].

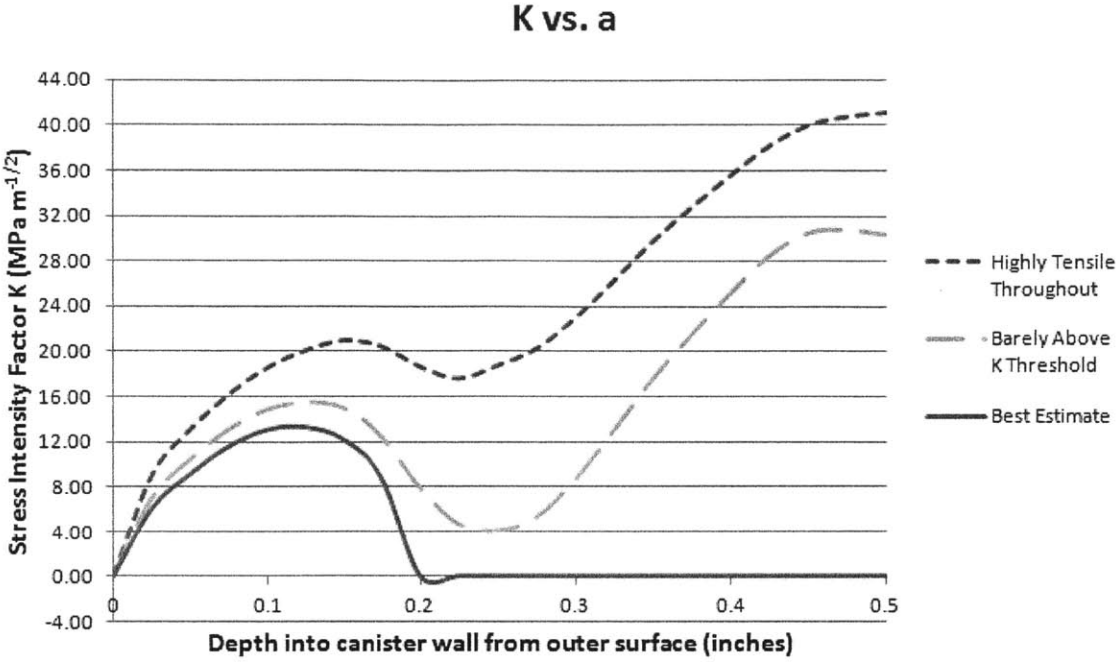

Figure 6.3 - Stress intensity factor vs. depth of crack penetration for three estimated residual stress distributions

6.C. Estimated Crack Growth Rate (da/dt)

Using the results of the crack growth rate literature review in Section 5.B. (summarized in Table 5.2), crack growth rates can be estimated from the graph of K vs. a in Figure 6.3. For values of K below the stress intensity factor threshold of 4MPa$\sqrt{m}$, a CGR of 0m/s is assigned (per the definition of the stress intensity factor threshold). Between 4 and 10 MPa$\sqrt{m}$, a CGR of 9.6×10^{-12}m/s is assigned. This is taken from [Kosaki, 2008] in which the natural exposure tests resulted in CGR values of 1.2×10^{-12} to 1.8×10^{-11}m/s in the K range of 0.6 to 9.0 MPa$\sqrt{m}$. 9.6×10^{-12}m/s is the average CGR over this range. Above 10MPa$\sqrt{m}$, a CGR of 3×10^{-11}m/s is assigned, taken from [Tani et al., 2009] in which 3×10^{-11}m/s was the CGR reported for stress intensity factors above 10MPa$\sqrt{m}$. These chosen CGRs are listed in Table 6.2.

Table 6.2- Crack growth rate approximations for estimated residual stress distributions

Stress Intensity Range ($MPa\sqrt{m}$)	da/dt (m/s)	Source
K < 4	0	Below threshold: [Brisson et al.]
4 ≤ K < 10	9.6E-12	Calculated average: [Kosaki 2008]
10 < K	3E-11	Reported value: [Tani et al.]

While this is an admittedly crude approximation for crack growth rate through the thickness of a canister weld, it is the most informed set of assumptions that can made based on the available literature until actual canister material can be received to measure residual stresses and perform crack growth rate experiments. While this may result in limited confidence in the final numerical results of this exercise, the approximation remains sufficient for demonstrating the magnitude of the effect of residual stress distributions on time to failure of canister material. A graph of these estimated crack growth rates vs. depth into canister material can be seen in Figure 6.4.

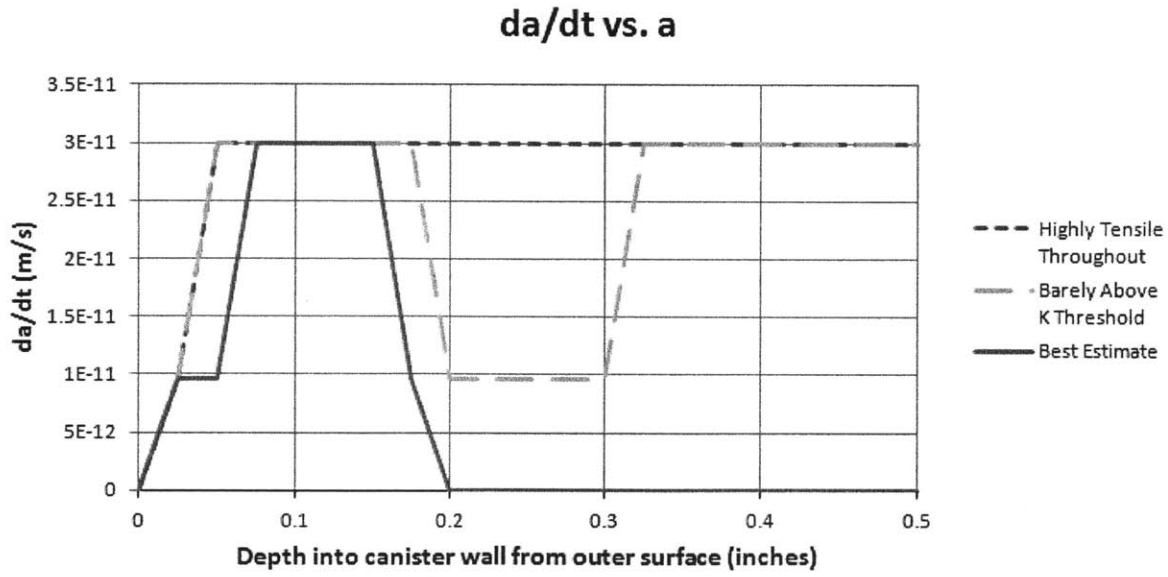

Figure 6.4 - Crack growth rate for three estimated residual stress distributions

In order to calculate the time to failure from da/dt and a, an adjustment must be made. Having a set of constant da/dt values over certain ranges of K, one can also obtain a set of

constant dt/da values over the same ranges of K by simply inverting the non-zero da/dt values. The inherent information is unchanged, but in the form of dt/da it allows one to estimate time to failure. By plotting a graph of dt/da vs. a (representing the amount of time it takes to penetrate through a unit of thickness at each location in the material), the area under can be integrated with respect to 'a' (in meters) in order to obtain the estimated time to failure.

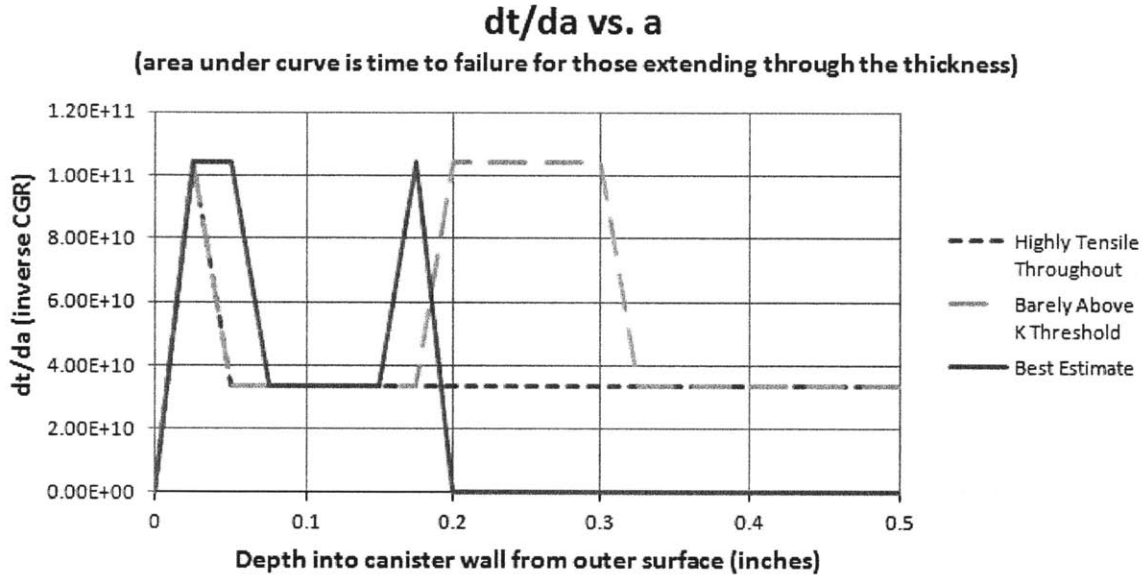

Figure 6.5 – dt/da vs. a, the area under which (for each distribution reaching 1.27cm or 0.5in with a nonzero stress intensity factor) is the total time to failure

Because the assumption is that once a crack's stress intensity falls below the threshold that the crack ceases to grow, integration will only give meaningful values to those distributions whose cracks penetrate through the entire thickness. The trapezoidal method (equation 9) was employed to calculate the area under the graph of dt/da vs. a:

$$\int_a^b f(x)\,dx \approx (b-a)\frac{f(a)+f(b)}{2} = (0.000635m)\frac{dt/da(a_i)+dt/da(a_{i+1})}{2} \qquad (9)$$

The estimated time to failure by SCC after crack initiation for the three residual stress distributions is shown below in Table 6.3.

Table 6.3- Estimated time to failure

Residual Stress Estimations:	Calculated Time to Failure:
Highly Tensile Throughout	15 years
Barely Above K Threshold	22 years
Best Estimate	Did not fail

Once again, because of the approximations that were made along the way to reaching these results, the times to failure reported in Table 6.3 should not be taken at face value, but rather should serve to demonstrate how greatly the time to failure can depend on the subtleties of the residual stress distribution. The "Barely Above K Threshold" distribution narrowly missed out on avoiding failure from cracking altogether. Also, in comparison with "Highly Tensile Throughout", while the residual stress distributions were not completely dissimilar, the time failure of each varied by over 30% from one another. From these results, it is clear that having high-resolution residual stress distributions of actual canister material will be vital in order to confidently predict the time to failure of used fuel storage canister material by SCC.

7. Conclusions and Future Work

7.A. Conclusions

This thesis has taken the first steps in the development of an estimate of the time to failure for canister material based on residual stress and uncertainties in residual stress. It has laid the groundwork for such a model to be built once the data is received, as well as proving the importance of accurate residual stress data in modeling time to failure by SCC. While the general shape of the residual stress profile has been shown to be governed by (among other factors) the joint geometry, within the bounds of a particular design (single-V, double-V, etc.) there is considerable uncertainty of the design as well as uncertainty within multiple welds of the same design. This level of variability and uncertainty will require a probabilistic time to failure model that accounts for uncertainty in time to failure.

Descriptions of the many dry fuel storage canisters, welding specifications, and residual stress factors have been compiled to aid in this endeavor. This compilation will be used moving forward as a reference for understanding the complex mechanical environment of the canister, as a basis for what to expect from canister residual stresses, and as a starting point for using residual stresses to predict time to failure.

It has been shown that the life prediction of used fuel storage canister material depends heavily on the extremely complex residual stress distribution through the thickness of the welded canister wall. Should the high-resolution residual stress measurements show that stresses go compressive or near-compressive, it could mean that dry storage can be relied on for longer than previously expected. If instead it is shown that stresses remain tensile throughout the wall thickness, then new work can begin on adopting welding techniques or surface treatments to create desirable residual stresses in order to improve the longevity of dry storage casks. It is of note that for a double-V configuration, it is possible for there to be a compressive region for σ_x (hoop stress in a circumferential weld or axial stress in an axial weld), and even more likely for σ_y (axial stress in a circumferential weld or hoop stress in an axial weld).

As was mentioned previously, this thesis focuses on crack propagation, and not on crack initiation. In many of the weld designs examined, a tensile residual stress is present at the surface. If one were to choose to solve the problem of SCC in canister welds by first choosing a joint geometry and welding procedure that result in a sub-surface region of compressive stresses, one might also attempt to induce near-surface compressive stresses with a technique such as shot peening or low plasticity burnishing. Caution should be taken, however, since the surface treatment would influence the underlying stress distribution.

7.B. Future Work

In order to obtain the information necessary to build a high-resolution model for predicting canister failure by SCC, residual stress measurements of actual canister welds are needed. Given the variability of the design of the major cask systems, it will be critical that actual residual stress distributions, including uncertainty, be measured with enough statistical confidence to be able to develop a probabilistic model for canister failure. As it would be near-impossible to take such high-resolution residual stress measurements on actual, loaded used fuel storage canisters, accurate mock-up canister shells should be fabricated, manufactured and welded to precisely the same specifications as the actual canisters, in order to mimic their residual stress distributions as closely as possible. They should be of the same thickness, diameter, and material as the canisters (though may be somewhat shorter in length), and must be fabricated and welded in precisely the same fashion (keeping in mind that some variation exists between different welders of the same canister design). A schematic of one such mock-up is included below in Figure 7.1

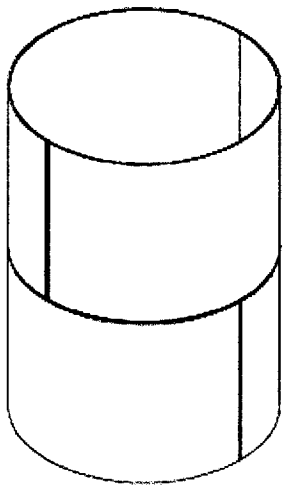

Figure 7.1- Drawing of a canister mock-up

Once received, these canister mock-ups should be sectioned for a number of experiments, including (but not limited to) using the contour method of residual stress measurement to obtain high-resolution residual stress distributions. Measurements should be taken in the HAZ of canister welds, both parallel and perpendicular with the circumferential and axial welds. Measurements should also be taken in the area of the intersection of the axial and circumferential welds (known as the 'T' joints), as it is likely that the σ_x of the axial welds will add to the σ_y of the circumferential weld, and vice-versa, potentially creating a region of unusually high tensile stress. In addition to these measurements, samples should be subjected to both on-site and experimentally accelerated crack growth studies to obtain more useful and relevant CGR data which takes into account the various environments endured by the canisters. Together, this information can then be used to build a high-confidence probabilistic model for time to canister failure as a function of residual stress distribution.

References

Andresen, P. L. "Emerging Issues and Fundamental Processes in Environmental Cracking in Hot Water." *Corrosion* 64.5 (2008): 439-64. Web.

ASME Boiler and Pressure Vessel Code, Sec. III (2007). Print.

ASTM International. ASTM C 1553 – 2008, "Standard Guide for Drying Behavior of Spent Nuclear Fuel," Pp. 1-16. (2008).

Atkinson, Barry Kean. "Subcritical Crack Propagation in Rocks: Theory, Experimental Results and Applications." *Journal of Structural Geology* 4.1 (1982): 41-56. Web.

Azom.com, "Tungsten Inert Gas (TIG) Welding of Aluminium Alloys - The Principles and The Process." *Azom.com.* N.p., 14 Aug. 2003. Web. 09 May 2013.

Bailly, Frederic. Spent Fuel Storage and Transportation Technologies, Nevada Workshop, Pahrump, Nevada, June 9, 2005.

Bare, W. C., and L. D. Torgerson. *Dry Cask Storage Characterization Project- Phase I: CASTOR V/21 Cask Opening and Examination*. Rep. No. INEEL/EXT-01-00183. Idaho National Engineering and Environmental Laboratory, 2001.

Black, J. Temple., Ronald A. Kohser, and E. Paul DeGarmo. *DeGarmo's Materials and Processes in Manufacturing*. 10th ed. Hoboken, NJ: Wiley, 2008. Print.

BNG FuelSolutions 2005, Steven Sisley, Licensing/Regulatory Compliance Manager, BNG Fuel Solutions, to U.S. NRC Document Control Desk, Subject: Amendment Request for the VSC-24 Ventilated Storage System Certificate of Compliance, BFS/NRC 05-014, Docket No. 72-1007, June 30, 2005.

Boyce, B. L., P. I. Reu, and C. V. Robino. "The Constitutive Behavior of Laser Welds in 304L Stainless Steel Determined by Digital Image Correlation." *Metallurgical and Materials Transactions A* 37.8 (2006): 2481-492. Web.

Bray, D. P., and R. J. Dennis. "Finite Element Residual Stress Analysis of a Girth-Butt Weld Joint." *Modelling Methodology and Analysis Procedure, FNC* 1 (2006)

Brisson, B. W., R. G. Ballinger, and A. R. Mcllree. "Intergranular Stress Corrosion Cracking Initiation and Growth in Mill-Annealed Alloy 600 Tubing in High-Temperature Caustic." *Corrosion* 54.7 (1998): 504-14. Web.

Brooks, J.A. and J.C. Lippold, ASM Handbook, 1996.

Callister, William D. *Materials Science and Engineering: An Introduction.* 7th ed. New York: John Wiley & Sons, 2007. Print.

Campbell, John. *Complete Casting Handbook.* Oxford, UK: Elsevier Butterworth-Heinemann, 2011. Print.

Cheng, W., I. Finnie, M. Gremaud, and M. B. Prime. "Measurement of Near Surface Residual Stresses Using Electric Discharge Wire Machining." *Journal of Engineering Materials and Technology* 116 (1994): n. pag. Web.

Cheng, Xiaohua, John W. Fisher, Henry J. Prask, Thomas Gnaupel-Herold, Ben T. Yen, and Sougata Roy. "Residual Stress Modification by Post-weld Treatment and Its Beneficial Effect on Fatigue Strength of Welded Structures." *International Journal of Fatigue* 25.9-11 (2003): 1259-269. Web.

Chu, S., S. DePaula, A. Hsia, J. Kessler, C. King, S. Leblang, M. Lombard, Z. Martin, R. McCullum, M. Nichol, and S. Ruffin. *Used Fuel Dry Storage Stainless Steel Canister Stress Corrosion Cracking Susceptibility Assessment: R&D Roadmap Leading to*

Identification of Canisters Potentially Susceptible to Stress-Corrosion Cracking. Issue brief. N.p.: EPRI, 2013. Print.

Content, Thomas. "Kewaunee Nuclear Power Plant Shutdown Cost Is Nearly $1 Billion." *JSOnline*. Milwaukee Wisconsin Journal Sentinel, 20 Apr. 2013. Web. 13 May 2013. <http://www.jsonline.com/business/kewaunee-nuclear-power-plant-shutdown-cost-is-nearly-1-billion-lr9j5fg-203912611.html>.

Davis, J. R. *Corrosion of Weldments*. Materials Park, OH: ASM International, 2006. Print.

Deng, Dean, and Hidekazu Murakawa. "Numerical Simulation of Temperature Field and Residual Stress in Multi-pass Welds in Stainless Steel Pipe and Comparison with Experimental Measurements." *Computational Materials Science* 37 (2006): 269-77. Web.

Deng, Dean, Hidekazu Murakawa, and Wei Liang. "Numerical and Experimental Investigations on Welding Residual Stress in Multi-pass Butt-welded Austenitic Stainless Steel Pipe." *Computational Materials Science* 42 (2008): 234-44. Web.

DePaula, Sara, and Greg Oberson. "Regulatory Issue Resolution Protocol (RIRP) Pilot: Marine Atmosphere Stress Corrosion Cracking." *NRC* (2012): n. pag. Web. <http://pbadupws.nrc.gov/docs/ML1212/ML12128A200.pdf>.

DOE, Office of Environmental Management, *License Renewal Application for the Fort St. Vrain (FSV) Independent Spent Fuel Storage Installation (ISFSI)* (Materials License SNM-2504), Docket 72-9, Status Updated, Presentation to the U.S. Nuclear Regulatory Commission, March 12, 2009.

Dong, P., and F. W. Brust. "Welding Residual Stresses and Effects on Fracture in Pressure Vessel and Piping Components: A Millennium Review and Beyond." *Journal of Pressure Vessel Technology* 122 (2000): n. pag. Web.

Dong, P., J. Zhang, and G. Rawls. "Crack Growth Behavior in Residual Stress Field in Vessel Type Structures." 2003.

"Dry Cask Storage of Nuclear Spent Fuel." Division of Spent Fuel Storage and Transportation, U.S. NRC, 2011, Web.

"Dry Casks." *www.storenuclearfuel.com.* Web. 08 May, 2013.

Effects of Marine Environments on Stress Corrosion Cracking of Austenitic Stainless Steels, EPRI, Palo Alto, CA: 2005. 1011820.

EPRI, *Industry Spent Fuel Storage Handbook.*, Palo Alto, CA: 2010. 102048.

Evans A, Johnson G, King A, Withers PJ. "Characterization of Laser Peening Residual Stresses in Al 7075 by Synchrotron Diffraction and the Contour Method". Journal of Neutron Research 15:147-154. (2007).

Garverick, Linda. *Corrosion in the Petrochemical Industry.* Materials Park, OH: ASM International, 1994. Print.

George, D., D. J. Smith, and P. J. Bouchard. "Evaluation of Through Wall Residual Stresses in Stainless Steel Weld Repairs." *Materials Science Forum* (2000): 646-51. Web.

Gideon, B., L. Ward, D. G. Carr, and O. Muransky. "Duplex Stainless Steel Welds: Residual Stress Determination, Magnetic Force Microscopy and Susceptibility to Intergranular Corrosion." (n.d.): n. pag. Web.

Hauk, V. M., R. W.M. Oudelhoven, and G. J.H. Vaessen. "The State of Residual Stress in the Near Surface Region of Homogeneous and Heterogeneous Materials after Grinding." *Metallurgical Transactions A* 13A (1982): Web.

Hayashibara, H., M. Mayuzumi, Y. Mizutani, and J. Tani. *Effect of Temperature and Humidity on Atmospheric Stress Corrosion Cracking of 304 Stainless Steel.* Corrosion, New Orleans, LA, Paper 08492, NACE International, 2008

Holtec. "Holtec International HI-STORM 100 Cask System Safety Evaluation Report." ML003711779 (2000): n. pag. Web.

"Holtec International Final Safety Analysis Report for the HI-STORM 100." Holtec International, 18 Jan. 2010. Web.

Holtec. "Topical Report on HI-STAR and HI-STORM 100 System Deployment at High ZPA ISFSI Sites." *Holtec Report No. HI-982004* Web. 1998. <http://pbadupws.nrc.gov/docs/ML0037/ML003709644.pdf>.

Iancu, Otto T., Dietrich Munz, Bernd Eigenmann, Berthoid Schoites, and Eckard Macherauch. "Residual Stress State of Brazed Ceramic/Metal Compounds, Determined by Analytical Methods and X-ray Residual Stress Measurements." *Journal of the American Ceramic Society* 73.5 (1990): Web.

Itzhak, D., and D. Eliezer. "The Stress Corrosion Cracking of Welded Austenitic Stainless Steels in MgCl2 Solutions in the Presence of NaI Additions." *Corrosion Science* 23.12: 1285-291. Web. 1983.

Johnson G, "Residual Stress Measurements Using the Contour Method," Ph.D. Dissertation, University of Manchester, 2008.

Jones, Denny A. *Principles and Prevention of Corrosion.* Upper Saddle River, NJ: Prentice Hall, 1996. Print.

Kingston, E. J. "Advances in the Deep-hole Drilling Technique for Residual Stress Measurement." PhD Thesis, University of Bristol, 2004.

Kok, Kenneth D. *Nuclear Engineering Handbook.* Boca Raton: CRC, 2009. Print.

Kopeliovich, Dmitri. "Principles of Arc Welding." *SubsTech Substances & Technologies.* N.p., 1 June 2012. Web. 09 May 2013.

Kosaki, A. "Example of Corrosion Resistance Evaluation around the Sealing Segment on Metallic Canister", Japan Weathering Test Center Report, Pp. 53, 2002.

Kosaki, Akio. "Evaluation Method of Corrosion Lifetime of Conventional Stainless Steel Canister Under Oceanic Air Environment." *Nuclear Engineering and Design* 238 (2008): 1233-240. Web.

Lambda Technologies. "X-Ray Diffraction Residual Stress Testing." *X-Ray Diffraction Testing.* Lambda Technologies, 2012. Web. 09 May 2013. <http://www.lambdatechs.com/x-ray-diffraction-testing.html>.

LANL. "The Contour Method for Measuring Residual Stresses." *Measure Full 2-D Residual Stress Maps Over a Cross-Section.* N.p., 2012. Web. 09 May 2013. <http://www.lanl.gov/contour/>.

Lewis, J. C., and George Sines. *Fracture Mechanics: Fourteenth Symposium.* Vol. 1. Philadelphia, PA: American Soc. for Testing and Materials, 1983. Print.

Lincoln Electric, "Waveform Control Technology." *Lincolnelectric.com.* Lincoln Electric, Jan. 2006. Web. <http://www.lincolnelectric.com/assets/en_US/Products/literature/NX4240.pdf>.

Mahmoudi, A. H., S. Hossain, C. E. Truman, D. J. Smith, and M. J. Pavier. "A New Procedure to Measure Near Yield Residual Stresses Using the Deep Hole Drilling Technique." *Experimental Mechanics* 49 (2009): 595-604. Web.

Masubuchi, K. "Residual Stresses and Distortion." *Welding Fundamentals and Processes* 6A, *ASM Handbook* ASM International, (2011): 158-68. Web.

Matweb.com "Online Materials Information Resource - MatWeb." *Online Materials Information Resource - MatWeb*. N.p., N.d. Web. 10 May 2013. <http://www.matweb.com/>.

Mintz, T., L. Caseres, X. He, J. Dante, G. Oberson, D. Dunn, and T. Ahn. "Atmospheric Salt Fog Testing to Evaluate Chloride-Induced Stress Corrosion Cracking of Type 304 Stainless Steel." *Corrosion* Salt Lake City, UT, March 11-15, 2012, NACE International, 2012.

Mintz, Todd S., Leonardo Caseres, Darrell S. Dunn, and Mekonen Bayssie. "Atmospheric Salt Fog Testing to Evaluate Chloride Induced Stress Corrosion Cracking of Type 304, 304L, and 316L Stainless Steel." Corrosion, San Antonio, Texas, NACE International, 2010.

Murugan, S., Sanjai K. Rai, P. V. Kumar, T. Jayakumar, Baldev Raj, and M.S.C. Bose. "Temperature Distribution and Residual Stresses Due to Multipass Welding in Type 304 Stainless Steel and Low Carbon Steel Weld Pads." *International Journal of Pressure Vessels and Piping* 78 (2001): 307-17. Web.

NAC International, "The MAGNASTOR System: The New Generation in Multipurpose Storage." *NAC International*. NAC International, Web. 08 May 2013.

Nara, Yoshitaka, Kazuya Morimoto, Naoki Hiroyoshi, Tetsuro Yoneda, Katsuhiko Kaneko, and Philip M. Benson. "Influence of Relative Humidity on Fracture Toughness of Rock: Implications for Subcritical Crack Growth." *International Journal of Solids and Structures* 49 (2012): 2471-481. Web.

NEI, *Industry Spent Fuel Storage Handbook*, NEI 98-01, May 1998.

Neider, Tara. The Transnuclear Future Licensing Objectives and New Project Overviews, NEI Dry Storage Information Forum, May 10, 2005.

NRC. "Dry Spent Fuel Storage Designs: NRC Approved for General Use." *Dry Spent Fuel Storage Designs: NRC Approved for General Use*. NRC, 29 Mar. 2012. Web. 08 May 2013.

NRC. Office of Nuclear Regulatory Research. *A Pilot Probabilistic Risk Assessment of a Dry Cask Storage System at a Nuclear Power Plant*. By A. Malliakos. NUREG-1864. Mar. 2007. Web.

"NRC Regulations." 10 CFR 72. 2013.

Ogawa, K., L. O. Chidwick, E. J. Kingston, R. Dennis, D. Bray, and N. Yanagida. "The Measurement and Modelling of Residual Stresses in a Stainless Steel Pipe Girth Weld." ASME Pressure Vessels and Piping Division Conference, 2008.

Pagliaro, P., M. B. Prime, H. Swenson, and B. Zuccarello. "Measuring Multiple Residual Stress Components Using the Contour Method and Multiple Cuts." *Experimental Mechanics* 50 (2010): 187-94. Web.

Pagliaro, Pierluigi. "Mapping Multiple Residual Stress Components Using the Contour Method and Superposition." Thesis. University of Palermo, 2008. Web.

Prevey, Paul S. "Current Applications of X-ray Diffraction Residual Stress Measurement." *Developments in Materials Characterization Technologies* (1996): 103-10. Web.

Prevey, Paul S. "X-ray Diffraction Residual Stress Techniques." *Metals Handbook* 10 (1986): 380-92. Web.

Prime, Michael B., and Alan L. Kastengren. "The Contour Method Cutting Assumption: Error Minimization and Correction." *Experimental and Applied Mechanics* 6 (2011): 233-50. Web.

Prime, Michael B. "Cross Sectional Mapping of Residual Stresses By Measuring the Surface Contour After a Cut." *Journal of Engineering Materials and Technology* 123 (2001): 162-68. Web.

Rainwater, Steven. "Submerged Arc Welding: Then and Now." *Superior Consumables*. N.p., 29 July 2008. Web.

Raju, I. S., and J. C. Newman. "Stress-Intensity Factors for a Wide Range of Semi-Elliptical Surface Cracks in Finite-Thickness Plates." *Engineering Fracture Mechanics* 11 (1979): 817-29. Web.

Rigby, Douglas B. *Evaluation of the Technical Basis for Extended Dry Storage and Transportation of Used Nuclear Fuel.* United States Nuclear Waste Technical Review Board, 2010.

Roberts, John P. *Safety Evaluation Report Related to the Topical Report for the Foster Wheeler Modular Vault Dry Store (M.V.D.S.) for Irradiated Nuclear Fuel.* Rep. N.p.: NRC, 1998.

Saegusa, T., G. Yagawa, and M. Aritomi. "Topics of Research and Development on Concrete Cask Storage of Spent Nuclear Fuel." *Nuclear Engineering and Design* 238.5 (2008): Web.

Shirai, K., J. Tani, H. Takeda, M. Wataru, and T. Saegusa. "SCC Evaluation Test of Multi-Purpose Canister." *Water Reactor Fuel Performance Meeting* (2011): n. pag. Web.

Shirzadi, A. A., H. K. D. H. Bhadeshia, L. Karlsson, and P. J. Withers. "Stainless Steel Weld Metal Designed to Mitigate Residual Stresses." *Science and Technology of Welding and Joining* 14.6 (2009): 559-65. Web.

Singh 2010, K.P. Singh, President and CEO, Holtec International, Recent Developments and Breakthroughs in the HI-STORM and HI-STAR Technologies, NEI Dry Storage Information Forum, May 5, 2010.

Singh, K.P. *Safety and Security of HLW Storage and Transport in the 21st Century*, NEI Dry Storage Information Forum, May 3-4, 2004.

Speidel, Markus O. "Stress Corrosion Cracking of Aluminum Alloys." *Metallurgical Transactions A* 6A (1975): 631-51. Web.

StoreFUEL. 13.164 (2012): n. pag. Web.

StoreFUEL. "Cask Report - The Month in Review." *StoreFUEL* 11.127 (2009): n. pag. Web.

"Strain Gauge Measurement - A Tutorial." *National Instruments Application Note 078* (1998): n. pag. Web.

"Submerged-arc Welding." *Submerged Arc Welding Process*. TWI, 2013. Web. 09 May 2013.

Tani, J. I., M. Mayuzumi, and N. Hara. "Initiation and Propagation of Stress Corrosion Cracking of Stainless Steel Canister for Concrete Cask Storage of Spent Nuclear Fuel." *Corrosion* 65.3 (2009): 187-94. Web.

Tateishi, K., T. Hanji, and S. Hanibuchi. "Improvement of Extremely Low Cycle Fatigue Strength of Welded Joints by Toe Finishing." *Welding in the World* 53 (2009): Web.

Teng, Tso-Liang, Peng-Hsiang Chang, and Wen-Cheng Tseng. "Effect of Welding Sequences on Residual Stress." *Computers and Structures* 81 (2003): 273-86. Web.

Todreas, Neil E., and Mujid S. Kazimi. *Nuclear Systems*. New York: Taylor & Francis Group, 1990. Print.

Uhlig, Herbert Henry, and R. Winston Revie. *Corrosion and Corrosion Control: An Introduction to Corrosion Science and Engineering*. 4th ed. New York: Wiley, 2008. Print.

University of Cambridge. "DoITPoMS." University of Cambridge, 2013. Web. 12 May 2013. <http://www.doitpoms.ac.uk/tlplib/brittle_fracture/same.php>.

VEQTER, "Deep-Hole Drilling Technique." *VEQTER Residual Stress Experts*, 2013. Web. <http://www.veqter.co.uk/assets/images/PDF%20Articles/VQT-DHD-TECH-V2.pdf>.

Wacid. N.p., 2 Feb. 2003. Web. 10 May 2013. <http://wacid.kins.re.kr/GALLERY/gallery_list.aspx?page=6>.

Weigand, J. M., and J. W. Berman. "Behavior of Butt-welds and Treatments Using Low-carbon Steel under Cyclic Inelastic Strains." *Journal of Constructional Steel Research* 75 (2012): 45-54. *ScienceDirect*. Web.

Weman, Klas. *Welding Processes Handbook*. Cambridge, Eng.: Woodhead Pub., 2003. Print.

Withers, P. J., M. Turski, L. Edwards, P. J. Bouchard, and D. J. Buttle. "Recent Advances in Residual Stress Measurement." *International Journal of Pressure Vessels and Piping* 85 (2008): 118-27. Web.

Appendix

Appendix A: Dry Cask Storage Dimensions, Quantity, and Location

Table A.1- Vendor Canister Totals (as of April 3, 2012) [DePaula and Oberson, 2012] which presented this information from [StoreFuel, 2012]

Vendor	Total Loaded
Transnuclear	603
Holtec	446
NAC	269
BFS/ES	66
GNB	26
Total	**1410**

Table A.2 - Dry Cask Storage in the U.S. (as of March 3, 2009) [StoreFUEL, 2009]

Utility	Reactor	Vendor	Cask System	Canister Type	Total Loaded	Assemblies Stored
APS	Palo Verde	NAC	**NAC-UMS**	**UMS-24**	57	1368
Connecticut Yankee	Conn. Yankee (Decommis-sioned)	NAC	**NAC-MPC**	**MPC-26**	43	1019
Constellation	Calvert Cliffs	Transnuclear	**NUHOMS**	**24P**	48	1152
Constellation	Calvert Cliffs	Transnuclear	**NUHOMS**	**32P**	12	384
Consumers Power Co.	Big Rock Point (Decommis-sioned)	BFS/ES	**Fuel-Solutions**	**W150**	8	441
DOE	INEEL	Transnuclear	**NUHOMS**	**12T**	29	177
Dominion	Millstone	Transnuclear	**NUHOMS**	**32PT**	8	256
Dominion	North Anna	Transnuclear	**NUHOMS**	**32PTH**	4	128
Dominion	North Anna	Transnuclear	**TN Metal Casks**	**TN-32**	27	864
Dominion	Surry	GNB	**Castor**	**V/21 and X33**	26	558
Dominion	Surry	Westinghouse	**MC-10**	**MC-10**	1	24
Dominion	Surry	NAC	**NAC-I28**	**NAC-I28**	2	56
Dominion	Surry	Transnuclear	**NUHOMS**	**32PTH**	6	192
Dominion	Surry	Transnuclear	**TN Metal Casks**	**TN-32**	26	832
Duke	Catawba	NAC	**NAC-UMS**	**UMS-24**	8	192
Duke	McGuire	NAC	**NAC-UMS**	**UMS-24**	21	504
Duke	McGuire	Transnuclear	**TN Metal Casks**	**TN-32**	10	320
Duke	Oconee	Transnuclear	**NUHOMS**	**24P**	84	2016
Duke	Oconee	Transnuclear	**NUHOMS**	**24PHB**	18	432
Duke (formerly Progress)	Robinson	Transnuclear	**NUHOMS**	**7P**	8	56
Duke (formerly Progress)	Robinson	Transnuclear	**NUHOMS**	**24PTH**	6	144
Energy Northwest	Columbia (formerly WNP-2)	Holtec	**HI-STORM**	**MPC-68**	27	1836
Entergy	Arkansas Nuclear One	BFS/ES	**Fuel-Solutions**	**VSC-24**	24	576
Entergy	Arkansas Nuclear One	Holtec	**HI-STORM**	**MPC-24**	17	408

Utility	Reactor	Vendor	Cask System	Canister Type	Total Loaded	Assemblies Stored
Entergy	Arkansas Nuclear One	Holtec	**HI-STORM**	**MPC-32**	12	384
Entergy	Fitzpatrick	Holtec	**HI-STORM**	**MPC-68**	9	612
Entergy	Grand Gulf	Holtec	**HI-STORM**	**MPC-68**	7	476
Entergy	Indian Point 1	Holtec	**HI-STORM**	**MPC-32**	5	160
Entergy	Indian Point 2	Holtec	**HI-STORM**	**MPC-32**	3	96
Entergy	Palisades	BFS/ES	**Fuel-Solutions**	**VSC-24**	18	432
Entergy	Palisades	Transnuclear	**NUHOMS**	**32PT**	11	352
Entergy	Palisades	Transnuclear	**NUHOMS**	**24PTH**	7	168
Entergy	River Bend	Holtec	**HI-STORM**	**MPC-68**	11	748
Entergy	Vermont Yankee	Holtec	**HI-STORM**	**MPC-68**	5	340
Exelon	Dresden	Holtec	**HI-STAR**	**MPC-68**	4	272
Exelon	Dresden	Holtec	**HI-STORM**	**MPC-68**	29	1972
Exelon	Limerick	Transnuclear	**NUHOMS**	**61BT**	2	122
Exelon	Oyster Creek	Transnuclear	**NUHOMS**	**61BT**	16	976
Exelon	Quad Cities	Holtec	**HI-STORM**	**MPC-68**	19	1292
Exelon (also PSEG)	Peach Bottom	Transnuclear	**TN Metal Casks**	**TN-68**	41	2788
FirstEnergy	Davis-Besse	Transnuclear	**NUHOMS**	**24P**	3	72
FPL	Duane Arnold	Transnuclear	**NUHOMS**	**61BT**	10	610
FPL	Point Beach	BFS/ES	**Fuel-Solutions**	**VSC-24**	16	384
FPL	Point Beach	Transnuclear	**NUHOMS**	**32PT**	9	288
FPL	Seabrook	Transnuclear	**NUHOMS**	**32PTH**	6	192
FPL	St. Lucie	Transnuclear	**NUHOMS**	**32PTH**	6	192
Maine Yankee	Maine Yankee (Decommisssioned)	NAC	**NAC-UMS**	**UMS-24**	64	1434
OPPD	Fort Calhoun	Transnuclear	**NUHOMS**	**32PT**	4	128
PG&E (Pacific Gas and Electric)	Humboldt Bay (Decommissioned)	Holtec	**HI-STAR**	**MPC-80**	5	390
Portland GE	Trojan (Decommissioned)	Holtec	**TranStor cask**	**MPC-24E/EF**	34	780
PPL	Susquehanna	Transnuclear	**NUHOMS**	**52B**	27	1404

Utility	Reactor	Vendor	Cask System	Canister Type	Total Loaded	Assemblies Stored
PPL	Susquehanna	Transnuclear	**NUHOMS**	**61BT**	26	1586
PS Colorado	Fort Saint Vrain (Deco- missioned)	DOE	**Foster Wheeler**	**MVDS**		1464
PSEG	Hope Creek	Holtec	**HI-STORM**	**MPC-68**	12	816
SMUD	Rancho Seco (Decommissioned)	Transnuclear	**NUHOMS**	**24PT**	21	493
Southern Cal Edison	San Onofre Unit 1 (SONGS 1, Decommissioned)	Transnuclear	**NUHOMS**	**24PT1**	17	395
Southern Cal Edison	San Onofre Unit 1 (SONGS 1, Decommissioned)	Transnuclear	**NUHOMS**	**24PT4**	14	336
Southern Nuclear	Farley	Holtec	**HI-STORM**	**MPC-32**	10	320
Southern Nuclear	Hatch	Holtec	**HI-STAR**	**MPC-68**	3	204
Southern Nuclear	Hatch	Holtec	**HI-STORM**	**MPC-68**	35	2380
TVA	Browns Ferry	Holtec	**HI-STORM**	**MPC-68**	4	272
TVA	Sequoyah	Holtec	**HI-STORM**	**MPC-32**	20	640
Xcel Energy	Monticello	Transnuclear	**NUHOMS**	**61BT**	10	610
Xcel Energy	Prairie Island	Transnuclear	**TN Metal Casks**	**TN-40**	24	960
YAEC	Yankee Rowe (Decommissioned)	NAC	**NAC-MPC**	**MPC-36**	16	533

Note from Table A.2 above that the most common dry storage systems as of 2009 were Transnuclear's NUHOMS (383 total), Holtec's MPC (237 combined between those in HI-STORM and HI-STAR overpacks), NAC's UMS (150 total), and Transnuclear's TN metal casks (128 total). The most common canisters were the Holtec MPC-68 (165 total in both HI-STAR and HI-STORM overpacks), the NAC-UMS-24 (150 total), and the Transnuclear NUHOMS 24P (135 total, not including variants).

Table A.3- Canister Shell Dimensions- [EPRI, 2010] and [Rigby, 2010] *

Vendor	Storage Design Model	ID (inches)	OD (inches)	Wall Thickness (inches)	Height (inches)	Source A [EPRI]	Source B [Rigby]
BNG Fuel Solutions/ EnergySolutions	VSC-24	60.5[b]	62.5[b]	1[b]	(164.2-192.2)[b]		Table 2
BNG Fuel Solutions/ EnergySolutions	FuelSolutions W21	64.8[b]	66.0[b]	0.6[b]	(182.3, 192.3)[b]		Table 4
BNG Fuel Solutions/ EnergySolutions	FuelSolutions W74	64.8[b]	66.0[b]	0.6[b]	192.3[b]		Table 4
Holtec	HI-STAR 100,	67.4[b]	68.5[a] or 68.4[b]	0.5[b]	(190.3)[a] (190.3-190.5)[b]	Table 4-3	Table 4
Holtec	HI-STORM 100	67.4[b]	68.5[a] or 68.4[b]	0.5[b]	(190.3)[a] (190.3-190.5)[b]	Table 4-3	Table 4
Holtec	HI-STORM 100U	67.4[b]	68.5[a] or 68.4[b]	0.5[b]	(190.3)[a] (190.3-190.5)[b]	Table 4-3	Table 4
NAC	MAGNASTOR		72[a]		(184.8-191.8)[a]	Table 4-4	
NAC	NAC-STC	69.4[b]	70.6[b]	0.6[b]	(122.6YC, 151.8CY)[b]		Table 4
NAC	NAC-MPC	69.4[b]	70.6[a,b]	0.6[b]	122.5[a], (122.5YC, 151.8CY)[b]	Table 4-4	Table 4
NAC	NAC-UMS	65.8[b]	67.1[a]	0.6[b]	(175.1-190.4)[a] (175.1-191.8)[b]	Table 4-4	Table 4
Transnuclear	NUHOMS-24P	65.9[b]	67.2[b]	0.6[b]	(186.17-196.3)[a] 186.2[b]	Table 4-6	Table 4
Transnuclear	NUHOMS-24PHB	65.9[b]	67.2[b]	0.6[b]	(186.17-196.3)[a] 186.2[b]	Table 4-6	Table 4
Transnuclear	NUHOMS-24PT1		67.2[a]		186.5[a]	Table 4-6	
Transnuclear	NUHOMS-24PT2	65.9[b]	67.2[b]	0.6[b]	(186.5-192.5)[b]		Table 4
Transnuclear	NUHOMS-24PT4		67.2[a]		196.3[a]	Table 4-6	
Transnuclear	NUHOMS-24PTH		62.2[a]		(186.5-193)[a]	Table 4-6	
Transnuclear	NUHOMS-32PT		67.2[a]		(186.5-193)[a]	Table 4-6	
Transnuclear	NUHOMS-32PTH		69.75[a]		(186.5-193)[a]	Table 4-6	
Transnuclear	NUHOMS-32PTH1		69.75[a]		193[a]	Table 4-6	
Transnuclear	NUHOMS-52B	65.9[b]	67.2[b]	0.6[b]	195.9[b]		Table 4
Transnuclear	NUHOMS-61BT	66.3[b]	67[a] 67.3[b]	0.5[b]	196[a,b]	Table 4-6	Table 4
Transnuclear	NUHOMS-61BTH		67[a]		196[a]	Table 4-6	
Transnuclear	TN-32		97.75[a]		(184, 201.88 with cover)[a]	Table 4-5	
Transnuclear	TN-40		99.52[a]		(175, 202 with cover)[a]	Table 4-5	
Transnuclear	TN-40HT		101[a]		(181.75, 199.6 with cover)[a]	Table 4-5	

Transnuclear	TN-68	69.5[b]	98[a,b]	14.3[b]	215[a,b]	Table 4-5	Table 4

*The information contained in this table was taken from two sources. The source of information for each individual value is denoted by a superscript. A superscript 'a' denotes [EPRI, 2010] as the source, and 'b' denotes [Rigby, 2010]. The table within these documents that the information was found within is indicated in the two columns on the right side of Table A.3.

Appendix B: Additional Dry Cask Storage Figures

Included in this section are additional figures of used fuel storage canisters that were not included in Section 2.

Appendix B.1.: Transnuclear

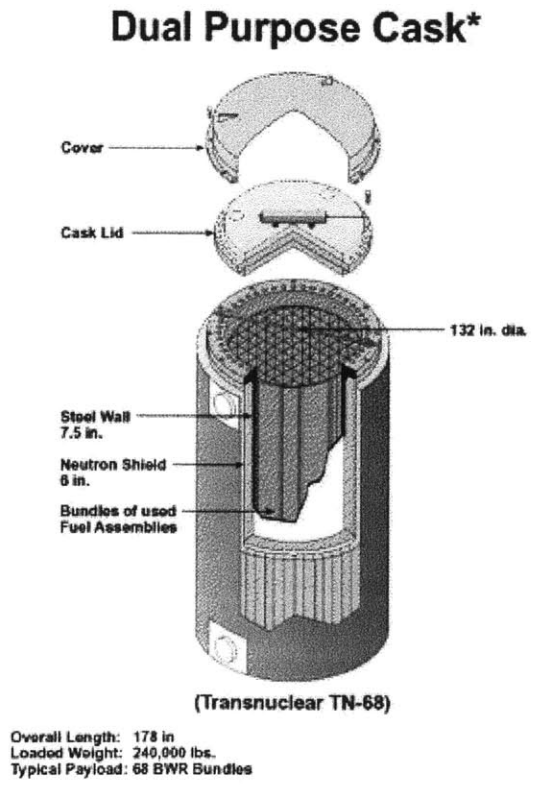

Figure B.1 – Transnuclear TN-68 Metal Bolted Cask [DOE, 2009]

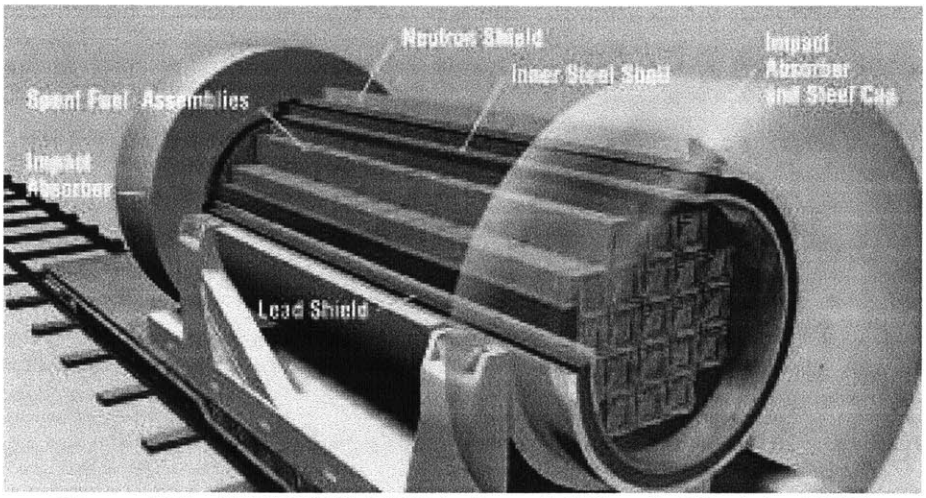

Figure B.2 – NUHOMS 32PT in transit [Lincoln Electric, 2006]

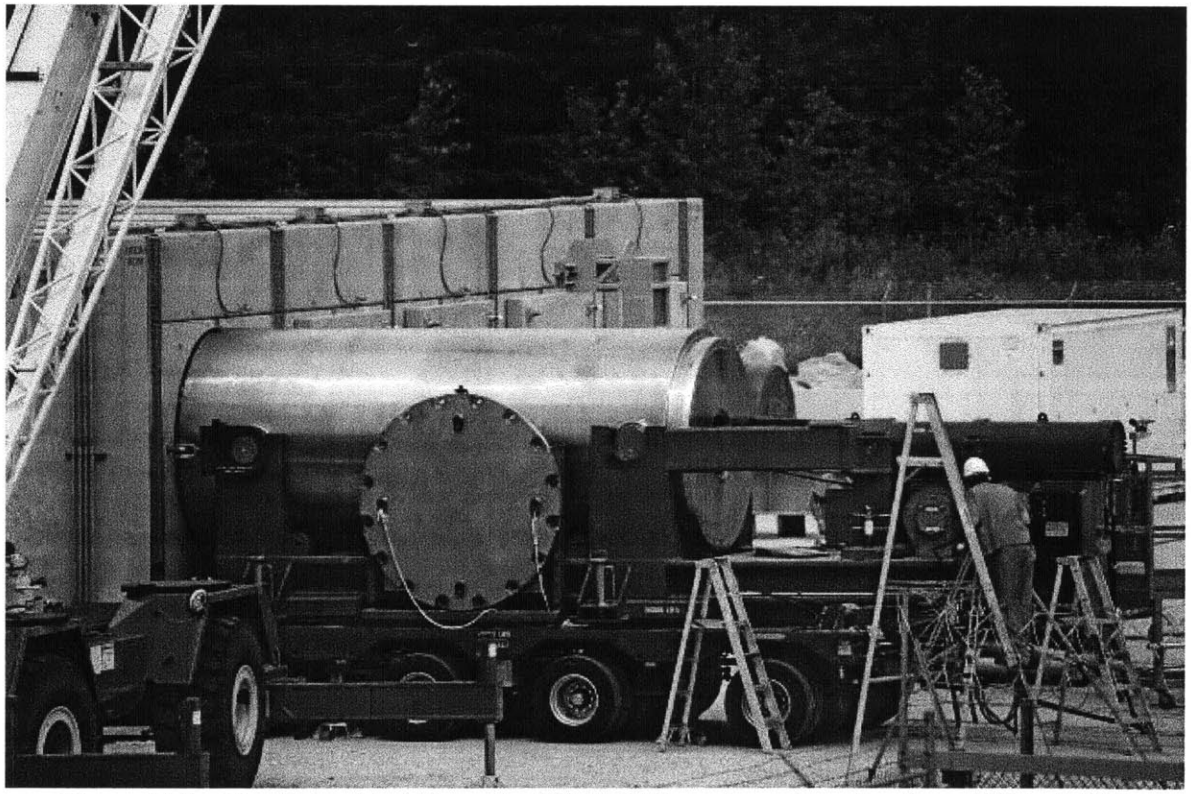

Figure B.3 - Dominion Test Run of a NUHOMS canister transfer from TC to HSM [Content, 2013]

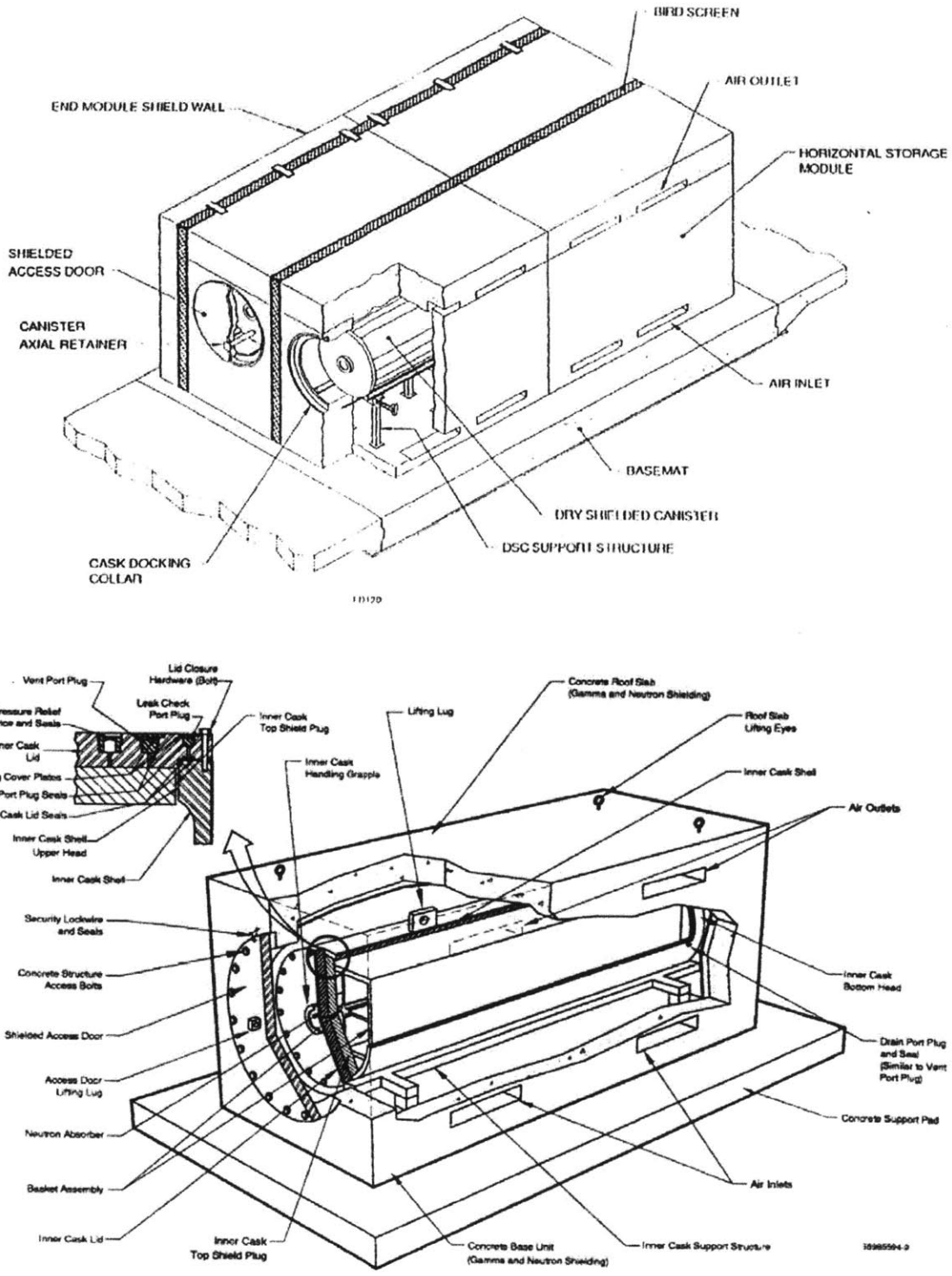

Figure B.4 – NUHOMS cask internals [Rigby 2010]

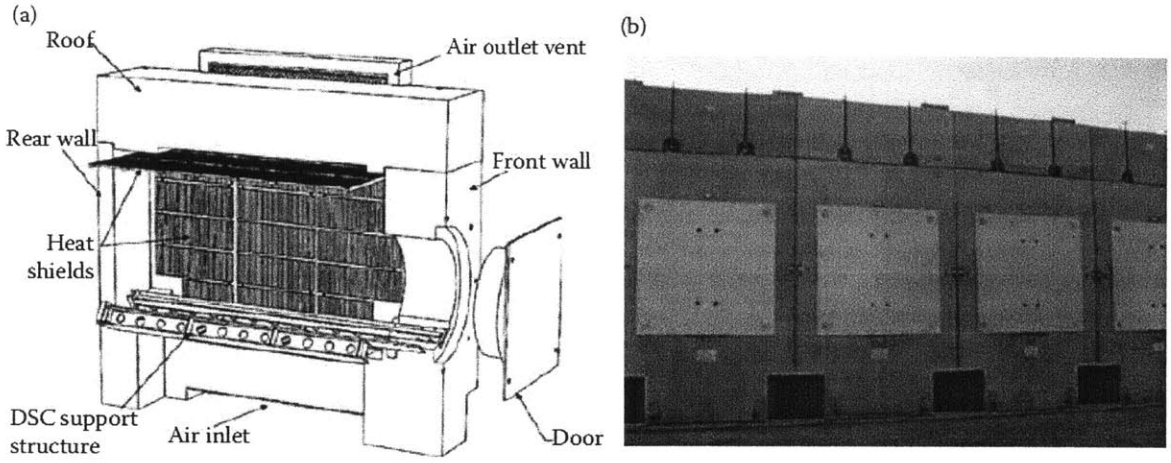

Figure B.5 – NUHOMS HD Schematic and exterior [Kok, 2009]

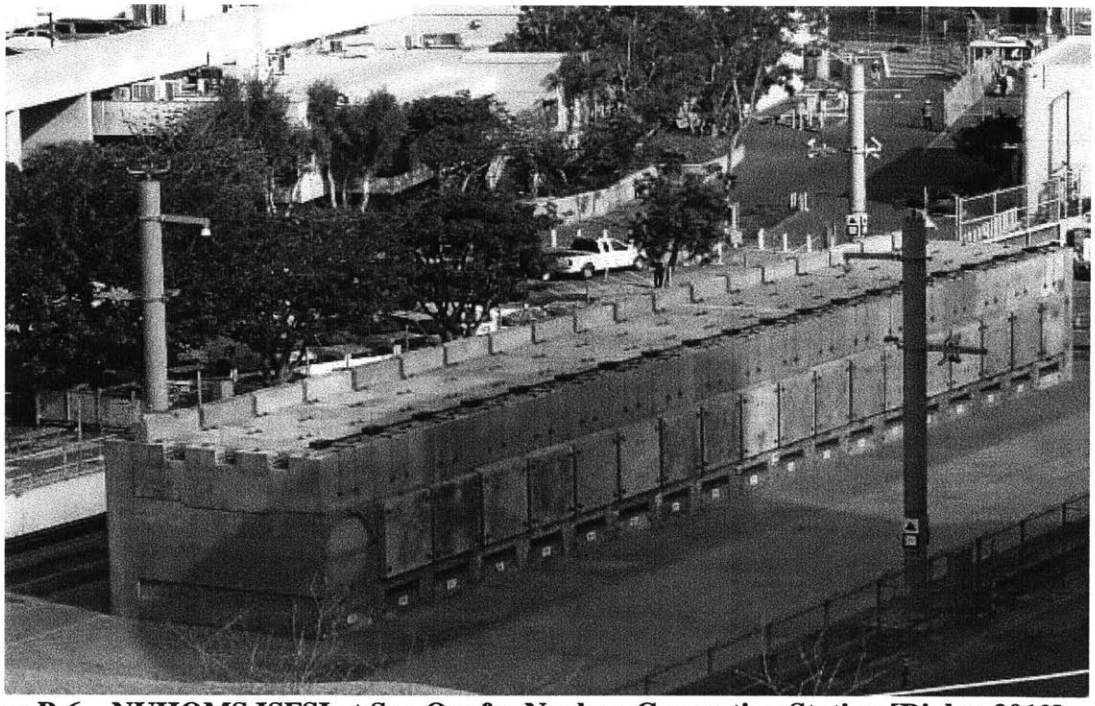

Figure B.6 – NUHOMS ISFSI at San Onofre Nuclear Generating Station [Rigby, 2010]

Appendix B.2.: Holtec

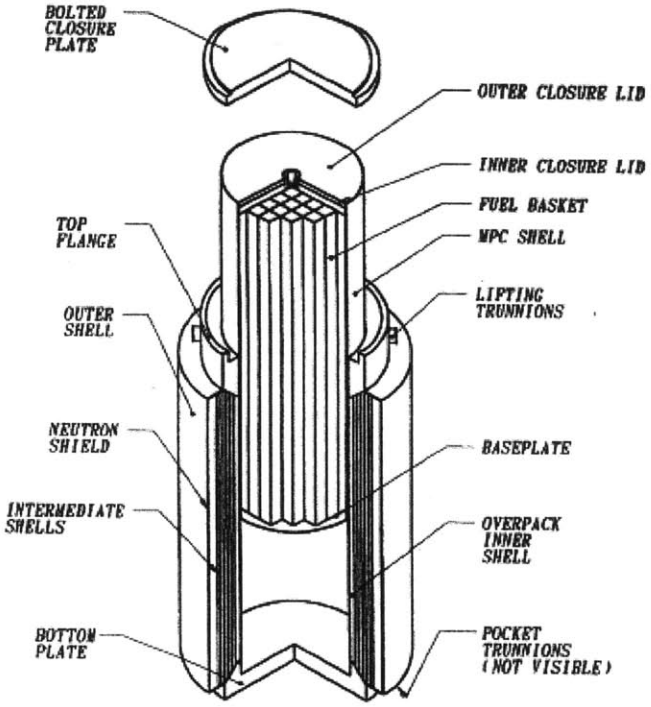

Figure B.7 – HI-STAR 100 overpack with MPC partially inserted [Holtec, 1998]

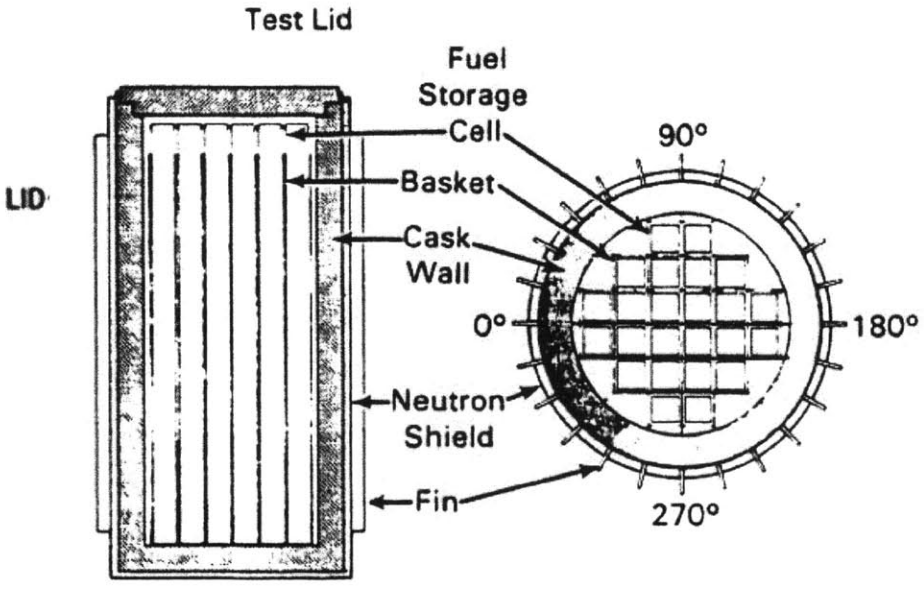

Figure B.8 – HI-STORM 100 basket and internals [Rigby, 2010]

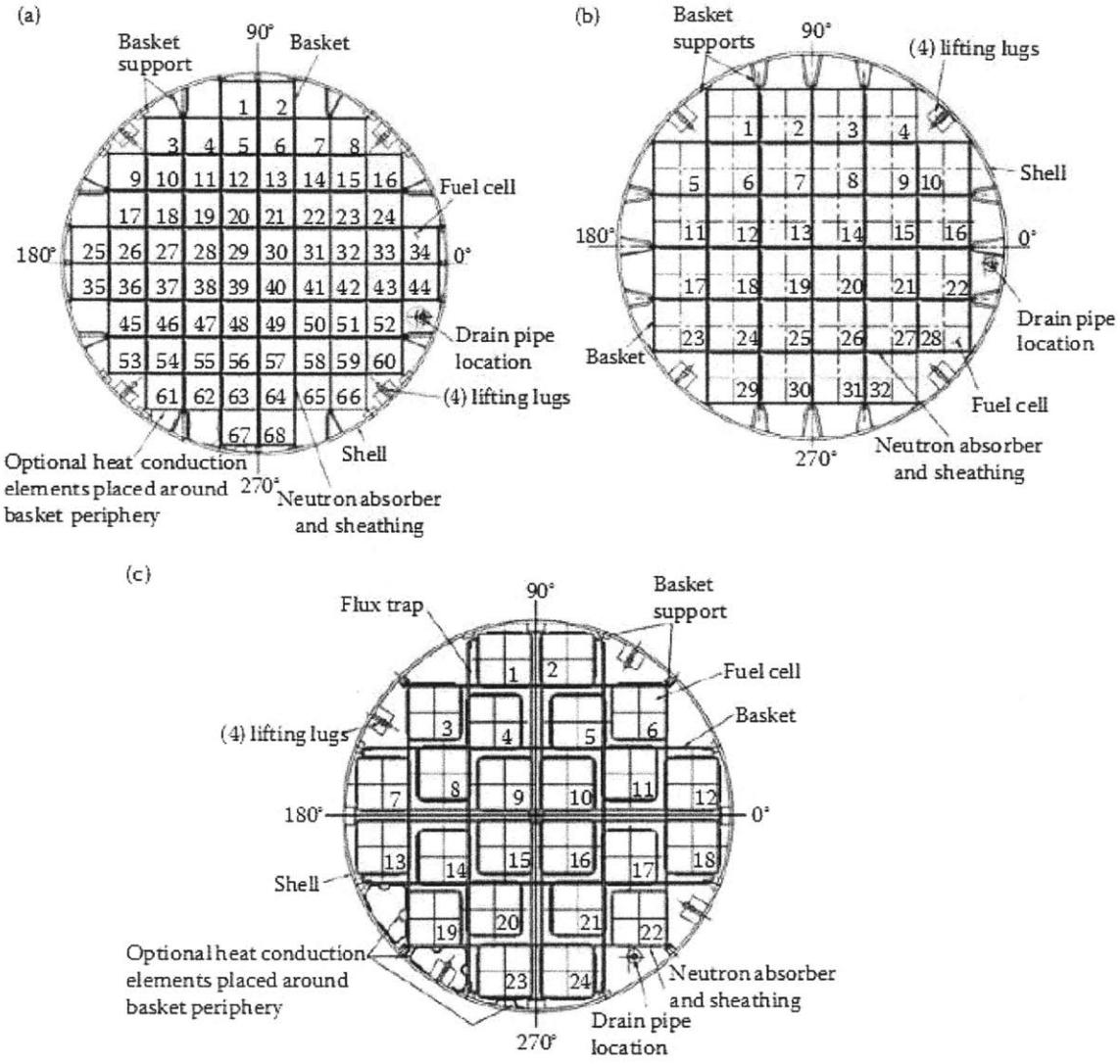

FIGURE 10.9
Cross-sectional view of various spent fuel storage canisters (Final Safety Analysis Report for the HI-STORM 100, Revision 6, USNRC Docket No. 72-1014).

Figure B.9 – Basket cross sections for various HI-STORM 100 canisters [Kok, 2009]

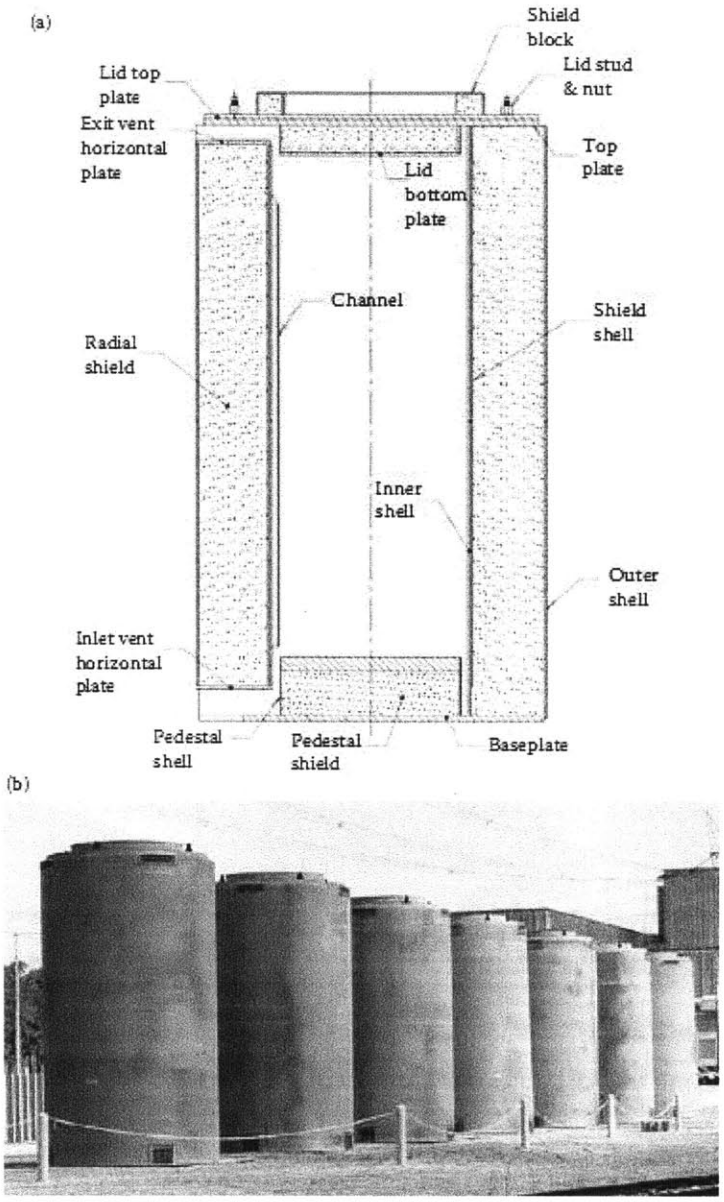

Figure B.10- HI-STORM 100 cask cross section and exterior [Kok, 2009]

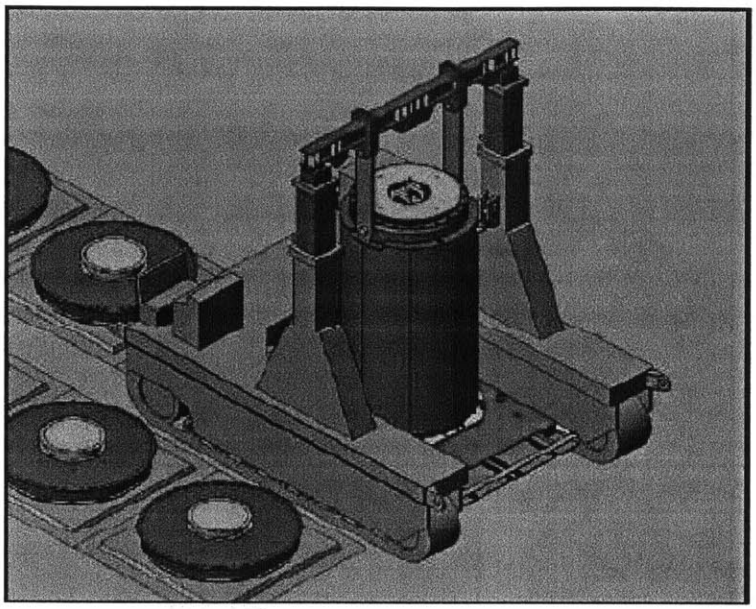

Figure B.11 - HI-STORM 100U Vertical Cask Transporter moving a loaded HI-TRAC Transfer Cask to HI-STORM 100U Storage Module [Singh, 2010]

Appendix B.3.: NAC

For a video of a NAC-MPC being loaded in a spent fuel storage pool and transferred to its cask, follow the link below, and click on "Yankee Rowe SNF Storage – Fuel Pool to Dry Cask Video."

http://www.storenuclearfuel.com/dry-casks/

Appendix B.4.: Other Vendors

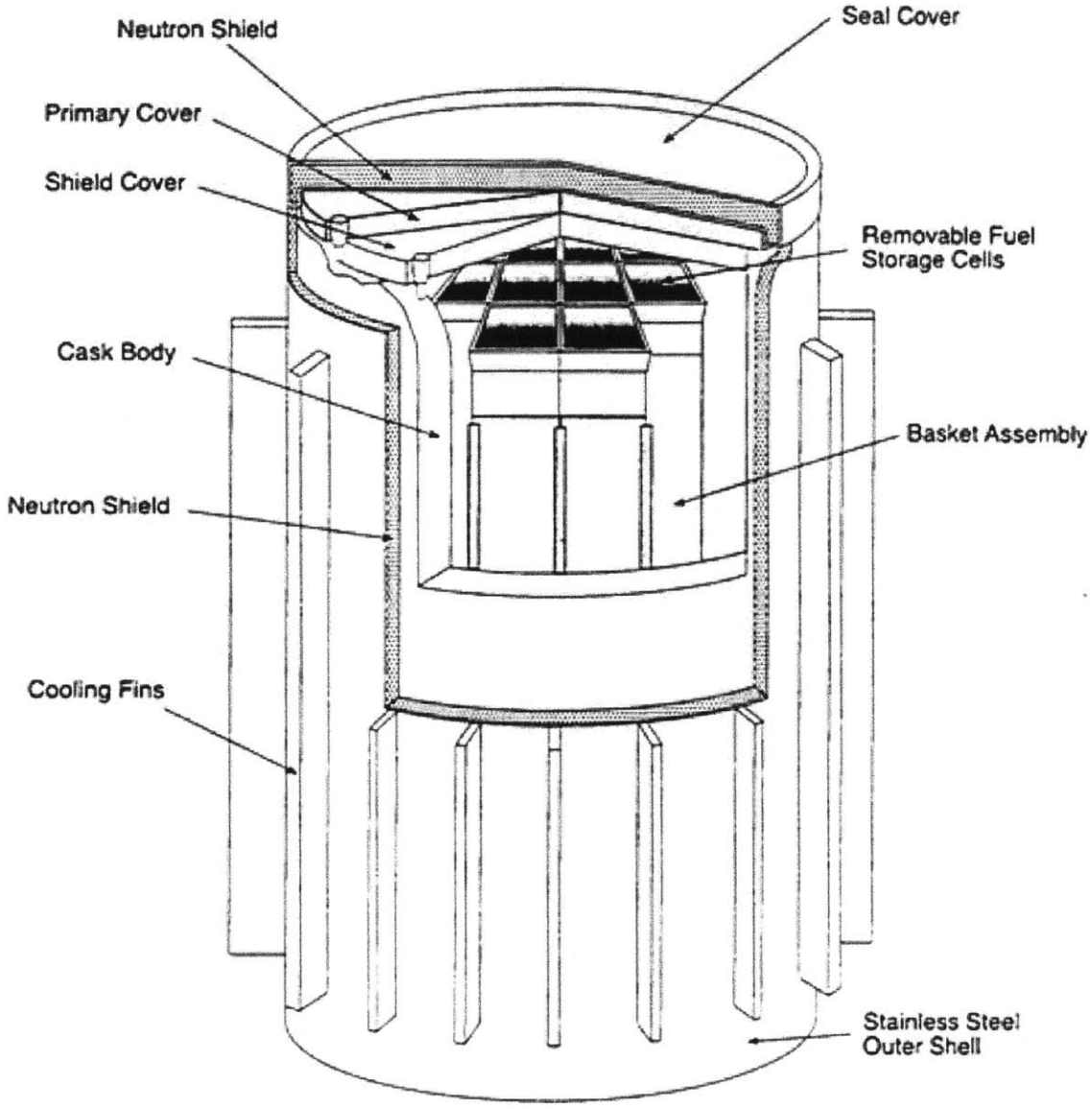

Figure B.12 – Westinghouse MC-10 Metal Storage Cask [NEI, 1998]

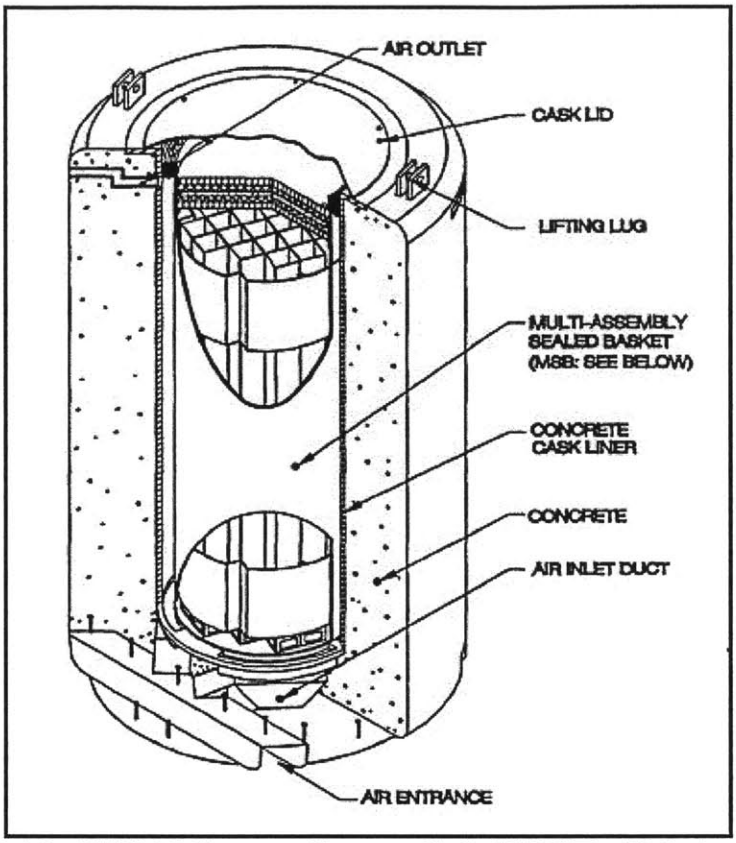

Figure B.13 – VSC-24 Concrete Storage Cask [BNG FuelSolutions, 2005]

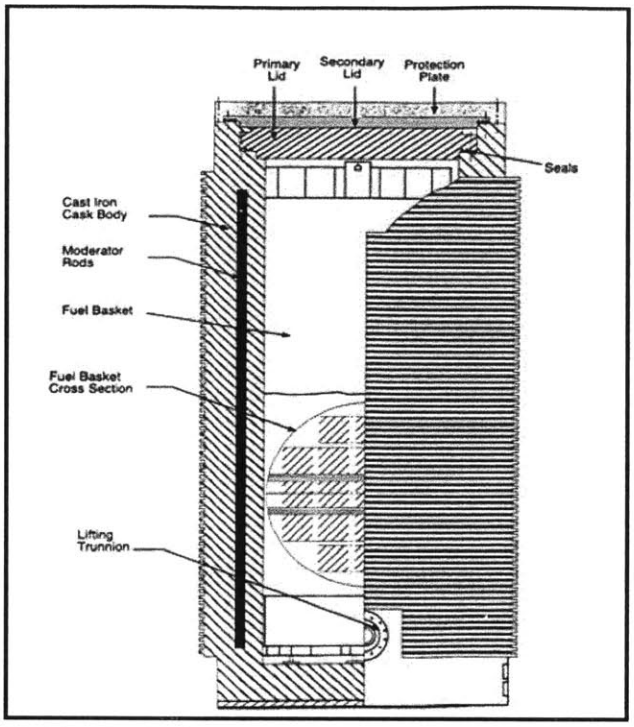

Figure B.14 - CASTOR V/21 Metal Storage Cask [NEI, 1998]

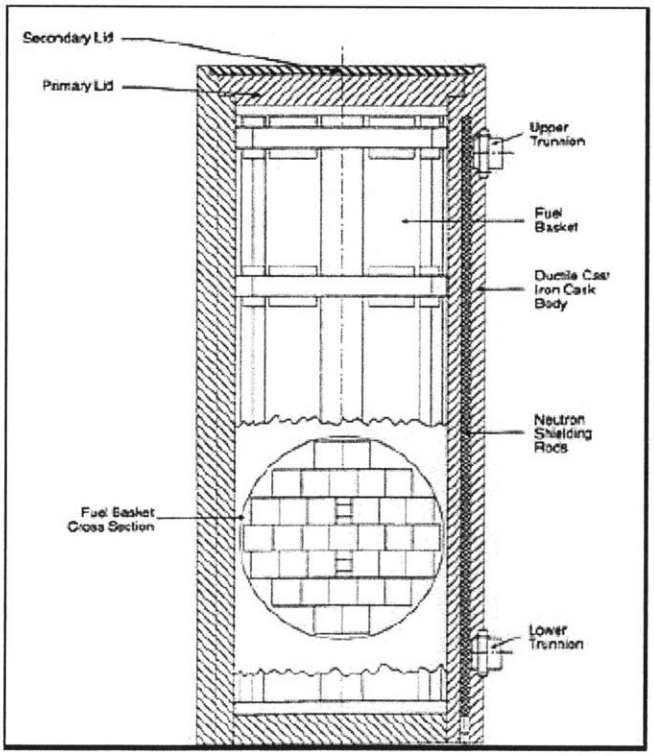

Figure B.15 – CASTOR X/33 Metal Storage Cask [NEI, 1998]

Appendix C: Welding Codes and Standards Outline

Included here is a summary of sections relevant to used fuel storage canisters in the Code of Federal Regulations (CFR), and American Society of Mechanical Engineers Boiler and Pressure Vessel (ASME B&PV) Code. This outline is the result of a literature review in attempt to uncover further information on canister welds by searching through their codes and standards. While it is by no means complete, it offers a useful insight into the standards of canister welds laid forth by 10 CFR and ASME B&PV.

- **Code of Federal Regulations (CFR) [NRC Regulations, 2013]**
  - **10 CFR 72 – Licensing Requirements for the Independent Storage of Spent Nuclear Fuel, High-Level Radioactive Waste, and Reactor-Related Greater than Class C Waste**
    - The only time in 10 CFR 72 that the word "weld" is mentioned:
      72.158 Control of Special Processes
      "The licensee, applicant for a license, certificate holder, and applicant for a CoC [Certificate of Compliance] shall establish measures to ensure that special processes, including welding, heat treating, and nondestructive testing, are controlled and accomplished by qualified personnel using qualified procedures in accordance with applicable codes, standards, specifications, criteria, and other special requirements."

      Here the NRC defers to "applicable codes, standards" to govern the welding procedures of used fuel storage canisters.

      The most frequently called out code and standard in the canisters' Certificates of Compliance is ASME Boiler and Pressure Vessel Code Section III, Subsection NB.

- **ASME (2007 Boiler and Pressure Vessel Code) [ASME, 2007]**

  The sections/subsections below are the most consistently called out in the cask system Certificates of Compliance issued to the NRC.

  - **Section III, Division 1 – Rules for Construction of Nuclear Facility Components**
    - **Subsection NB – Class 1 Components**

      According to the Holtec HI-STORM 100's Safety Evaluation Report, "while ASME Code Section III was intended for the design and fabrication of reactor

vessels, the NRC accepts its use, to the extent practical, for spent fuel storage systems" [Holtec, 2000]. Subsection NB is referenced throughout.

- **2400- Welding Material**
  a) "All welding material used in the construction and repair of components or material, except welding material used for cladding or hard surfacing, shall conform to the requirements of the welding material specification or to the requirements for other welding material as permitted in Section IX [Rules for Inservice Inspection of Nuclear Power Plant Components]. In addition, welding material shall conform to the requirements stated in this Subarticle [NB] and to the rules covering identification in NB-2150."
  b) "The Certificate Holder shall provide the organization performing the testing with the information listed below, as applicable.
     1) Welding process;
     2) SFA Specification and classification;
     3) Other identification if no SFA Specification applies;
     4) Minimum tensile strength [NB-2431.1(e)] in the as-welded or heat-treated condition or both [NB-2431.1(c)];
     5) Drop weight test for material as-welded or heat treated, or both (NB-2332)
     6) Charpy V-notch test for material as-welded or heat treated, or both (NB-2331); the test temperature and lateral expansion or the absorbed energy shall be provided;
     7) The preheat and interpass temperatures to be used during welding of the test coupon [NB-2431.1(c)];
     8) Postweld heat treatment time, temperature range, and maximum cooling rate, if the production weld will be heat treated [NB-2431.1(c)];
     9) Elements for which chemical analysis is required per the SFA Specification or Welding Procedure Specification and NB-2432;
     10) Minimum delta ferrite (NB-2433)"

This indicates that while not publicly available, information such as welding process, preheat and interpass temperature, temperature range, and minimum delta ferrite must be disclosed to the testing organization. This means that the

fabricators must keep track of and/or monitor this information, and provide it for the tests detailed below.

- **2430- Required Tests**- "Tensile and impact tests shall be made, in accordance with this paragraph, of welding materials which are used to join P-Nos. 1, 3, 4, 5, 6, 7, 9, and 11 base materials in any combination, with the exceptions listed in a-d below:
  a) Austenitic stainless steels and nonferrous welding material used to join the listed P-Numbers;
  b) Consumable inserts (backing filler material)
  c) Welding material used for GTAW root deposits with a maximum of two layers
  d) Welding material to be used for the welding of base material exempted from impact testing by NB-2311 shall likewise be exempted from the impact testing required by NB-2330 and this paragraph"
  - **2431.1- General Test Requirements**- "The welding test coupon shall be made in accordance with a-f below, using each process with which the weld material will be used in production welding.
    a) Test coupons shall be of sufficient size and thickness such that the test specimens required herein can be removed.
    b) The weld metal to be tested for all processes except electroslag welding shall be deposited in such a manner as to eliminate substantially the influence of the base material on the results of the tests. [Next several points were about electroslag were covered]
    c) The welding of the test coupon shall be performed within the range of preheat and interpass temperatures that will be used in production welding. Coupons shall be tested in the as-welded condition, or they shall be tested in the applicable postweld heat-treated condition when the production welds are to be postweld heat treated. The postweld heat treatment holding time shall be at least 80% of the maximum time to be applied to the weld metal in production application. The total time for postweld heat treatment of the test coupon may be applied in one heating cycle. The cooling rate from the postweld heat treatment temperature shall be of the same order as that applicable to the weld metal in the component. [Weld coupons for electroslag then discussed]
    d) [Some information on electrodes, impact test specimens] "The longitudinal axis of the specimen

shall be at a minimum depth of 1/4 t from a surface, where t is the thickness of the test weld.

- **3350- Design**- Design of Welded Construction
  - 3351- Welded Joint Category- This section defines Weld Categories A-D, as I have defined in Section 3 above.

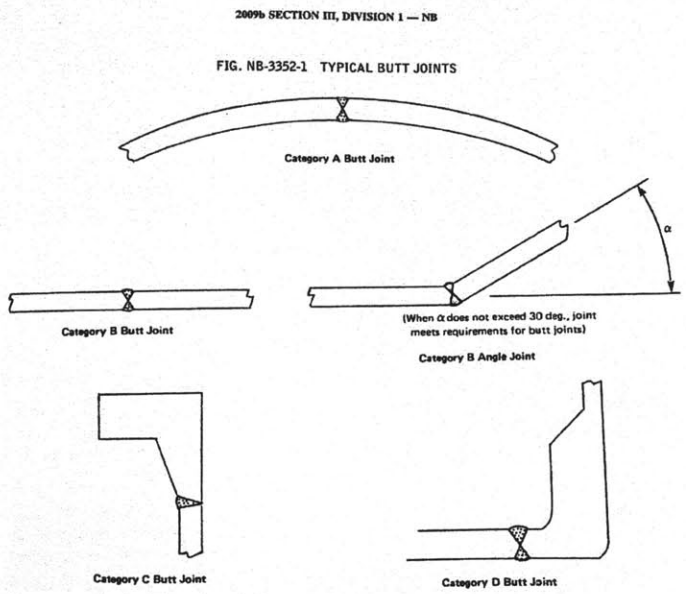

Figure C.1- Typical Butt Joints [ASME, 2007]

Note that the type of butt joint shown in Figure C.1 above for Category A (axial weld) is a Double-V.

  - 4240- Requirements for Weld Joints in Components- Relevant excerpts from here were included in Section 3 of this thesis.
- **4400- Rules Governing Making, Examining, and Repairing Welds**
  - **4420- Rules for Making Welded Joints**
    - 4422- Peening- "controlled peening may be performed to minimize distortion. Peening shall not be used on the initial layer, root of the weld metal, or on the final layer unless the weld is postweld heat treated."
    - 4423- Miscellaneous Welding Requirements-
      a) "Before applying weld metal on the second side to be welded, the root of full penetration double welded joints shall be prepared by suitable methods, such as chipping, grinding or thermal gouging, except for those processes of welding by which proper fusion and penetration are otherwise obtained and demonstrated to be satisfactory by welding procedure qualification."
- **4600- Heat Treatment**

- 4610- Welding Preheating Requirements- Essentially references to BP&V Section IX
- 4612- Preheating Methods- Basically, any method can be used as long as the base or weld metals are not harmed and harmful material is not introduced to the weld
- 4622- PWHT (Post weld heat treatment) Time and Temperature Requirements- "Except as otherwise permitted in NNB-4622.7, all welds, including repair welds, shall be postweld heat treated"
- Table NB-4622.1-1 – P-No. 8: PWHT neither required nor prohibited (see Table C.1 of this thesis for identification of P-No. 8)

▪ **5200- Required Examination of Welds for Fabrication and Preservice Baseline**

- 5210- Category A- "Category A welded joints in vessels and longitudinal welded joints in other components shall be examined by a volumentric[2] and either the liquid penetrant or magnetic particle method."
- 5221- Category B (particularly for Vessels rather than piping or valves)- "Category B welded joints in vessels shall be examined by a volumetric[2] and either the liquid penetrant or magnetic particle method."

[2] "A radiographic examination [NB-5111(a)] is required; a preservice examination [NB-5111(b)] may or may not be required for compliance to the Design Specification [NCA-3252(c)]."

- 5111(a)- Radiographic examinations shall be performed in accordance with Section 5 Article 2, with some exceptions
- 5111(b)- Preservice Examinations- Ultrasonic must follow Section XI Appendix I, eddy current shall follow Section V Article 8, and surface examinations should follow 5111(a)

▪ **5300- Examination Acceptance Standards**- This section gives acceptance standards specifics (including "indication" dimensions) for radiographic, ultrasonic, magnetic particle, liquid penetrant, eddy current, visual acceptance for brazed joints, and bubble formation testing.

o **ASME Section IX- Qualification Standard for Welding and Brazing Procedures, Welders, Brazers, and Welding and Brazing Operations [ASME, 2007]**

▪ **Article I- Welding General Requirements**

- "A Welding Procedure Specification (WPS) is a written document that provides direction to the welder or welding operator for making production welds in accordance with Code requirements".
- **Tension Tests-** Minimum specified tensile stresses listed in QW/QB-422 in [ASME, 2007], the relevant parts of which can be seen in Table C.1 below. For plate sections with thicknesses up to and including 2.54cm (1in), a full thickness specimen shall be used for each required tension test.
- **Guided Bend Tests-** depending on thickness, several side bend, face bend, and root bend tests could be required (for groove welds). The requirements tabulated in QW-450 of [ASME, 2007].
- **Notch Toughness Tests**
- **Fillet-Weld Tests-** more detail tabulated in QW-451.3-4
    - Fracture Tests
    - Macro-Examination-Procedure Specimens
    - Macro-Examination- Performance Specimens
- **Other Tests and Examination [relevant sections only]**
    - **Radiographic Examination**
        - Imperfection limits:
            - Linear Indications (when the length is more than 3x the width- cracks, incomplete fusion, inadequate penetration, and slag)
                - Any type of crack or zone of incomplete fusion or penetration
                - Any elongated slag inclusion which has a length greater than 3mm for t up to 10mm, inclusive OR $1/3t$ for t over 10mm-57mm, inclusive OR 19mm for t over 57mm.
                - Any group of slag inclusions in line that have an aggregate length greater than t in a length of $12t$ except when the distance between the successive imperfections exceeds 6L where L is the length of the longest imperfection in the group
            - Round Indications (length 3x the width or less-porosity and inclusions such as slag or tungsten)
                - Maximum permissible dimension for rounded indications shall be 20% of t or 3mm, whichever is smaller
                - For welds in material lass than 3mm thick, the maximum number of acceptable rounded indications shall not exceed 12 in a 150mm length of weld. A proportionately fewer number of

rounded indications shall be permitted in welds less than 150mm in length.
    - For welds in material 3mm or greater in thickness [here it references several charts for more information].
- **Visual Examination – Performance**
    - "performance test coupons shall show complete joint penetration with complete fusion of weld metal and base material"
- **Liquid Penetrant Examination**
    - Must meet the requirements of Section V Article 6
    - Relevant Indications- defined as indications with major dimensions greater than 1.5mm
    - Linear indications- defined as indications with length greater than 3x width
    - Rounded indications- circular or elliptical indications with length less than or equal to 3x width

- **Article II- Welding Procedure Qualifications**
    - **QW-250: Welding Variables-** Tables are given for the type of variable (essential/nonessential) for all the types of welding (GTAW, SAW, etc.)
        - Essential Variables- "those in which a change, as described in the specific variables, is considered to affect the mechanical properties of the weldment, and shall require requalification of the WPS"
        - Supplementary Essential- required for materials for which other Sections specify notch-toughness tests and are in addition to the essential variables for each welding process.
        - Nonessential Variables- "those in which a change, as described in the specific variables , may be made in the WPS without requalification"
- **Article III- Welding Performance Qualifications**
    - **Qualification for Test Coupons-** "the dimensions of the welding groove on the test coupon used in making qualification tests for double-welded groove welds or single-welded groove welds with backing [full penetration] shall be the same as those for any WPS qualified by the manufacturer, or shall be as shown in figure QW-469.1" (seen in Figure C.2).

QW-469.1 BUTT JOINT

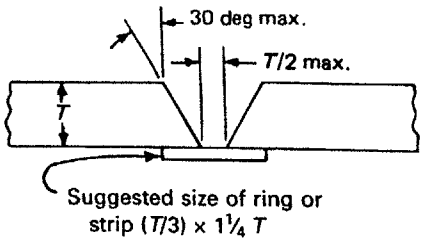

Figure C.2 - Test Coupon Butt Joint Dimensions [ASME, 2007]

"A single-welded groove-weld test coupon with backing or a double-welded groove-weld test coupon shall be considered welding with backing. Partial penetration groove welds and fillet welds are considered welding with backing."

"The dimensions of the welding groove of the test coupon used in making qualification tests for single-welded groove welds without backing shall be the same as those for any WPS, or as shown in Figure QW-469.2" (seen in Figure C.3).

QW-469.2 ALTERNATIVE BUTT JOINT

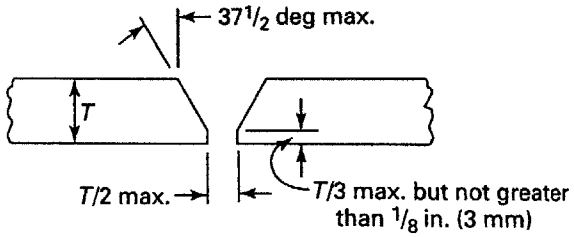

Figure C.3 - Test Coupon Alternative Butt Joint Dimensions [ASME, 2007]

- **Article IV- Welding Data**
  - Lists/specifies all deviations that require requalification of welding procedure.
  - P80-81: QW/QB-422 - Base Metals for Qualification- the welding coupons are put through tensile tests to ensure they can withstand the tensile pressure listed below (Table C.1). For specimens under 3/4in thick, 2 tensile tests are required.

Table C.1 - Selection from QW/QB-422 regarding relevant base materials for canister applications [ASME, 2007]

Type/ Grade	UNS No.	Minimum Specified Tensile (MPa)	Welding P-No.	Welding Group No.	Nominal Composition
304	S30400	515	8	1	18Cr-8Ni
304L	S30403	485	8	1	18Cr-8Ni
316	S31600	515	8	1	16Cr-12Ni-2Mo
316L	S31603	485	8	1	16Cr-12Ni-2Mo

- **F-Numbers:** each "F number" refers to a grouping of electrodes and welding rods. For steel and steel alloys, the F Numbers are 1-6, with each having 4-14 different ASME and AWS specifications as given in Table QW-432.
  "The following F-Number grouping of electrodes and welding rods in table QW-432 is based essentially on their usability characteristics, which fundamentally determine the ability of welders to make satisfactory welds with a given filler metal."
- **Test Positions:** See Figure C.4 below. Circumferential canister welds look as though their test position would be 2G. However, if the canisters happen to be treated as plates rather than pipes (given the large diameter) the circumferential weld could be treated as a horizontal plate, either 1G or 5G. Axial welds look as though they would be 3G (vertical groove weld on a plate as there is no pipe equivalent).

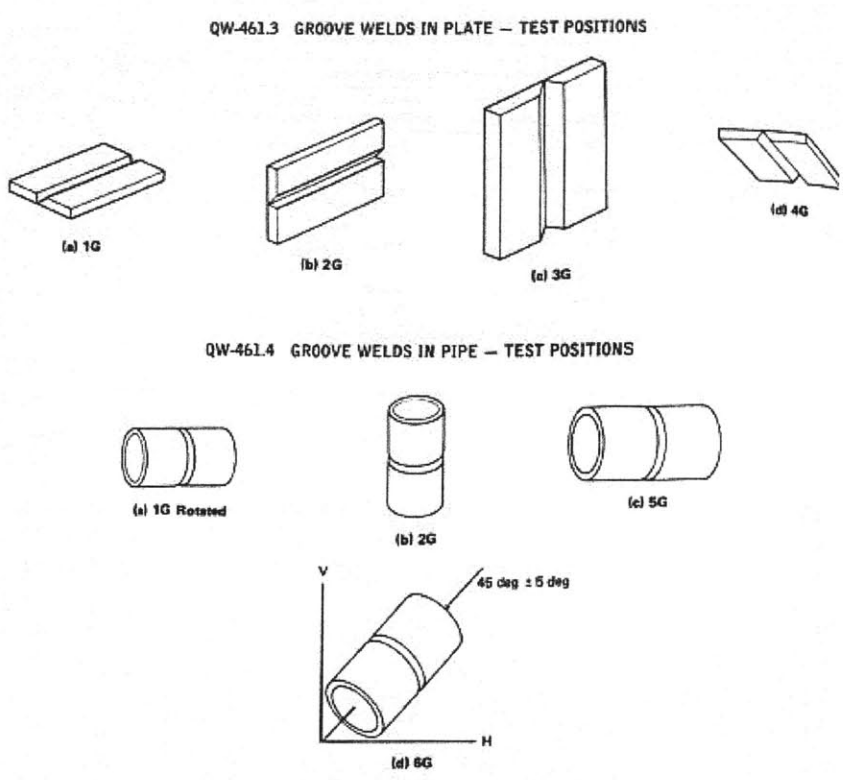

Figure C.4 - Groove Weld Test Positions [ASME, 2007]

- Relevant Definitions included in Article IV: (all verbatim)
  - *Butt Joint*- a joint between two members aligned approximately in the same plane
  - *Ferrite number*- an arbitrary, standardized value designating the ferrite content of an austenitic stainless steel weld metal. It should be used in place of percent ferrite or volume percent ferrite on a direct on-to-one replacement basis.
  - *Heat-affected zone*- the portion of the base metal which has not been melted, but whose mechanical properties or microstructures have been alerted by the heat of welding or cutting
  - *Interpass Temperature*- the highest temperature in the weld joint immediately prior to welding, or in the case of multiple pass welds, the highest temperature in the section of previously deposited welded metal, immediately before the next pass is started.
  - *Welding, gas metal-arc (GMAW)*- an arc welding process that uses an arc between continuous filler metal electrode and the weld pool. The process is used with shielding from an externally supplied gas and without the application of pressure

- *Welding, gas tungsten-arc (GTAW)*- an arc welding process which produces coalescence of metals by heating them with an arc between a tungsten (nonconsumable) electrode and the work. Shielding is obtained from a gas or gas mixture. Pressure may or may not be used and filler metal may or may not be used. (This process has sometimes been called TIG welding, a nonpreferred term).
- *Welding, submerged-arc (SAW)*- an arc welding process that uses an arc or arcs between a bare metal electrode or electrodes and the weld pool. The arc and molten metal are shielded by a blanket of granular flux on the workpieces. The process is used without pressure and with filler metal from the electrode and sometimes from a supplemental source (welding rod, flux or metal granules).

- **Article V- Standard Welding Procedure Specifications (SWPS)**
  - QW-510d- The information recorded on a SWPS shall include the following:
    - The specification, type, and grade of the base metal welded
    - Groove design
    - Initial cleaning method
    - Presence or absence of backing
    - The ASME or AWS specification and AWS classification of electrode or filler metal used and manufacturer's trade name
    - Size and classification of tungsten electrode for GTAWW
    - Size of consumable electrode or filler metal
    - Shielding gas and flow rate for GTAW and GMAW
    - Preheat temperature
    - Position of the groove weld and, if applicable, the progression
    - If more than one process or electrode type is used, the approximate weld metal deposit thickness for each process and or electrode type
    - Maximum interpass temperature
    - Post weld heat treatment used, including holding time and temperature range
    - Visual inspection and mechanical testing results
    - The results of radiographic examination when permitted as an alternative to mechanical testing by QW-304

Note: See also the American Welding Society (AWS) codes for further standards followed on the welding of used fuel storage canisters.